# CAN SOLAR RADIATION MANAGEMENT COOL EARTH WITHOUT REDUCING PRECIPITATION IN HEAVILY POPULATED AND CULTIVATED REGIONS?

By

COREY J. GABRIEL

A dissertation submitted to the

Graduate School-New Brunswick

Rutgers, The State University of New Jersey

In partial fulfillment of the requirements

For the degree of

Doctor of Philosophy

Graduate Program in Atmospheric Science

Written under the direction of

Alan Robock

And approved by

_____

_____

_____

_____

New Brunswick, New Jersey

May, 2017

ABSTRACT OF THE DISSERTATION

Can Solar Radiation Management Cool Earth Without Reducing Precipitation In Heavily Populated and Cultivated Regions?

By COREY J. GABRIEL

Dissertation Director:

Alan Robock

Geoengineering is the large-scale intentional manipulation of climate processes designed to reduce global temperature. Absent the implementation of an effective global mitigation strategy, it may be difficult to avoid experiencing an amount of anthropogenic global warming that would adversely impact both civilization and natural ecosystems without solar radiation management (SRM) geoengineering. One of the major issues with global warming is a possible increase in tropical precipitation over already wet tropical land regions. A major risk associated with stratospheric SRM, an intervention designed to reduce the impacts of global warming, is a reduction of tropical precipitation over land.

In this thesis, I will explore the climate response to SRM with a special focus on impacts in tropical regions, particularly with regard to changes in precipitation patterns. Changes in the El Niño Southern Oscillation (ENSO) are either not present in Geoengineering Model Intercomparison Project (GeoMIP) G1-G4 output, or not detectable, due to the short simulation duration and to the large inherent variability of

ENSO. The changes in precipitation distribution and monsoon strength relative to anthropogenic global warming or the historical climate under G1-G4 cannot be attributed to changes in ENSO.

After determining that no possible marine cloud brightening scheme could be an effective method of cooling Earth without reducing tropical precipitation, in heavily populated, highly cultivated tropical regions, I developed the G4Foam experiment, which achieved significant global cooling and a large redistribution of precipitation from ocean to land. No direct forcing was applied to tropical latitudes, but G4Foam cooled the tropics by 0.6 K, while increasing precipitation in most areas, including areas that typically get less precipitation with global warming. However, the Southern Hemisphere (SH) regional forcing was, as expected, not effective in cooling Northern Hemisphere (NH) continents.

In an attempt to cool the entire planet while maintaining tropical precipitation at present day levels, I combined stratospheric solar radiation management and regional ocean albedo enhancement in designing the G4SSAFoam experiment. In this experiment, 1.5 K of global mean cooling was achieved and tropical precipitation remained at or near RCP6.0 levels and slightly above G4SSA levels. However, the spatial distribution of positive and negative precipitation and precipitation minus evaporation (*P-E)* anomalies in the tropics was heterogeneous, with some heavily populated areas experiencing large increases, while others experience large decreases. The severe cooling of about 2 K in the SH extratropics causes a precipitation reduction of almost 6% in G4SSAFoam when compared to RCP6.0. While *P-E* anomalies over land in the SH are only negative in certain regions, future research would be needed to

determine the full societal and ecological impact of the SH extratropical temperature and precipitation perturbations.

The deployment of microbubbles in the ocean is currently not possible and significant innovation would need to occur if a need to conduct geoengineering in the manner of G4Foam arose, for example, in the event of a stratospheric solar radiation management deployment that reduced tropical precipitation to the extent that it or reduced tropical temperature.

## ACKNOWLEDGEMENTS

First and foremost, I wish to thank Professor Alan Robock (Rutgers) for teaching me how to think like a scientist. Professor Robock's overall leadership and guidance enabled me to produce this thesis. I also wish to acknowledge several others. Dr. Lili Xia (Rutgers) and Dr. Mike Levy (NCAR) generously taught me how to use the CESM. Dr. Ben Kravitz (Pacific Northwest National Laboratory) has chronicled the locations of all GeoMIP data knowable, which is no trivial task, and that effort made my ENSO paper possible. Dr. Kravitz also suggested GeoMIP testbed experiments (Kravitz et al., 2016), which inspired me to create G4Foam. Dr. Tom Collow (Innovim) generously took the time to teach me to use GrADS. Brian Zambri (Rutgers) taught me how to produce clear and eye-catching figures during the preparation of G4Foam. Professor David Keith (Harvard) provided valuable suggestions about G4Foam and geoengineering more generally. I also wish to thank the entire faculty of the Graduate Program in Atmospheric Science at Rutgers. I wish to thank the staff of the Department of Environmental Sciences at Rutgers, in particular, Mike Ferner, Martha Pineda and Melissa Arnesen. This work was supported by U.S. National Science Foundation (NSF) grants AGS-1157525, GEO-1240507, and AGS-1617844. Computer simulations were conducted on the National Center for Atmospheric Research (NCAR) Yellowstone supercomputer. NCAR is funded by NSF. The CESM project is supported by NSF and the Office of Science (BER) of the U.S. Department of Energy. I thank all the climate modeling groups for conducting the GeoMIP simulations and making their output available. Two

anonymous reviewers offered many valuable suggestions, which were incorporated into Gabriel et al. (2017), making it a far better paper. Six anonymous reviewers offered valuable feedback on G4Foam and G4SSAFoam when they approved Alan Robock's NSF proposal that contained G4Foam and G4SSAFoam.

## TABLE OF CONTENTS

## LIST OF TABLES

## LIST OF FIGURES

# CHAPTER 1: INTRODUCTION

In this thesis, I will address the following scientific questions: 1) Will ENSO amplitude and frequency be different under a regime of stratospheric geoengineering from that under a global warming scenario? 2) Is it possible to cool Earth while concurrently maintaining or increasing precipitation in highly populated and heavily cultivated regions, particularly in regions dependent on monsoon precipitation? 3) If one geoengineering method alone is insufficient to cool the planet without reducing precipitation, particularly in heavily populated and cultivated areas, can two methods of geoengineering be imposed concurrently do so?

## 1.1. Background on geoengineering and why it is being considered

The current rate of increase in global mean surface temperature is unprecedented in the last 1,000 years (Marcott et al., 2013). This warming is concurrent with a rate of increase in the atmospheric concentration of carbon dioxide ($CO_2$) and other greenhouse gases that exceeds any other increase in the recent record by one or two orders of magnitude, and the atmospheric concentration of $CO_2$ is higher now than at any time in the last 650,000 years (Siegenthaler et al., 2005). It is extremely likely that the warming since 1950 is primarily the result of anthropogenic emission of heat-trapping gases rather than natural climate variability (IPCC, 2013).

A global consensus on the need for mitigation has led to the December 2015 Paris Agreement at the 21$^{st}$ Conference of the Parties of the United Nations Framework Convention on Climate Change (UNFCCC). However, the UNFCCC lacks enforcement mechanisms, unlike the successful 1987 Montreal Protocol on Substances That Deplete

the Ozone Layer, which legally obliged the signatories to phase out chlorofluorocarbons by 1998. Further, the Paris Agreement relies on nonbinding pledges from nations and avoids explicit emissions targets for specific countries. Societies' abilities to reach the aspirations set out in the Paris Agreement will largely rely on these voluntary contributions to mitigation efforts. The nature of these voluntarily contributions is to be determined on the national level. Even then, attaining the Paris targets will likely require large-scale removal of carbon dioxide from the atmosphere (Fuss et al. 2014; Sanderson et al. 2016). Large-scale carbon dioxide removal is not yet possible, and development of the required technology is likely very expensive.

Even if all 143 countries that are parties to the Paris Agreement were to successfully implement all of the voluntary national contributions put forward in Paris, a global mean surface temperature change of more than 2 K above preindustrial is still likely. Falling short of the 2 K target would require not only the Paris voluntary emission targets being met, but additionally rests on either the hope that technological developments could cause a more rapid adoption of low-carbon technologies, or the hope of massive demand substitution brought about by drastic changes in consumer preferences relating to direct and indirect consumption of greenhouse gases. Sophisticated adaptation efforts, including the planning of infrastructure projects in anticipation of an increase in extreme events, are underway (Miller et al., 2013; Fischbach et al., 2015). However, resources are finite and the planning of and execution of sophisticated large-scale projects necessary for adaptation has been largely limited to the world's richest countries.

Under these conditions, it is easy to see that the combination of mitigation and adaptation may be insufficient to spare society from progressively more disruptive impacts of global warming. This reality elevates the discussion of SRM geoengineering to relevance. SRM has been proposed as a method of reducing global mean temperature, thereby ameliorating many of the negative effects of global warming (Crutzen, 2006). The most discussed SRM approach involves injection of sulfur dioxide ($SO_2$) into the tropical stratosphere. The $SO_2$ reacts with water, and aqueous sulfuric acid ($H_2SO_4(aq)$) is formed. It is theorized that this will then form a relatively stable layer of $H_2SO_4(aq)$ droplets with diameters of less than about 1 μm and mix globally through the Brewer-Dobson circulation, reflecting incoming shortwave (SW) radiation at all latitudes. Other suggested SRM geoengineering methods include marine cloud brightening **(**Jones et al., 2009; Rasch et al., 2009; Latham et al., 2012**)** and surface albedo modification (Irvine et al., 2010; Cvijanovic et al., 2015; Mengis et al. 2016; Gabriel et al. 2017). Each of these methods has the potential to cool Earth's surface, but each comes with known potential side effects. For example, Robock (2008, 2014, 2016) enumerates and describes specific risks and benefits of stratospheric geoengineering.

The cost of implementing stratospheric geoengineering is most likely not prohibitive (Robock et al., 2009). Any decision about the implementation would likely be based on substantive issues of risk and feasibility of governance (Caldeira et al., 2013).

Assessment of the efficacy and risk profile of stratospheric geoengineering is underway in a series of standardized climate modeling experiments as part of the Geoengineering Model Intercomparison Project (GeoMIP) (Kravitz et al., 2011). Any

assessment of the impact of geoengineering on climate must include analysis of how geoengineering could alter patterns of natural climate variability and how geoengineering could change the mean climate state in such a way that natural climate variability would evolve differently in an intentionally-forced world. Since ENSO is the most important and most heavily studied source of interannual climate variability, particularly in the tropics where ENSO is the dominant source of interannual climate variability, even more important than the seasonal cycle in some regions, I concentrate on studying potential changes in that mode of variability.

**1.2. Does geoengineering impact ENSO and why is this question so important?**

Will ENSO amplitude and frequency be different under a regime of geoengineering from that in a global warming scenario? In addition to an exploration of changes in ENSO frequency and amplitude under different scenarios, I seek to determine how sea surface temperatures in the tropical Pacific will evolve under geoengineering, relative to historical and global warming scenarios over the entire length of the simulations.

ENSO's amplitude, frequency and the attendant teleconnection patterns have critical consequences for global climate (McPhaden, 2006). ENSO exhibits a spectral peak every 2-7 years, with warm (El Niño) and cold (La Niña) events each lasting for around one year, and peaking during the DJF season. Typically a La Niña event will follow a strong El Niño event. This understanding is based on a well-established ENSO delayed oscillator paradigm. However, the delayed oscillator paradigm does not always hold up. This may in part be due to the randomness introduced by weather in the equatorial Pacific. However, it is also possible that the widely accepted delayed

oscillator paradigm is wrongly established and that any of several different ENSO mechanisms could be the basis for a model that simulates ENSO just as well as the Zebiak-Cane delayed oscillator (Zebiak and Cane, 1987).

MacMartin and Tziperman (2014) showed that the delayed oscillator paradigm may be useful in describing some of the dynamics associated with ENSO, but that any other plausible ENSO mechanism could be used in place of the delayed oscillator and achieve similar levels of skill in simulating ENSO in a model. They use transfer function tools typically applied in engineering control analysis to evaluate the dynamics of ENSO. By estimating process parameters, they are able to identify compensating model errors that lead to seemingly physically realistic simulations of ENSO. Despite incorrect physics relating to the response of the coupled system to an initial forcing, beginning with an incorrect representation of the magnitude of the SST response, and therefore the surface wind response to the initial downwelling Kelvin wave, compensating errors lead to offsets, and a plausible ENSO simulation results. These errors are present in both general circulation models (GCMs) and simpler models, including the Zebiak-Cane model.

The possibility of a connection between warm ENSO events subsequent to stratospheric aerosol loading via volcanism has been explored both in proxy records and model simulations. Despite the flaws described above, the Zebiak-Cane (ZC) model (Zebiak and Cane, 1987) is a simple model that produces a plausible ENSO, based on a physical representation of the coupled ocean-atmosphere dynamics of the tropical Pacific. By forcing ZC with the calculated radiative forcing from each eruption in the past 1000 years, Emile-Geay et al. (2007) showed that El Niño events tend to occur in the year

subsequent to major tropical eruptions, including Tambora (1815) and Krakatau (1883). A strong enough cooling by a volcanic event is likely to cause warming in the eastern Pacific over the next one to two years (Mann et al., 2005).

The dynamical "ocean thermostat" describes the mechanism underlying differential heating in the eastern and western Pacific. In the presence of strong reduction in insolation, the western Pacific will cool more quickly than the eastern Pacific. This is because the western Pacific mixed layer's heat budget is almost exclusively from solar heating, while, in the east, both horizontal divergence and strong upwelling contributes to the mixed layer heat budget. Therefore, a uniform solar dimming is likely to result in a muted zonal sea surface temperature (SST) gradient across the equatorial tropical Pacific (Clement et al., 1996). A diminished SST gradient promotes a weakening of trade winds, resulting in less upwelling and an elevated thermocline, further weakening the cross-basin SST gradient. This "Bjerknes feedback" describes how muting of the SST gradient brought on by negative radiative forcing alone is exacerbated by ocean-atmosphere coupling (Bjerknes, 1969). Following the initial increase in El Niño likelihood, La Niña event probability peaks in the third year post-eruption, and the statistical likelihood of ENSO events is changed for at least five years (Maher et al., 2015).

The likelihood of an ENSO event in a given year is 31% (Trenberth et al., 1997). To investigate whether the statistical probability of an ENSO event in the year following a volcanic eruption is different than it would be absent the eruption, Emile-Geay et al. (2007) applied the radiative forcing associated with every volcanic eruption in the past 1000 years by dimming the sun in the ZC model by the amount that corresponds to the radiative forcing from each volcano-year in the past 1000 years. This includes 1991

Pinatubo, 1783 Laki, 1257 Sumatra and many other notable eruptions. It also includes many years where the volcanic forcing is very small. They then run 200 simulations of the ZC model for each forcing to see how the tropical Pacific responds over the next year. When the applied forcing is less than -0.8 W $m^{-2}$, the probability of an El Niño event in the year after the simulated volcanic forcing never exceeded 43%, with modeled next year El Niño probabilities clustered around the unforced average of 31%. Volcanic events with radiative forcing ranging from –0.8 W $m^{-2}$ to –3.3 W $m^{-2}$ fit into a transition regime, with the number of El Niño events approaching or exceeding the 43% probability maximum. For all modeled volcanic events with radiative forcing exceeding –3.3 W $m^{-2}$, the probability of a next year El Niño exceeded 43%. This is a forced regime – negative radiative forcing applied to the ZC model forced El Niño likelihood out of a free regime and into a regime where enhanced variability would be more likely (Emile-Geay et al.. 2007). In the transition and forced regimes, El Niño event amplitude is also larger following moderate to strong volcanic events.

Geoengineering schemes simulated in modern GCMs, such as the G4 experiment, introduce long-lasting radiative forcing of around -1 W $m^{-2}$. This magnitude of forcing corresponds to that found in the ENSO transition regime, identified using the ZC model by Emile-Geay et al. (2007). This means that radiative forcing of about -1 W $m^{-2}$ does not force the probability of a next year El Niño event to exceed the 43% free oscillation maximum threshold. However, a radiative forcing of about -1 W $m^{-2}$ does fit into a range in which the statistical probability of an El Niño is higher than it would be absent the volcanic forcing. Will solar dimming lasting many years, as a proxy for sulfate injections, or sulfate injections lasting many years as simulated by models alter El Niño

or La Niña event frequency and amplitude? This is studied by using various geoengineering experiment designs in GCMs to determine whether forcing from stratospheric aerosol injections, added continuously, alter the probability and potential strength of ENSO. Gabriel and Robock (2015) evaluated the impact of long term solar dimming or continuous stratospheric sulfate injections on ENSO. However, little other work had been done to assess the ENSO response to SRM until very recently..

Since this comparison is between El Niño and La Niña amplitude and frequency under a geoengineering regime and under a scenario of unabated global warming, the evolution of ENSO behavior under global warming, independent of geoengineering, is also of interest. Overwhelming evidence from climate model experiments shows that geoengineering could effectively reduce or offset the surface temperature increase resulting from global warming by limiting the amount of incoming shortwave radiation, compensating for global warming (Robock et al., 2008; Jones et al., 2010). An alternative theory for why ENSO amplitude and frequency may be different in the future under a geoengineering regime than under global warming is based on the fact that ENSO events may evolve differently from a warmer tropical Pacific mean state under global warming than if a geoengineering scheme were imposed. For example, Cai et al. (2015) shows in a study using 21 CMIP5 models that simulate the Representative Concentration Pathway 8.5 (RCP8.5), the maritime continent heats faster than the Central Pacific while the Walker Circulation weakens. This results in strong La Niña events occurring twice as frequently than under the control simulations.

Kirtman and Schopf (1998) showed that tropical Pacific mean-state changes on decadal timescales are more responsible than atmospheric noise for changes in ENSO frequency

and predictability. This does not imply any external cause for the changes in ENSO, but does imply that a uniform warming of the tropical Pacific may cause changes in ENSO. Despite the lack of a robust multi-model ENSO signal in the Coupled Model Intercomparison Project 5 (CMIP5) models (Taylor et al., 2012), there are suggestions that strong El Niño events may become far more likely under global warming, specifically in a multi-model ensemble experiment using the RCP8.5 scenario (Meinshausen et al., 2011). As global warming continues, background state tropical Pacific SSTs are expected to warm faster along the Equator than off the Equator, and faster in the east than in the west – the inverse of the ocean dynamical thermostat mechanism (Held et al., 2010). With the weaker zonal SST gradient in the tropical Pacific, there will be more occurrences of higher SSTs in the eastern Pacific, promoting large scale organization of convection further to the east, with twice as many strong El Niño events over 200 years of RCP8.5 runs (Cai et al., 2014). In order to offset RCP8.5 with a geoengineering experiment, it is necessary to inject about 50 Tg yr-1 into the stratosphere (Niemeier and Timmreck, 2015), which may be very difficult and could have serious side effects. However, GeoMIP simulations facilitate comparison between various geoengineering scenarios and several other global warming scenarios, RCP4.5, 4xCO2 and +1%$CO_2$ $yr^{-1}$ and those will be used as the global warming reference scenarios in this ENSO experiment.

**1.3 Representation of the Tropical Pacific in CMIP3 and CMIP5**

Proper depiction of ENSO in a GCM is confounded by the fact that ENSO is a coupled ocean-atmospheric phenomenon, generated by the interaction of many processes, each occurring on one of several different time scales. Nearly all CMIP3 models were

able to produce an ENSO cycle, but significant errors were evident (Guilyardi et al., 2009). Analysis of CMIP5 models has shown significant improvement, but the improvement has not been revolutionary. Such a comparison is facilitated by standardized "metrics developed within the CLIVAR [Climate and Ocean: Variability, Predictability and Change] Pacific Panel that assess the tropical Pacific mean state and interannual variability" (Bellenger et al., 2013). The following metrics were used in the CLIVAR CMIP3/CMIP5 comparison: ENSO amplitude, structure, spectrum and seasonality. Some process-based variables were also studied, including the Bjerknes feedback.

Key results included that 65% of CMIP5 models produce ENSO amplitude within 25% of observations as compared to 50% for CMIP3. Other results included improved seasonal phase locking and the proper spatial pattern of SSTs at the peak of ENSO events. Despite the improvement in these result-based variables, analysis of process-based variables, such as the Bjerknes feedback, showed less consistent improvement. This gives rise to the possibility that the bottom-line improvement in ENSO depiction was at least partially the result of error cancellation, rather than clear improvements in parameterization and simulation of physical processes (Yeh et al., 2012; Guilyardi et al., 2012; Bellenger et al., 2013). A particularly striking area of divergence between modeling and observations is in the absence of a shift from a subsidence regime to a convective regime in the equatorial central Pacific during evolution of El Niño events. Many models maintained a subsidence regime or convective regime at all times over the equatorial central Pacific (Bellenger et al., 2013). This error likely led to the muting of the negative shortwave feedback in many models, leading to muted damping of ENSO

events in those models.

Both the improvement in depiction of ENSO amplitude and seasonality from CMIP3 to CMIP5 and the ability to understand the simulation of key process-based variables motivate an analysis of ENSO and geoengineering using CMIP5 GCMs.

It is difficult to draw robust conclusions about future ENSO variability. By comparing time slices of a 4,000-year unforced control run Wittenberg et al. (2013) demonstrate that multidecadal episodes of extreme ENSO behavior can arise entirely randomly or as a result of inherent climate variability. There is no unambiguous signal of how ENSO may change under global warming in CMIP5. However, several recent studies have been able to detect statistically significant changes in ENSO. For example, Cai et al. (2015) shows a statistically significant increase in the frequency of extreme La Niña events under RCP 8.5 as compared to a non-global warming control scenario. They selected 21 of 32 available CMIP5 models, because of their ability to accurately simulate processes associated with extreme ENSO events. Each model simulation lasted for a period of 200 years.

This is done by comparing various time slices of a 4,000-year unforced control run to each other. The detectability of changes in ENSO variability in future SRM modeling experiments will likely be buoyed by the availability of more models and longer simulations. Additionally, future SRM experiments that attempt to offset or partially offset more extreme AGW scenarios, such as RCP 6.0 and RCP 8.5, may improve detectability. Given that detecting an ENSO change in a 200-year record with 21 different participating GCMs is not straightforward, I anticipate that detecting changes in ENSO by analyzing GeoMIP may be difficult. Further, I recognize that even if

significant differences between ENSO in a geoengineered world as opposed to an AGW world are evident, a large number of comparisons will have to be made, and further analysis of significant results will need to be performed to determine whether the result is robust. Despite these substantial caveats, it would be irresponsible for geoengineering research to progress without consideration of how a geoengineering regime could alter ENSO.

**1.4 Background on G4Foam experiment**

While the examination of ENSO changes under stratospheric geoengineering requires the examination of as many models as possible in an attempt to identify a signal, the methodology for the next part of this thesis, G4Foam, is extremely different. In the ENSO analysis, I seek to answer a specific important question about the potential changes in climate variability brought on by SRM geoengineering. G4Foam is motivated by a desire to offer a modeled solution of a known problem with stratospheric SRM: not enough precipitation falls, particularly in the tropics, during periods of modeled geoengineering. To address this question, I need to identify, and implement, in a climate model, a novel geoengineering approach.

The G4Foam experiment, a GCM simulation consisting of three ensemble members from 2020-2089 was performed. The period 2020-2089 is simulated in order to facilitate comparison with G4SSA (Tilmes et al., 2015; Xia et al. 2016), where forcing commences in 2020 and is gradually turned off in 2070 and then run for an additional 20 years to assess what happens after the forcing is removed. Fifty years of forcing is sufficient since the climate responds to G4Foam relatively quickly and the 2030-2069 period is a long enough period from which to identify significant differences between the

climates. G4Foam forcing is removed in 2070 and the climate adjusts back quickly. By 2089, the G4Foam, RCP6.0 and G4SSA climates are very similar.

G4Foam is unique for several reasons. Most importantly, G4Foam changes the surface energy budget only in carefully chosen regions. The radiative forcing alone is modest and designed to induce via powerful positive cloud feedbacks, which are responsible for much of the cooling. Further, the G4Foam precipitation changes are large-scale circulation anomalies intentionally introduced by the hemispherically asymmetric cooling of the SH. G4Foam seeks to harness the power of positive feedbacks rather than relying on forcing alone. Specifically, the area appropriate for brightening in this experiment is confined to three specific regions in the SH. For the G4Foam scheme to achieve enough cooling, the forcing must trigger powerful positive feedbacks, which amplify the temperature response and facilitate the circulation changes. Sections 1.6-1.7 of this thesis explain why I hypothesize that G4Foam will work in this manner.

G4Foam simulates a particular implementation of an idealized form of the technology described by Aziz et al. (2014), where stable, reflective foam suitable for use as SRM in ocean regions with limited nutrients that support little marine life, is made in the laboratory. The broad idea of microbubble deployment as a form of SRM is explored by Seitz (2010). I only examine the potential benefits and risks of such a surface albedo scheme, and I do not advocate deployment of any form of geoengineering even if it were presently possible. Robock (2011) has cautioned against the potential implications of ocean albedo modification as presented by Seitz (2010).

Stratospheric SRM is the most discussed, and given the current state of research, probably the most feasible, form of geoengineering (Dykema et al., 2014, Keith et al.,

2014). Implementation of the G4Foam regional ocean albedo modification scheme could be considered with or without concurrent SRM. G4Foam could be used concurrently with stratospheric SRM in an attempt to restore the strength of the hydrological cycle should the hydrological cycle be weakened by performing stratospheric SRM only. G4Foam is also a potential alternative to SRM with a far different latitudinal distribution of benefits. The focus here is solely on the second scenario, as it allows for the elucidation of the impacts of the G4Foam experiment forcing alone.

While G4Foam and stratospheric SRM are aimed in part at reducing surface temperature, their objectives vary in two profound ways. First, G4Foam primarily aims to enhance water supply by repositioning the tropical rain belts into highly populated, heavily cultivated areas. Second, unlike stratospheric SRM, where the surface temperature in the high latitude Northern Hemisphere (NH) is reduced the most, G4Foam is most effective in cooling Earth's surface south of 30°N.

**1.5. Can G4Foam reduce global warming without reducing tropical precipitation?**

One of the major issues with stratospheric aerosols is a reduction of precipitation, especially for summer monsoons. The intervention discussed here attempts to reduce warming without reducing precipitation. Is it possible to cool the planet while concurrently maintaining or increasing precipitation in highly populated and heavily cultivated regions, particularly in regions dependent on monsoon precipitation? I begin by determining whether a forcing can be applied in a GCM that will result in the model responding with the northward and landward shift of tropical precipitation needed to achieve my objective. To that end I conducted simulations with The Community Earth System Model 1/Community Atmospheric Model 4 fully coupled to tropospheric and

stratospheric chemistry (CESM1 CAM4–Chem) model (Lamarque et al., 2012; Tilmes et al., 2015, 2016). I ran the model with horizontal resolution of 0.9° x 1.25° lat-lon and 26 levels from the surface to about 40 km (3.5 mb), as was done for G4SSA (specified stratospheric aerosol) by Xia et al. (2016).

The experiments consisted of three ensemble members of a simulation from 2020-2089 in which the ocean surface albedo is raised as described above from a daytime average of 0.06 to a daytime constant 0.15 on the SH subtropical ocean gyres for 50 years, 2020-2069, and then returned to unforced values from 2070-2089 to assess how quickly the G4Foam climate returns to RCP6.0 after the forcing is removed. . My hypothesis is that the tropical rain belts will move northward largely as a result of increased moisture convergence over land regions, particularly during NH summer (June-July-August, JJA) in NH monsoon regions. Enhanced divergence over the already strong subtropical highs, due to increased subsidence over the increased albedo ocean regions in the subtropical Southern SH, would help the cooler air from the forced subtropical regions advect throughout the SH troposphere. The asymmetric cooling would force changes in the Hadley Cell, enhancing cross equatorial flow, which would cool the surface in the NH tropics, especially during JJA, when heat related mortality and morbidity is highest. Finally, the resulting cooling of low latitude NH land areas would not dampen the monsoon. The wet season monsoon circulation is initiated and maintained by the moist static energy gradient, not the surface temperature gradient. A wetter, more cloudy land mass will strengthen, not dampen the circulation relative to a warmer, drier continent (Hurley and Boos, 2014), especially with a cooler, lower specific humidity environment under the descending branch of the meridional circulation.

The strength of this response will be very sensitive to the cloud feedbacks that result from the surface albedo forcing, and hence the results are likely to be model dependent. The basis of this comprehensive hypothesis is described in detail, below, specifically in sections 1.6 and 1.7. The details of the experiment are discussed in detail in section 2.2.

**1.6 Stratospheric geoengineering weakens the hydrological cycle**

With global warming, low-level specific humidity scales with Clausius-Clapeyron, and will increase by about 7% $K^{-1}$ within the tropical planetary boundary layer. This response will be approximately spatially homogeneous throughout the tropics. However, the precipitation response will be different. Increased moisture convergence in areas that already get a lot of precipitation will result in the wet getting wetter, while increased moisture divergence in dry areas will result in the dry getting drier (Held and Soden, 2006).

The rich get richer, poor get poorer paradigm does not hold up in an SRM world (Tilmes et al., 2013), where the response is very different from that under global warming. Based on the results of an observational study, Trenberth and Dai (2007) pointed out the possibility that drought, particularly in the tropics, could result from geoengineering. This is based on a study of tropical volcanism, which provides a good analog to stratospheric SRM, particularly by sulfate injections. They found that after the eruption of Mount Pinatubo (15°N) in 1991, precipitation dropped over land and record drops in runoff and river discharge were observed from October 1991 to September 1992.

Using a comprehensive atmosphere-ocean GCM, the National Aeronautics and Space Administration Goddard Institute for Space Studies ModelE, Robock et al. (2008)

used a simulation of injections of tropical and Arctic stratospheric of sulfate aerosol precursors and generated a reduction in rainfall over China and India, especially during NH summer, which is associated with a weakened monsoon. Changes in precipitation patterns also imply a southward shift of the intertropical convergence zone (ITCZ) over the Atlantic and Pacific Oceans. Additional similar experiments showed similar results.

In the GeoMIP G1 experiment, abrupt 4xCO2 forcing is applied to a year 1850 control climate, and the $CO_2$ forcing is fully offset by concurrent solar dimming (Kravitz et al., 2011). To explain the different hydrological cycle responses to surface and atmosphere energy balance responses to greenhouse gas and solar forcings, Kravitz et al. (2013) compared G1 with the experiment abrupt 4xCO2 and the Pre-Industrial Control experiment (picontrol), which is the reference experiment for both abrupt 4xCO2 and G1. They found a reduction in precipitation in G1 relative to abrupt 4xCO2 that can be separated into a fast component, due to the radiative response, which scales with the applied forcing, and a slow response, which is a temperature effect. Tilmes et al. (2013) analyzed the hydrological cycle in most of the GeoMIP participating Coupled Model Intercomparison Project 5 (CMIP5) (Taylor et al., 2012) models by comparing abrupt 4xCO2, picontrol, and G1. They found a robust reduction in global monsoon rainfall, including in the Asian and West African monsoon regions in G1 relative to both abrupt 4xCO2 and picontrol. Haywood et al. (2013) explored the impact of stratospheric SRM in one hemisphere only and found a movement of the ITCZ away from the hemisphere that was cooler as a result of the asymmetric cooling of the hemispheres.

This consensus about the potential for reduced tropical rainfall under a regime of stratospheric SRM motivates me to identify an alternative or stratospheric SRM-

concurrent geoengineering approach that could cool the planet, without reducing monsoon precipitation in highly cultivated areas. However, many of the studies that assess the hydrological cycle's response to SRM involve geoengineering experiments that cool the planet to preindustrial levels and if geoengineering is performed, it is not likely necessary to cool the planet to preindustrial levels and the precipitation response could be much smaller if geoengineering were used to offset only a small portion of the anthropogenic warming that has occurred.

**1.7 Extratropical forcing impacts the position of the ITCZ**

Under global warming, tropical rainbelts will move toward the hemisphere that warms more (Chiang and Bitz, 2005, Frierson and Hwang, 2012). Early atmosphere-ocean coupled models involved prescribed clouds. Increasing low cloud cover, and thereby inducing cooling, in one hemisphere relative to the other caused the tropical rainbelts over the Pacific Ocean to move toward the other hemisphere (Manabe and Stouffer, 1980). The impacts of asymmetric heating of the hemispheres became highly relevant during the Sahel drought. Much of the rainfall deficit during the devastating 20-30 year drought can be attributed to cooling initiated by increased tropospheric sulfate emissions in the NH (Hwang et al., 2013). The forced cooling over the NH was enhanced by a positive dynamical feedback in the North Atlantic Ocean. This hemispheric asymmetry moved Earth's energy flux equator, the vertical surface boundary where the vertically integrated meridional energy flux is zero, southward (Broccoli et al. 2006; Kang et al. 2008). Hence, the ITCZ and associated tropical rainbelts migrated south. Since the Sahel is at the northern margin of the ITCZ's annual migration, or at the

northern terminus of the West African monsoon, southward displacement of the ITCZ led to a devastating drought (Folland, 1986).

Broccoli et al. (2006) diagnosed the energy balance mechanism that causes the ITCZ to shift in response to asymmetric heating of the extratropics. Using models of varying complexity, Broccoli et al. (2006) imposed an anomalous cooling of the NH, both via a last glacial maximum simulation and hosing of the North Atlantic. The heating asymmetry causes the extratropics in the NH to demand more heat and the extratropics in the SH to demand less heat. Since cross equatorial heat transport is achieved principally via the Hadley Cell, the SH Hadley Cell strengthens, particularly in austral summer, in response to the NH cooling, and net energy flow in the upper branch intensifies, redistributing energy into the NH from the relatively warm SH.

Net flow of energy in the Hadley cell is achieved by the flow of moist static energy, which flows in the direction of the upper troposphere branch of the Hadley Cell. This is because moist static energy is higher at higher altitudes in the troposphere due to the increased contribution of the geopotential energy term overwhelming the moisture and internal energy terms in the moist static energy equation for the high altitude air. Net transport of energy, occurring in the upper branch of the Hadley cell from the SH to the NH, leads to increased moisture advection to the SH in the lower branch of the Hadley Cell. This redistribution of energy causes the ascending branch of the Hadley cell to migrate to the warmer SH where moisture convergence is increased and convective quasi-equilibrium is achieved under the relatively narrow poleward shifted ascending branch of the stronger SH winter Hadley Cell. This mechanism leads to the southward-displaced tropical rain belts (Broccoli et al., 2006).

This result is consistent with Lindzen and Hou (1988), who used a relatively simple model to show, based primarily on angular momentum considerations, that even a small movement of maximum heating poleward into one hemisphere causes great asymmetry in the Hadley Cell, with the winter cell intensifying. Further simplified model studies continued to elucidate the mechanism of extratropical forcing of the ITCZ. Kang et al. (2008) heated the SH poleward of 40°S while cooling the NH poleward of 40°N by an equal amount. The overall energy in the system was unchanged. In that study, the atmosphere was coupled to a simple ocean, that is actually just a wet surface with no heat capacity and no currents on which SST is calculated based on surface energy fluxes only. Through this design, interhemispheric heat exchange could only be achieved through the atmosphere. In this model, the energy flux equator and tropical rain bands moved to the SH.

The ocean also plays a vital role in pushing the ITCZ into the warmer hemisphere. This is well described by Xie and Philander (1994). They used a mixed layer ocean model, coupled with a simple atmosphere, which was capable of transporting momentum and heat to the ocean. This design allows for SST changes to occur as a result of surface wind-induced mixing and latent heat flux. Asymmetric heating produced a single ITCZ that forms in one hemisphere only. The atmosphere forced enhanced equatorial upwelling in the asymmetric Hadley Cell solution. This pushed the ITCZ toward warmer SSTs in the warmer hemisphere.

GCM results confirm this mechanism and connect the changes due to northward displacement of the ITCZ with the onset of active periods in the Asian summer monsoon (Chao and Chen 2001). It is evident that a geoengineering technique that could

preferentially cool the SH could shift the tropical rain bands northward. However, in a GCM there are clouds. How would clouds respond in the hemisphere cooled by geoengineering? Would clouds change in the area being directly cooled? Would a cooling of the subtropics either directly, or indirectly via eddy flux from the artificially cool high latitudes, cause an increase in subtropical subsidence? Would this increase in the sinking of air above the intensified subtropical highs cause water vapor to be trapped in the lower troposphere, forming low clouds and suppressing water vapor mixing into the free troposphere, where the water vapor may instead be used up in formation of high clouds, which tend to reduce outgoing longwave radiation?

Informed by these established diagnostic mechanisms associated with the impacts of asymmetric heating of the hemispheres, I seek to concurrently cool the entire SH and the NH tropics, modestly cool the NH extratropics and, most importantly, induce an anomalous tropical overturning circulation and redistribute rainfall from ocean to land and from south to north across the tropics. The success of G4Foam in achieving these objectives will determine the design of the final, and shortest, chapter of this thesis, which will consist of a report of the results of a GCM simulation combining G4Foam with stratospheric SRM.

**1.8 G4Foam combined with stratospheric SRM**

Since the latitudinal distribution of forcing in G4Foam is far different from that in stratospheric SRM, I anticipate that G4Foam alone may be ineffective in cooling the NH extratropics. Will it be possible to combine G4Foam with stratospheric SRM in such a way that will cool the entire planet without reducing tropical precipitation? Since G4SSA branches from RCP6.0, which is also the reference run for G4Foam, and since

G4SSA is the control experiment for G4Foam, I conducted and analyzed simulations that combine G4Foam and G4SSA into the G4SSAFoam simulations. Microbubble deployment in the form of G4Foam was not a first choice method. Marine Cloud Brightening (MCB) is far more heavily studied and likely more feasible at this time, a simulation of microbubble foam was chosen over MCB because MCB is only feasible in relatively small regions, and forcing those regions does not preferentially increase rainfall over land. The next section provides what I believe to be a needed discussion of the potential ecosystem impacts of MCB, which have barely been studied as well as a realistic estimate of the amount of radiative forcing and global cooling that is achievable via MCB.

# CHAPTER 2: MARINE CLOUD BRIGHTENING (MCB): LIMITS ON ITS POTENTIAL EFFICACY AND MCB ECOSYSTEM IMPACTS

I began investigating the question of whether a regional geoengineering technique or a combination of geoengineering techniques could effectively cool the planet without reducing precipitation in heavily populated and highly cultivated regions by reviewing the existing research on MCB and determining what climate objectives could be achieved with MCB. It was evident that MCB could not achieve the objectives of cooling Earth without reducing tropical precipitation, and G4Foam was designed.

It also became evident that it would be useful to provide an estimate how much radiative forcing and what distribution of radiative forcing and therefore cooling could actually be achieved via MCB and whether applying such a large local forcing to biologically productive areas, MCB susceptible regions are for the most part ecologically rich, could be dangerous to important ecosystems. This ecosystem risk urgently requires further consideration, as the potential benefits of MCB must be weighed against the risks, and I include a discussion of the potential ecological consequences and how best to research these consequences because the potential negative impacts on the ocean and its biota have not been the focus of as much research as is appropriate, given the potential risks and the importance of preserving ocean ecosystems, both in a mankind as a fiduciary sense and because society relies on the ocean for food and commerce. Finally, MCB may only be effective to achieve substantial radiative forcing in the three marine regions with persistent marine stratocumulus decks, which cover about 3.3% of Earth: the South Pacific region, off the coast of South America, the North Pacific region, covering

the area of the California current system and in the South Atlantic region, off the coast of tropical and subtropical West Africa. This limits potential efficacy.

**2.1 MCB background**

Highly reflective marine low clouds have been extensively observed in the wake of large ships that emit exhaust after these ships pass through stable marine boundary layer environments. The ship tracks are a source of radiative forcing in the current climate system on the order of -0.1W $m^{-2}$ (IPCC, 2013), but that radiative forcing estimate is rather uncertain. The ship track clouds are highly reflective, owing not to changes in liquid water availability, but to a high concentration of cloud droplet nuclei concentration (CDNC). Liquid water clouds form around the particulate matter (e.g. sulfate and secondary organic aerosols, which form volatile organic carbons) emitted from the ships as exhaust. The high reflectivity and persistence of the ship tracks are consequences of the first and second aerosol effects (Twomey, 1974; Albrecht, 1989). A necessary assumption for the first aerosol indirect effect is that cloud albedo increases with the same liquid water being shared among more condensation nuclei in the presence of increased aerosol concentration. The second indirect effect increases cloud lifetime as the result of precipitation suppression, owing to the smaller droplet size. Since these ship tracks create negative radiative forcing, it is natural to ask if the ship-track-induced persistent cloud formation process can be emulated by humans in some manner. Is there a way to enhance these aerosol indirect effects to increase the amount of sunlight reflected by marine stratocumulus decks and cool the planet (Latham, 1990)? Many MCB simulations that include actual aerosol injections into the marine boundary layer also include the direct effect of these aerosols scattering solar radiation, contributing to

the negative radiative forcing achieved. However effective this is not marine cloud brightening per se. MCB is only effective in specific persistent stratocumulus regions that cover only 3.3% of the planet. More recent studies that incorporate parameterizations of injections and cloud aerosol interactions derived from very high resolution simulations that consider small scale processes like coagulation and local evaporation indicate that earlier studies that prescribe cloud droplet number concentration (CDNC) are prescribing CDNC values may be impossible to actually achieve.

**2.2 Where, when and how would the clouds be brightened?**

The planetary boundary layer is the area above the Earth's surface where the properties of the layer (e.g. temperature, wind, convection) are largely governed by that layer's interaction with Earth's surface. Stratocumulus clouds cover large areas of the world's oceans and they reflect a lot of solar radiation without absorbing much longwave radiation. A global increase of 0.06 in cloud albedo would offset the warming from a doubling of $CO_2$ (Latham et al., 2012). The albedo of these stratocumulus clouds depends on a nonlinear combination of many factors: liquid water path, CDNC, how long the clouds last, how efficiently the clouds produce precipitation and other microphysical properties that govern the dynamics of cloud droplet activation and cloud formation. Furthermore, the reflectivity of these clouds is a function of the synoptic and mesoscale properties of the planetary boundary layer in which the clouds develop. If MCB is applied, the impacts of performing MCB on the structure of the boundary layer must be taken into account.

The marine planetary boundary layer (PBL) best suited for MCB involves a strong inversion at an altitude above the lifting condensation level, which is the level at

which clouds develop when air rises in the turbulent capped marine planetary boundary layer. This situation occurs where barometric pressure is relatively high and there is relatively strong mixing at the surface. Air rises to the base of the inversion. Clouds develop. The vertical motion of clouds is capped by the inversion, where the previously rising air loses its positive buoyancy. If a strong inversion is in place, these stratocumulus clouds will not dissipate as much during the day, as surface mixing will not break the inversion, leading to entrainment and evaporation of the stratocumulus layer at the base of the inversion, preserving a high albedo. The presence of a shallow boundary layer and a relative balance between entrainment and subsidence must be maintained. An unpolluted boundary layer is also necessary for maximum impact as low background CDNC facilitates a larger forcing. A boundary layer that generally meets these criteria will be referred to subsequently as a region that is susceptible to MCB (Wood and Bretherton, 2004; Wood and Bretherton, 2006; DeSzoeke et al., 2016).

Finally, the efficacy of injections depends on when in the diurnal cycle the injection occurs. Jenkins et al. (2013) find that the optimal time to perform the injections is 03:00 local time. This gives the clouds a chance to persist as a non-precipitating cloud before solar heating takes hold. Simulations of injections at 13:00 local time are ineffective in raising cloud albedo. This would mean that the fleets of MCB ships could only inject at certain times of day and coordination of the fleets would have to account for this logistical issue.

Turning now to examination of the specific MCB susceptible regions, MCB seeks to further increase the lifetime and reflectivity of these clouds in an attempt to deflect solar insolation and reduce global mean surface temperature. There are three distinct

regions in which the marine boundary layer typically meets these conditions. One is off the west coast of the United States, another off the west coast of Africa in the SH tropics and subtropics and off the west coast of South America. Each area coincides with the eastern boundary current in each ocean basin. Partanen et al. (2012) estimate the area of earth susceptible to MCB to be about 3.3% and brighten those regions in Partanen et al. 2012 and 2016. The susceptible areas tend to be in regions favorable for upwelling and biological productivity, which are close to large population centers and robust economic regions.

The exact details of how MCB might be implemented vary from experiment to experiment, but the broad idea of large scale MCB deployment was well-described by Salter et al. (2008). Ships will sail back and forth across the susceptible areas, perpendicular to the prevailing wind so that the injected plume of sea salt did not trail the ship. Aligning ships at all times perpendicular to an always-changing wind would require excellent weather forecasting and the ability to communicate these forecasts to these ships and automatically adjust route in response to anticipate wind changes. It is suggested these ships could be powered by wind. While doing this over the Earth's entire ocean surface could require as many as 16,000 ships (Alterskjaer et al., 2013) working at all times, brightening only the susceptible areas could probably be achieved with fewer ships. The ideal wet diameter of the injected seawater particles emitted from these ships is less than 100 nm (Salter et al., 2008).

The combination of a relatively fast moving ship and relatively strong winds perpendicular to the direction the ship will allow for maximum spray coverage of available sky. The dry particles formed after the sea spray is shot up to the top of the

boundary layer and the spray evaporates could serve as a dense layer of condensation nuclei, upon which many water droplets will collect, forming highly reflective stratocumulus clouds. The proposed ships will power themselves and harness the excess energy they generate to pump a large quantity of sea spray into the air, which, if MCB is done over the entire ocean, adds up to an emission of about 3.4% of the annual total global flux of sea salt between the atmosphere and the ocean. A number of studies subsequent to Salter et al. (2008) have evaluated the feasibility of MCB, the global climate impacts of MCB, very fine scale simulation of actual aerosol injection and models that primarily depict the actual process by which these clouds will form. Some studies also evaluate the potential impact of MCB on ocean ecosystems and the same studies suggest additional ecosystem research.

First, I look at studies of MCB global climate models, which prescribe either CDNC or raise cloud albedo. Some of these studies brighten only specific regions and some studies that brighten over all or most ocean areas. In Alterskjaer et al., (2013), actual salt is injected into the marine boundary layer across vast ocean areas and 71% of the radiative forcing is achieved via the direct effect of the salt injected in the boundary layer. While this study and others that involved brightening vast areas were exceptionally useful in determining MCB susceptibility and elucidating mechanisms associated with changes in atmospheric circulation, the studies where only regions with persistent marine stratocumulus layers are treated are likely to be more accurate representations of the amount and spatial distribution of radiative forcing actually possible via a regime of MCB.

Recent studies that include small-scale processes like evaporation of the injected sea spray and particle coagulation and present a general estimate of how much radiative forcing could be achieved with MCB. There are few studies that consider some of the ecological impacts that MCB may have and the studies that exist suggest that MCB researchers should endeavor to include more research relevant to the ecosystems that exist in the MCB susceptible regions and how the temperature and insolation changes may impact marine biota (Russell et al., 2012).

**2.3 MCB impacts on atmospheric circulation**

Rasch et al. (2009) increased CDNC to 1000 $cm^{-3}$ and simulated several sea spray strategies. Although effective in reducing temperature, no simulation could concurrently stabilize global mean temperature, maintain current precipitation, and maintain sea ice extent in a 2xCO2 climate relative to a preindustrial climate. This particular study uses a baseline $CO_2$ of 355 ppm (late $20^{th}$ century level) and a 2xCO2 value of 710 ppm. This departs from the typical convention of 280 ppm preindustrial $CO_2$ and 560 ppm 2xCO2.

Jones et al. (2009) increased CDNC from background of between 50 and 100$cm^{-3}$ to 375 $cm^{-3}$ in three regions of marine stratocumulus clouds. They brightened all three regions and then brightened the South Atlantic, South Pacific and North Pacific. In this experiment, there was an alarming decrease in precipitation that caused substantial drying of the Amazon. This drying was found to be largely a consequence of the brightening of the South Atlantic region. However, this simulated decrease in rainfall over the Amazon was only found in simulations using the Hadley Centre Coupled Model, version 3.

Even if the Amazon drying in Jones et al. (2009) is model dependent, the simulated drying is an example that shows that applying large amounts of local radiative

forcing in a climate model can cause changes in the general circulation of the atmosphere, which can result in persistent anomalous patterns of precipitation. However, it also shows that selective brightening can avoid some of these negative impacts brought about by regional homogeneous radiative forcing.

Hill and Ming (2012) apply a forcing with a particular spatial distribution, which triggers a long term La Niña like mean state in the tropics. The Alterskjaer et al., (2013) forcing induced an intensified hydrological cycle over land with a weakened hydrological cycle over the ocean. An intensified hydrological cycle over land is not necessarily seen in studies that brighten only susceptible regions (Jones et al., 2009; Stuart et al., 2013). The Kravitz et al. (2013) review lists prescribed CDNC for many MCB experiments, as well as the radiative forcing achieved, the background CDNC and the amount of Earth's surface over which CDNC was raised to the prescribed level (Kravitz et al., 2013). The amount of global mean negative radiative forcing that humans can achieve via MCB and therefore global cooling, that humans can achieve via MCB, when modeled by prescribed CDNC, is determined by many factors. These factors include by how much the CDNC is increased, how clean the pre-injection boundary layer is and over how much ocean area CDNC is increased. Several studies described by Kravitz et al. (2013) perform actual sea-spray injections, and the efficacy of the MCB in these simulations is unsurprisingly also governed by how much the CDNC is increased, how clean the pre-injection boundary layer is and over how much ocean area CDNC is increased.

Studies that actually inject sea salt into the boundary layer or resolve clouds in some manner are useful in helping to determine an actual achievable CDNC. If I further assume that MCB is possible over about 3-4% of the planet and additionally take into

account the actual physics of injecting sea salt into the boundary layer in order to alter how clouds form, including coagulation and the temperature and buoyancy effects of the sea spray the evaporates after injection, it is possible to bound the amount negative radiative forcing. If the spatial pattern of the forcing is also understood, the homogeneity of regional climate responses can also be considered. The consequences of the homogeneity of forcings may not only produce unique climate feedbacks, but as a result of the potential heterogeneity of impacts, it may cause different regions to have different preferences for how MCB would be implemented. Future research into MCB governance and economic impacts would be needed to address the potential for different regions to have different MCB policy preferences.

**2.4 Coagulation and evaporation of the injected sea-spray may limit MCB efficacy**

Recognizing an important limitation in MCB climate modeling studies, Stuart et al. (2013) omitted the assumption that sea spray is emitted relatively uniformly into a particular array of ocean grid boxes. Previous sea spray climate models would simply fill grid boxes with sea salt spray at a fixed value. Since the Stuart et al. (2013) model depicts a homogeneous distribution of aerosols in a grid box, neither the behavior of the sea spray at the point of emission, nor away from the point of emission is explicitly considered. In reality, the concentration of sea salt particles would be much higher at the source of emission and rather low away from the source. Using proposed emission rates from other studies on the order of 10 kg $s^{-1}$, between 10% and 90% of particles are lost, mostly due to surface deposition and coagulation (Stuart et al., 2013), and an average of 50%, with rates of loss varying with the from under 10% to over 90% depending on the atmospheric conditions at the time of injection. This modeling is then used to

parameterize sub-grid scale coagulation in both cloud resolving models and global climate models. When this parameterization is fed into a global climate model, the radiative forcing achieved by the MCB regime falls 46% from -1.5 W $m^{-2}$ to -0.8 W $m^{-2}$. The authors suggested that their coagulation parameterization be applied in global climate model simulations to eliminate a common overestimate on how much aerosol actually reaches the cloud base. The mean CDNC at cloud-top in each of the three Stuart et al. (2013) MCB regions varied somewhat from region to region, but in simulations without coagulation, mean CDNC ranged from 600-750 $cm^{-3}$, while when coagulation is accounted for CDNC ranges from 300 to 450 $cm^{-3}$. The achievable radiative forcing is considerably less when coagulation is accounted for.

The Jenkins et al. (2013) model included the process of evaporation. By comparing the sea salt plume behavior of wet and dry aerosols in a large eddy simulation and found that in the wet case, evaporation of the water from the sea salt aerosols caused local cooling, which limits how high the injection plume heights could reach to around 40 m. The weaker plume results in a smaller cloud albedo increase both in the weakly-precipitating (favorable) night time scenario and in the daytime injection into nonprecipitating clouds case. These results suggest that the achievable albedo increase is actually 0.01 lower in the favorable case. The authors suggested that a parameterization of evaporation of the water from injected sea salt droplets, which leads to the formation of cold pools, and additional sinking air, be included in future modeling assessments.

The effect of including evaporation and coagulation into parameterizations, which can then be incorporated into global climate models may tend to produce global climate model simulations where the ultimate amount of radiative forcing achievable via MCB is

lower than what is achieved in idealized prescribed CDNC studies. The tolerance of the risk for negative local impacts of MCB must be weighed against the global benefit of what cooling is actually achievable, according to simulations that include parameterizations as many relevant processes as possible. The former will be larger if the latter is also larger. However, many other factors, including but certainly not limited to, unexpectedly high climate sensitivity or the presence of an imminent tipping point that could somehow be foreseen and then avoided by MCB cooling would change the context in which MCB would be viewed and likely increase the local and regional risk tolerance.

In summary, MCB can be very effective in areas where marine stratocumulus persist, a relatively strong inversion is in place, there is adequate mixing below the inversion, atmospheric pressure is relatively high, the clouds are weakly precipitating and the injections are performed in the morning. The benefit of implementing MCB to cool Earth needs to be balanced against any possible consequences on the marine ecosystems that exist in the areas that are being cooled dramatically so that a future decision about MCB implementation takes into account all elements of the Earth system.

**2.5 Modeling of the impact of MCB on marine ecosystems and considerations for potential field tests of MCB**

Global mean radiative forcing and radiative forcing in each region, South Pacific, South Atlantic, North Pacific, are lower in simulations where the effects of coagulation or evaporation are taken into account. However, radiative forcing in each of the three MCB regions still exceeds 20 W $m^{-2}$ to achieve -1 W $m^{-2}$ of global mean radiative forcing (Stuart et al., 2013). Such a large perturbation in each of these regions, which are all home to extremely rich and diverse ecosystems is something that should be very carefully

studied. However, this is difficult. To properly model MCB, one has to accurately model, or model and then parameterize and integrate the emission of sea spray, the evaporation of the spray, the interaction of the wet and dry sea salt particles and accurately model boundary layer turbulence meaning the correct amount of aerosol reaches the cloud top. These processes must then be parameterized and placed into cloud resolving models and global climate models. Many modern global climate models do include ocean biogeochemistry, but global climate models do not incorporate ecosystems at the same level of detail as an ecological model.

The concern associated with MCB and ecology exists because to get a global mean temperature reduction via MCB there must be very significant light limitation and local cooling in specific areas. This strong regional cooling has been shown in Jones et al. (2009) to disrupt the coupled ocean-atmosphere West African Monsoon. In Hill and Ming (2012), ENSO is changed as a result of a strong cooling in the Eastern Pacific. These atmospheric and oceanic changes may have major ocean ecosystem impacts and these impacts must be assessed.

A reasonable research plan to evaluate impacts of MCB on ecology would start with developing criteria for detection and attribution of changes. How could a robust ecological signal be extracted from natural variability? It would likely be best to study one method of geoengineering at a time, rather than, say, combining SRM and CDR (Hardman-Mountford et al., 2015). The determination of a range of natural variability for a large number of ecological variables would also be imperative for proper attribution. This would be greatly helped by observations, reanalysis and model simulations.

Field experiments would be useful. However, in order to optimize the value of information gleamed from the field experiments, there would need to be an integrated assessment of what could be learned from the experiment. There would also need to be an objective preliminary risk assessment conducted by a disinterested authority (Robock, 2012).. The spatial scales of the experiments should also be limited to the minimal useful amount (Russell et al., 2012). If the spatial scale of a field experiment were large enough to impact multiple political divisions, there would need to be complete integration between both parties.

The amount of information that could be gained about aerosol cloud interactions and the novel parameterizations that could be incorporated into global climate models as the result of the observations gleamed from MCB field studies could reduce the uncertainties associated with climate sensitivity to increased atmospheric $CO_{2,}$ which would actually reduce the uncertainty associated with whether or not some form of geoengineering will ultimately be necessary.

There is no reason to assume that indoor or outdoor field studies would increase the likelihood of large-scale implementation. The argument that testing makes large-scale deployment more likely suffers from the slippery-slope logical fallacy, and such an argument can easily be refuted with the assertion that a field test could just as easily reduce the perceived feasibility and attractiveness of such a regime. However, it is possible that the potential negative impacts or even the potential goals of the experiment could be distorted in both traditional and social media if the greatest possible care was not taken to be completely transparent or the research community failed to engage deeply and substantively with the public and stakeholders living near the area of the field

experiment. To the extent that the use of primarily public funds implies there is public say, in the form of legislative or administrative oversight, in how public funds are being used, the presence of public funding implies some level of prior public assent to the particular area of research.

There are only two comprehensive studies that evaluate the impact of MCB on ocean ecosystems. Partanen et al. (2016) used an Earth System Climate Model to simulate how the ocean would respond to a sea salt spraying for the purpose of MCB in three regions though to be susceptible to MCB: South Pacific, South Atlantic and North Pacific. The model did have a relatively complex dynamical ocean model, but was coupled only to a simple atmosphere model. However, atmospheric $CO_2$ was calculated online throughout the simulation. This calculation not only took into account prescribed emissions, but the flux coupler in the model calculated land and ocean interactions with the atmosphere as well as changes in the land and ocean carbon cycles. The biogeochemistry module divides phytoplankton into nitrogen fixers and nonnitrogen fixers and also model zooplankton. DIC, oxygen, nitrate, phosphate and total alkalinity are also simulated in the model. Primary productivity is sensitive to iron limitation in this model. Geoengineering commenced in 2030 and the simulations ended in 2100.

The global mean annual mean forcing was around -1 W $m^{-2}$. However, in the MCB susceptible regions (North Pacific, South Pacific and South Atlantic) a given location will receive highly variable forcing, ranging from -10 W $m^{-2}$ to -100 W $m^{-2}$. This large variability in forcing in the MCB regions occurs even with an assumption that there is no interannual variability in the amount of radiative forcing achieved by the MCB approach. This is a useful simplification that makes the results much easier to interpret,

but the seasonal cycle in each region will vary greatly over a given year. The annual cycle in variables such as dissolved inorganic carbon (DIC) is quite large and there is also a good deal of natural variability. This variability is the result of many different things and interpreting the ecological consequences of MCB would require the ability to extract, if it exists, a MCB response in variables such as DIC. Not only is there a seasonal cycle in ecological variables, there is a large seasonal cycle in the atmospheric conditions in much of the MCB susceptible areas. The local forcing will likely be larger in local summer when the boundary layer conditions are most ideal and the local forcing may be negligible in local winter, particularly in the North Pacific regions due to the influence of the midlatitude storm track.

Specific to Partanen et al. (2016), on a global mean basis, up to about -0.7 K of cooling is achieved when compared to the global warming scenario. However, much of this cooling is achieved over the ocean and confined to the MCB areas. Under global warming alone, global mean ocean net primary productivity (NPP) was 3.2% lower in 2090–2099 than in 1990-1999. The 3.2% NPP reduction in this model was close to the large ensemble global warming NPP change projection of over 30 Earth system models during this time of 3.6%. In this experiment, geoengineering studies are compared against control climate simulations in which global warming occurs. This allowed a comparison between a world experiencing the negative consequences of global warming and a world attempted to manage these consequences with geoengineering, which is the relevant comparison, since those are the options for the future, absent unexpected technological breakthroughs. Results were given for both GEO, geoengineering that includes temperature effects as well as sunshade effects, and GEO-SHADE, which

considers only the sunshade effects. On a global mean basis, NPP was 0.9% lower in the geoengineering GEO simulations than in the global warming only simulations. For the GEO-SHADE simulation, NPP was only altered significantly over the South Pacific region.

These global mean results come with some important nuances. First, the negative NPP effects may be transient, as the strongest effects occurred around 2030 (the beginning of the simulation) and the differences almost vanished by the end of the simulation. Second, the global mean differences being discussed are actually the net combination of a complex pattern of local changes in or near the MCB areas. Basically, there were large decreases in one place and large increases in nearby places. For example, local changes in the area of the Peru Current had the largest range. One area had a 27% decrease while another nearby area has an 84% increase in NPP and the proximity of large increase to large decrease areas suggests nutrients may have been being transported from regions with diminished NPP to fuel NPP elsewhere (Partanen et al., 2016). It is also possible that circulation changes had changed the locations of maximum upwelling. Therefore, in this simulation, there was a clear redistribution of NPP around the MCB areas, with some net reduction, rather than a clear change in total NPP. Third, of the MCB treated areas, only the South Pacific region coincided with a region of very high NPP. The North Pacific region has a very rich ecosystem, but the richness of the California current system is not well captured by considering NPP alone, meaning NPP paints a very incomplete picture of ecological changes in that region. Fourth, some of the GEO simulations were stopped after ten years and these were then called the GEO-STOP simulations. After MCB was stopped, NPP conditions returned to

control simulation global warming conditions within a decade. This demonstrates the reversibility of the effects of MCB on NPP if MCB is stopped after a ten-year period.

In summary, MCB can cause large regional redistributions of NPP in a simulation with this particular configuration. This could be a significant local impact on a marine ecosystem and the cascade of events that could begin from the reduced NPP include changes in fisheries and broad changes that are not captured by a model with such a simple depiction of the marine ecosystem. Both temperature and light availability effects were included, but light availability, as quantified in GEO-SHADE was only a limiting factor in the South Pacific region. These are significant potential ecosystem effects and the consequences of these changes in NPP have not been examined in terms of how they would propagate through the food web and how human interaction with a MCB treated marine ecosystem would have to change.

Hardman-Mountford et al. (2015) used a very different model configuration to examine the biogeochemical changes and changes in ocean biota that could be brought about by MCB. They exclusively studied the relationship between light availability and productivity in a one-dimensional ecosystem model. They selected a water column with the stratification properties of what one would find in a subtropical ocean gyre. The model incorporated numerous forms of plankton and although the ecosystem is richly depicted, it is a one dimensional column model, so there is no horizontal motion of nutrients. Under this design, they found that light limitation of up to 90%, which could be experienced locally with MCB, only redistributed productivity within the vertical water column. However, It did not decrease net productivity. The authors concluded by cautioning that more complete consideration of marine ecosystems and feedbacks needs

to be taken into account before robust conclusions about light limitation's effect on an ecosystem can be drawn. At the very least, Hardman-Mountford et al. (2015) could be repeated in a water column that was more typical of the water column in the MCB region. A more comprehensive ecological model may also be useful. The results showing a spatial redistribution of NPP in Partanen et al. (2016) should be followed up with a model study that includes biota other than primary producers.

**2.6 MCB Conclusions**

Additional research on the local ecological impacts of MCB is needed. The benefit of MCB, which, at best, given current estimates, could achieve a highly spatial heterogeneous radiative forcing of about 1 W $m^{-2}$ and a global mean cooling of about 0.5 K, needs to be weighed against the climate risks of both the MCB induced circulation anomalies that have been modeled multiple times, beginning with Jones et al. (2009) and the heretofore understudied local ecological impacts. Ecological impacts are very important to consider in MCB since the MCB susceptible regions all coincide with extremely rich cold current ecosystems that sustain societies' and have their own inherent value.

# CHAPTER 3: ENSO AMPLITUDE AND FREQUENCY DO NOT DIFFER SIGNIFICANTLY FROM THAT UNDER GLOBAL WARMING IN GeoMIP G1-G4 SIMULATIONS

## 3.1 Methods.

The results described in this chapter are from Gabriel and Robock (2015). This part of the thesis consisted of me comparing a large sample of GeoMIP G1-G4 simulations from 9 different modeling groups and matching them with their AGW or preindustrial control simulations do determine whether is there a statistically significant change in ENSO amplitude or frequency in any of the GeoMIP experiments relative to its respective control simulations? I began with the simple question of whether or not, in a single GeoMIP participating model that simulates ENSO well, a difference in ENSO amplitude or frequency is evident in a comparison between one experiment and its control. Unsurprisingly, given the large inherent variability in ENSO, such a change is not detectable in one model. Given that, I adopt an approach in which I use output from nine GeoMIP-participating GCMs, each running between one and three ensemble members of each experiment G1-G4. The simulations are then analyzed. These GeoMIP experiments are described by Kravitz et al. (2011). See Fig. 3.1 for schematics of GeoMIP experiments G1-G4 and Tables 3.1 and 3.2 for details about the GCMs used in these experiments. The G1 experiment – instantaneous quadrupling of $CO_2$ coupled with a concurrent fully offsetting reduction of the solar constant – was designed to elicit robust responses, which then facilitate elucidation of physical mechanisms for further analysis. I compared G1 output to a control run in which the atmospheric carbon dioxide concentration is instantaneously quadrupled. The G2 experiment combines a 1% $yr^{-1}$ $CO_2$ increase with a fully offsetting reduction in the solar constant. The G3 experiment

combines RCP4.5 with a nearly fully offsetting sulfur dioxide injection. The G4 experiment – stratospheric loading of 25% the $SO_2$ mass of the 1991 Mt. Pinatubo volcanic eruption (5 Tg) each year concurrent with RCP4.5, with top-of-atmosphere radiation balance not fixed at zero – attempts to replicate a physically and politically plausible large scale geoengineering deployment scenario.

Each experiment (G1–G4) is compared to its respective control scenario: 4xCO2 for G1, 1% annual $CO_2$ increase for G2 and RCP4.5 for G3 and G4. I compare the means of each sample by applying a two-tailed Welch's independent sample *t*-test assuming unequal variance. To apply this test, the populations making up the two samples being compared must both follow a normal distribution and the two populations must be measured on an equal-interval scale. In this case, I must establish normality to move forward to performing a valid *t*-test. If the samples were a bit larger ($n > 30$, where $n$ is the size of the sample), the central limit theorem would likely make analysis of the normality of the respective samples moot. However, due to somewhat small sample size, additional statistical analysis was performed and that analysis suggested that each sample was normally distributed. (D'Agostino, 1990, DeCarlo, 1997, Gabriel and Robock, 2015).

I chose to use 90% confidence intervals to enhance detectability. However, by narrowing the confidence intervals, I am forced to supplement the finding of a significant result by either subsequently applying a bootstrapping method for an original finding pertinent to geoengineering and AGW, or to consult the appropriate studies to establish the veracity of a significant finding that matches the findings in other work, such as in a comparison between control or historical runs.

Even with carefully applied methods for analysis, detection of changes in future ENSO variability under different scenarios is challenging. As I am limited in both the length and number of geoengineering simulations, I aggregate geoengineering experiments, when appropriate, to increase sample size. I combine experiments only when the aggregated experiments form a group that is neatly distinct from its matching comparison group. Aggregated experiments must simulate a future climate that both starts from a similar mean climate and follows a similar trend, or lack of a trend, throughout the experimental period. After applying this standard, I am able to aggregate G1 and G2, since the experiments both start from a preindustrial climate and the anthropogenic warming imposed in the runs are fully offset by imposed solar dimming. I am also able to aggregate G3 and G4, since both start from a year 2020 climate and follow trajectories in which RCP4.5 is either fully (G3) or largely (G4) offset by constant sulfur dioxide injections during the experimental period. Application of this standard for aggregation of experiments precludes the aggregation of all GeoMIP experiments G1-G4 into a single ensemble, as the experiments start from different climates and follow independent trajectories thereafter. This standard is also applied when I consider aggregating control experiments. Since each control experiment – instantaneous quadrupling of $CO_2$, 1% $yr^{-1}$ $CO_2$ increase runs and RCP4.5 – depicts climates that are distinct from each other, no aggregation of control experiments is performed.

To identify and analyze ENSO variability and amplitude, absent the contamination of the signal induced in the immediate aftermath of application of initial solar dimming or stratospheric aerosol forcing, the first 10 years of each geoengineering model run were removed. The relevant comparison periods become either "Years 11-50"

in G1 and 2030-2069 in G2-G4. Initial forcing is applied in "Year 1" in G1 and in 2020 in G2-G4. This 40-year interval is then compared to RCP4.5 2030-2069 and historical 1966-2005 for each respective model and to observations. I used the Kaplan (1998) SST data set because it is well documented and used in many of the referenced papers. Differences between the Kaplan data and other available data sets are small during the period of data used.

I used several SST-based indices to quantify the amplitude and phase of the ENSO cycle. For each ensemble member of each model, a time series of the Niño3.4 index was generated. I chose Niño3.4 over Niño3 or Niño4 because the Niño3.4 region remains the center of action for ENSO variability both in observations and models. The Niño3.4 region is the area 120°W-170°W and 5°N-5°S. The Niño3 region misses a good deal of the so-called Modoki ENSO-type variability, while Niño4 misses a good deal of canonical ENSO-type variability. I define an ENSO event as a departure of the 5-month running mean Niño3.4 index (computed over 5°S-5°N, 120°W-170°W) of greater than 0.5 K from the 2030-2069 climatology, with the linear trend removed from the 2030-2069 climatology before anomalies are calculated. Cold and warm events have the same definition, just with opposite sign. Anomalies in the historical data and the observational record are calculated relative to a 1966-2005 climatology, which is also detrended before anomalies are calculated. G1 output is analyzed absent detrending, as there is no trend in the data. I used skin temperature ($T_S$) anomalies rather than SST anomalies to build the Niño3.4 time series for the BNU, IPSL and MPI models, because they were available on a regular grid. For the purpose of computing an anomaly-based index, the variable $T_S$ is an excellent SST proxy variable, which is interchangeable with SST.

Gabriel and Robock (2015) contains a lengthy discussion of my attempts to use non-SST based indices as an ENSO index and why these efforts were not productive. For example, considering changes in zonal wind and sea level pressure is prevented by both the large inherent variability of SLP and zonal winds in the tropical Pacific, and the difficulty in deconvolving the possible Walker Circulation weakening and ENSO change signals (Vecchi et al., 2006 and 2007). In the observational record, 30-50 year changes in the Walker Circulation can occur concurrently with extended periods of more frequent ENSO warm events (Power and Smith, 2007). Hence, the observed weakening of the Walker Circulation during a period of somewhat more frequent ENSO warm events is not necessarily the result of a anthropogenically forced change in the Walker Circulation, but is instead convoluted by increased ENSO warm events and other inherent variability in the Tropical Pacific. The period of time required to robustly detect and attribute changes in the tropical Pacific Walker Circulation is found to be up to 130 years (Vecchi, 2006, 2007) and no less than 60 years (Tokinaga et al., 2012). Because I cannot deconvolve the two signals in such a 40-year interval, I reject using zonal wind or SLP spatial pattern or trend as a proxy for ENSO. Additionally, as mentioned earlier, Cai et al. (2015) showed that a robust weakening of the Walker Circulation under RCP8.5 counterintuitively co-occurs with a period of anomalously strong La Niña events as a result of increased heating over the Maritime Continent. Therefore, while changes in atmospheric Walker Circulation over the tropical Pacific can be impacted by ENSO on decadal time scales, the changes may also be entirely unrelated to ENSO variability.

Next, I turn to defining what constitutes an ENSO event in my experiments. Presently the National Oceanic and Atmospheric Administration Climate Prediction

Center defines the climatological base period from which to calculate the departure from the current value and define an ENSO event as 1981-2010. I depart from this definition due to the robust warming trend in tropical SST in the Pacific both during the 1966-2005 comparison, and in 2030-2069 model runs, which show continued warming of the tropical Pacific. The detrended 40-year average produces a more realistic assessment of the base climate from which a particular ENSO event would evolve. This avoids the trap of identifying spurious ENSO events toward the end of the time series, which are really artifacts of the warming trend. Ideally, a climatological period in a rapidly changing climate would span less than 40 years. However, longer term natural trends in Pacific SST variability, including extended ENSO warm or cold periods, force use of a lengthy climatological base period to avoid comparing variability against a climatology that also includes that same variability.

The ENSO parameters evaluated are amplitude and frequency. El Niño amplitude is defined here as the peak anomaly value (in K) found during each El Niño event in the time series of Niño3.4. La Niña amplitude is defined here as the mean negative peak anomaly value (in K) found during each ENSO event in the time series. Frequency is counted as the number of warm and cold events in each 40-year time slice. These parameters are chosen because ENSO frequency and amplitude have particular importance as global climate drivers.

The ENSO frequency and amplitude calculated in each ensemble member of each experiment (G1-G4) are compared 1) to other ensemble members from the same model for the same experiment, if available, 2) to their respective control runs, 3) to runs from other models with the same experimental design and 4) with different experimental

designs, 5) to historical model runs, and 6) to observations. From this I seek to identify significant differences between model output from geoengineering scenarios, global warming, and historical runs compared to each other and to observations, as well as differences between models running the same G1-G4 experiment. Not only do I seek to analyze differences in ENSO amplitude and frequency between different scenarios, but I also seek to identify ENSO tendencies specific to particular models. The discussion below includes the successes and limitations of CMIP5 GCMs in depicting ENSO.

Lastly, in addition to seeking to identify changes in ENSO variability, I attempt to describe the evolution of Niño3.4 SSTs during a period of geoengineering as compared to AGW or the historical record. To do this, I calculate the linear trend in the Niño3.4 index during the period 2030-2069 for G3, G4 and RCP4.5, 1966-2005 for historical simulations and Years 11-50 for G1, G2, +1% $CO_2$ and 4xCO2. Could imposition of a geoengineering regime partially or fully offset warming in Niño3.4 over a 40-year period?

**3.2 Results**

Changes in ENSO event frequency and amplitude in a geoengineered world are either not present, or not large enough to be detectable, relative to the historical record, global warming simulations, and the observational record, using the approach employed in this experiment and described in the methods section above.

Data from three GeoMIP participating GCMs were excluded from final comparison. While many models depict realistic ENSO variability in terms of both the location of strongest ENSO variability (Fig. 3.2) and the amplitude and frequency of ENSO (Fig. 3.3), not all models are yet able to simulate a realistic ENSO cycle. Prior to

further analysis, I applied two simple amplitude-based filters to exclude unreasonable ENSO time series data. The BNU-ESM output was excluded, because runs from more than one of several experiments found unrealistic 40-year ENSO time series where the substantial portion of warm and cold events maximum amplitude exceeded 3 K. Some BNU-ESM events exceeded 4 K, nearly a factor of 2 greater than the largest amplitude warm or cold events in the observational record. The model also produced nearly annual swings from implausibly strong warm events to cold events and back, implying an almost constant non-neutral state (Fig. 3.4).

The MIROC-ESM and MIROC-ESM-CHEM output were also both excluded. Runs from more than one experiment in those models resulted in unrealistic 40-year ENSO time series without a single positive anomaly of more than 1 K of the Niño3.4 Index. Negative anomalies were similarly suppressed in simulations from both models (Fig. 3.5). After excluding those models, I considered output from six GeoMIP participating GCMs: CanESM, CSIRO, GISS, HadGEM, IPSL and MPI (Tables 3.1 and 3.2). As an initial test of model performance, I first evaluated agreement between the models used and the observational record. I found good agreement between 150 years of model data and the full observational record dating back 150 years. The strong agreement between simulations and observations includes the period after 1960, when the spatial and temporal density of Niño3.4 in situ observations increased dramatically. Specifically, the 1966-2005 observational record shows nine warm events, eight cold events, a maximum warm amplitude of 2.3 K, and maximum cold amplitude of 1.9 K. A multi-model ensemble of historical simulations of the same period shows 9.0 (±1.9)

warm events, 8.5 (±1.7) cold events, maximum warm amplitude of 1.9 (±0.5) K and maximum cold amplitude of 1.7 (±0.6) K.

I also compared several selected 40-year periods from the historical simulations with historical simulations and observations from different 40-year periods in order to assess ENSO variability within the historical record (Fig. 3.6). Are there 40-year periods in the historical record where ENSO variability is different than other 40-year periods, and, if so, is my detection method sensitive enough to detect the difference? The statistically significant differences (90% confidence) found are for comparisons made between warm event frequency between 1966 and 2005 and warm event frequency between 1866 and 1905 ($p = 0.07$) or 1916 and 1955 ($p = 0.06$). There is good agreement between models and observations throughout the record and this includes extremely close agreement between 1966-2005 historical simulations and the 1966-2005 observations in terms of ENSO warm event frequencies being elevated relative to the rest of the period. This also lends support to the validity of the 1966-2005 enhanced warm event finding. While the overall fit between historical models and observations is excellent, there is a good deal of model spread (Figs. 3.7 and 3.8).

I believe this finding is robust in part because it is buttressed by the results of numerous studies using various combinations of observations and proxy records and historical modeling to reconstruct past ENSO behavior. A number of studies show similar findings about enhanced ENSO variability in the late 20$^{th}$ century. For example, Gergis and Fowler (2006) show that late 20$^{th}$ century El Niño frequency and intensity is significantly greater than it had been at any point since 1525. They further demonstrate that the post-1940 period accounts for between 30% and 40% of extreme and protracted

El Niño events (Gergis and Fowler, 2006). Li et al. (2013) used 700 years of tree ring records from multiple locations to show that ENSO activity has been unusually high in the late 20th century. Additionally, a synthesis of multiple proxies over the past 400 years showed that the period 1979-2009 was more active than any 30-year period from 1600-1900 (McGregor et al. 2013). Based on 7,000 coral records, late 20th century ENSO is unusually strong, 42% greater than the 7,000 year average (Cobb et al., 2013). However, I cannot conclude that the unusually strong ENSO variability in the late 20th century is the result of anthropogenic forcing, as there are other periods in the extended record where ENSO is either significantly enhanced or suppressed.

This finding from the historical record may not be germane to geoengineering, but it does test the limits of my method's detectability threshold and also demonstrates that ENSO behavior has exhibited significantly different properties during distinct portions of the historical record.

I now turn back to the thrust of this chapter of my thesis, attempting to detect whether or not ENSO variability under a regime of geoengineering is distinct from ENSO variability under AGW. To do this, I perform a series of comparisons. First, each experiment G1-G4 is matched with and compared to its respective control simulation, to the 1966-2005 historical period (during which observations are spatially and temporally dense) and to the full 150 years of available historical simulations. I find that there are no statistically significant differences in ENSO frequency or amplitude between G1-G4 and their respective controls, or from the observations or historical simulations. Because only six CMIP5 GeoMIP models produce a reasonable ENSO, I have a limited number of ensemble members available with which to perform comparisons. This limits my ability

to detect differences and I suggest future GeoMIP experiments include an extended G1, to run for as long as 200 years. If all of the participating GeoMIP modeling groups produced these runs, it may be possible to extract a geoengineering behavior in ENSO behavior from the large inherent ENSO variability.

The criteria used for aggregating experiments are provided in the methods section above. The purpose of aggregation is to construct the largest possible ensemble of simulations, which can then be compared. The inherent variability and usually subtle character of changes in ENSO compels the use of as many data as possible to filter out all of the internal variability and detect the ENSO change attributable to a particular forcing. Based on the aggregation criteria, I am only able to aggregate G1 with G2 and G3 with G4. In the G1/2 comparisons with 4xCO2, I see significantly more frequent (90% confidence) La Niña events - 8.32 ± 2.5 per 40 years for G1/2 and 6.71 ± 1.7 for 4xCO2. I also see more frequent (90% confidence) La Niña events in the G1/2 ensemble than in the 1% annual $CO_2$ increase ensembles - 8.32 ± 2.5 per 40 years for G1/2 and 7.37 ±1.7 for 1% annual $CO_2$ increase.

Without additional analysis, only one estimate of the difference of medians of the amplitude or frequency of ENSO events in each comparison can be taken from each aggregation of simulations. The number of simulations is limited and the statistically significant results of the comparisons may have been obtained by chance. When two samples with large standard deviations are compared, it will take a larger sample to draw robust conclusions about the difference between the medians of the two samples than it would if the samples had small standard deviations. When the simulations are aggregated

by experiment, each aggregation of simulations has a large standard deviation (Figure 3.6).

G1/2 was compared to 4XCO2 and the comparison of the aggregation of the mean number of La Niña events was higher in G1/2 than 4XCO2 statistically significant with 90% confidence. However, the frequency of La Niña events in the G1/2 and 4XCO2 aggregations both had large standard deviations (Figure 3.6), so I decided to apply a simple resampling technique to test the statistical power of the two significant results. First, I chose a sample, with replacement, from the G1/2 ensembles. Next, I chose a sample, with replacement, from 4xCO2. After calculating the median of each of the two samples, I repeated this process 500 times. Next, I calculated the differences between the medians in each of the 500 samples. This gave me an array of 500 integers, which were the differences between medians. The 25 highest and lowest differences between medians were stored, and the remaining 450 integers formed a 90% confidence interval. Since the difference between the medians in the G1/2 ensemble and the 4xCO2 ensemble fall within the 90% confidence interval of differences between medians that I obtained via resampling, I conclude that the result showing increased ENSO frequency in G1/2 relative to control was likely obtained by chance.

The same process was carried out for the G1/2 comparison with 4XCO2. Although the original comparison showed a significant result (90% confidence), after resampling, the difference between the G1/2 and 1% annual CO2 medians was shown to be within the 90% confidence interval. Therefore, despite the initial presentation of results, based on a simple resampling technique, which allows for replacement, I find that there are no significant differences between G1/2 and the applicable controls.

Next, I turn to the final aggregated comparison, G3/4 and RCP4.5. Among all experiments and control simulations RCP4.5 simulations showed both the strongest and most frequent ENSO events. However, error bounds are large due to relatively small sample size ($n$ = 21) for RCP4.5 and G3/4, and no difference in ENSO frequency or amplitude was detected in this comparison.

These results show the absence of a significant difference between GeoMIP experimental runs and AGW runs. However, the comparisons were limited by a number of factors. First, I had to exclude simulations from several GeoMIP participating modeling groups due to an implausible ENSO in the models. Second, current generation GeoMIP runs may not be long enough to detect changes in ENSO. Third, the signal-to-noise ratio in RCP4.5 is low. A geoengineering experiment that seeks to offset a stronger forcing may improve my chances of detecting potential changes in future ENSO. These detectability issues will be covered in greater detail in the discussion section.

Comparisons between models and with observations show intermodel differences and differences between models and observations (Fig. 3.9). One of the features most readily apparent across all models was the confinement of the most robust coupling between the ocean and the atmosphere too close to the Equator and not extending as far eastward as in observations. The ENSO center of action in the models was over a small area in the central Pacific, whereas the center of action extended further into the equatorial eastern extent of the basin in the observational record.

Next I make model vs. model comparisons - comparing all ensemble members of runs from each model against each other. Figs. 3.8 and 3.9 show ENSO event amplitude and frequency simulated by each model. Of the models not excluded, the CanESM

results diverged far more than the other models from the overall mean on all four parameters evaluated. CanESM depicts ENSO warm and cold events that are both more frequent and stronger than that documented in the Kaplan SST observational record. The CSIRO model depicts the lowest number of both cold and warm events, as well as event amplitudes that are lower than the other models included. GISS, HadGEM, IPSL and MPI models are not in close agreement on all four parameters, but they agree more than the CSIRO and CanESM. The best agreement between models existed between the GISS, HadGEM, MPI and IPSL, which agreed on all but cold event amplitude. Had I excluded the CanESM (most frequent and strongest ENSO events) and CSIRO models (least frequent ENSO events), agreement between the remaining four models would have been reasonable. However, both the CanESM and CSIRO produce a physically plausible ENSO. During especially active periods, ENSO has behaved in line with the CanESM results. During relatively quiescent periods in the observational record, the CSIRO results are not out of line with observations.

In addition to my analysis of ENSO variability, I also examined some longer-term trends in the Tropical Pacific under a regime of SRM, relative to global warming. While ENSO is a dominant source of interannual variability both in the tropical Pacific and globally, the evolution of conditions in the Niño3.4 region on time scales much longer than that of ENSO are also of importance to regional and global climate. Individual ENSO events are modulated by the complex interaction of positive and negative feedbacks. The long-term trend in SSTs in this region is heavily influenced by other sources of natural variability on decadal time scales. However, over a 40-year period of global warming or geoengineering, the SST trend in this region will be largely dependent

on anthropogenic forcing or the combination of geoengineering and anthropogenic forcing. To examine the change in Niño3.4 over the full duration of each experiment, I calculate the linear trend of warming or cooling in the Niño3.4 index over the applicable 40-year period. The linear trends are calculated over 2030-2069 for G3, G4 and RCP4.5, and over years 11-50 for G1, G2, 4xCO2 and +1% $CO_2$ $yr^{-1}$ (Table 3.3, Fig. 3.10).

An objective of geoengineering could be to cool Earth's surface sufficiently so as to offset some of the negative impacts of global warming. The amount of temperature change expected over an extended period of geoengineering as opposed to under AGW alone is an obvious indicator of the potential efficacy of geoengineering in a particular region. SSTs over Niño3.4 region change considerably under global warming and under some geoengineering scenarios. Under G1 and G2, the linear trend of SSTs in Niño3.4 is negative, and very close to zero. In both experiments, a $CO_2$ increase is imposed on a steady-state preindustrial climate concurrently with a fully offsetting solar constant reduction. G1 and G2 generally depict little change in global mean temperature. In terms of variability between models simulations of Niño3.4 linear trend, the coarsest error bars can be found with the G1 and G2 experiment. Climate was fully stabilized in most runs, but some runs exhibited evidence of either a warming or cooling trend.

G3 and G4 initialize from a warming climate and seek to offset RCP4.5 with $SO_2$ injections. In both experiments, the positive temperature trend in the Niño3.4 region despite the $SO_2$ injections. In G3, the warming trend is 0.07 K $decade^{-1}$. However, the G3 experiment is designed so that the RCP4.5 warming is fully offset to generate zero net forcing. Offsetting radiative forcing by injecting a layer of stratospheric aerosols does

not prevent continued warming in the ocean. Put simply, the ocean has a huge thermal mass. Rising or falling air temperatures take time before their impact is felt in the ocean.

For G4, the initial $SO_2$ forcing is fully offset at first, but during the experiment, the amount of $SO_2$ being injected into the atmosphere does not change, even as the RCP4.5 forcing grows. Therefore, it is unsurprising that Niño3.4 continues to warm under G4. However, the trend of 0.13 K decade$^{-1}$ is rather robust, and is only 23% weaker than the trend observed from 1966-2005 of 0.16 K decade$^{-1}$.

Only the geoengineering scenarios that are physically implausible (G1-G2) fully offset global warming-induced SST changes in Niño3.4. The more realistic scenarios (G3 and G4) are able to significantly reduce the magnitude of warming under RCP4.5. The RCP4.5 warming trend of 0.21 K decade$^{-1}$ is three times stronger than G3 and 62% stronger than the warming trend seen in the G4 experiment.

The warming trends are 0.22 K decade$^{-1}$ in +1% $CO_2$ yr$^{-1}$ and 0.17 K decade$^{-1}$ in 4xCO2. About 60% of the 4xCO2 warming occurs in the first 10 years and then a relatively slow trend develops for the next 50 years during which another approximately 15% of the total warming occurs (Table 3.3). Frietas et al. (2016) reported calculating the rate of 4xCO2 warming as described in Gabriel and Robock (2015) and they got similar results. After about 60 years the warming flattens out substantially and it takes several thousand years for the full extent of the warming to be evident. I calculated the time series of global mean temperature in the models included, and about 10% to 15% (0.6 K to 0.9 K) of the ~6 K of warming that occurs in 4xCO2 to occur over the experimental period.

The key finding in my experiment with regard to the long-term behavior of the Niño3.4 Index is that under RCP4.5 the warming trend will be 62% stronger between 2030-2069 than if geoengineering was imposed as simulated by G4 beginning in 2020.

**3.3. Sample size and model spread make detecting of ENSO changes difficult**

Changes in ENSO event frequency and amplitude in a geoengineered world relative to the historical record, global warming simulations, and the observational record are either not present, or not large enough to be detectable. This conclusion comes with a number of very strong caveats, including the relatively brief simulation length and the considerable model spread. Despite the absence of a detectable change in ENSO amplitude and frequency in my experiments, I take this opportunity to explicitly state the conditions under which changes in ENSO variability could have been detected. Therefore, I assess the sensitivity of my method for identifying differences in ENSO frequency and amplitude between an experiment and its control. I begin by calculating the minimum increase in event frequency or amplitude that would be detectable.

Since GISS is a relatively well-performing model, and the standard deviation of event amplitude and frequency is relatively low, I address the minimum detectability issue with the GISS model first. I take the GISS runs and randomly assign each simulation into one of two groups of 11. The random assignment to each group is repeated many times. The amplitude and frequency statistics of the two groups are then compared using a two-sample *t*-test assuming unequal variance. I select the comparison that generates a probability of wrongly rejecting the hypothesis that there is no difference between the means that is closest to but not greater than 0.05 (0.03-0.05 in all cases). This corresponds to a significant result at the 95% level. The difference between these

two means, expressed as a percentage increase, is then reported as the threshold value of detectable change in ENSO frequency or amplitude.

In the GISS model, to detect a 31% increase in El Niño frequency, two groups of 11 ensembles of 40-year simulations are required. A 26% increase in La Niña event frequency is required for detectability. In terms of amplitude, an 18% increase in El Niño amplitude was detectable, as was a 17% increase in La Niña frequency.

I then use the same approach to test the minimum detectability threshold in the CSIRO model; I expect to find increased sensitivity to changes in event frequency, but not necessarily to amplitude. In fact, a 25% increase in warm event frequency and a 21% increase in cold event frequency are both detectable. The ENSO event amplitude detectability threshold in CSIRO is close to that found in the GISS model: 17% for warm events and 16% for cold events.

Lastly, I examine the CanESM model, which featured the largest and most frequent ENSO events, but also featured close agreement between ensemble members. The thresholds for detectability for the CanESM are increases of 16% for both warm and cold event frequency, 18% for an increase in warm event amplitude, and 15% for an increase in cold event amplitude.

**3.4. Future GeoMIP experiments may be better suited to diagnose changes in ENSO**

A priority in subsequent experiments would be to reduce the detectability thresholds. For the purposes of improving detectability, steady-state simulations that simulate 100 years or more of geoengineering in which a large $CO_2$ forcing is offset would likely be of most interest for additional detailed analysis, especially if a large

number of simulations were available. This has been proposed for future GeoMIP experiments (Kravitz et al., 2015).

The next generation of GeoMIP experiments that will be part of CMIP6 will extend G1 simulations to 100 years and also provide simulations in which a more extreme AGW scenario – RCP6.0 or RCP8.5 – is offset by constant stratospheric sulfate injections or solar dimming. These new experimental designs result from the need to understand extreme precipitation and temperature events, changes in regional climate and to examine modes of internal variability (Kravitz et al., 2015).

A potential future GeoMIP experiment could apply my detection methodology and proceed as follows. Compare the 100-year 4xCO2 scenario with 100 years of preindustrial control and G1 (G1extended; Kravitz et al., 2015). Given the length of this simulation and the large differences in depiction of future climate between 4xCO2, G1 and the preindustrial control, this would likely be the comparison most likely to show a difference sufficient to exceed my detectability threshold.

I would also recommend comparing the extended GeoMIP simulation results to the late 20$^{th}$ century ENSO record. The availability of ENSO observations increased by at least an order of magnitude during the 1950s and 1960s. Even after the next generation of GeoMIP simulations has been released, the ability for those experiments to potentially detect future changes in ENSO variability will still be limited by how well each model performs.

Lastly, it is evident that diagnosing ENSO variability in the current generation GCMs is hindered by their abilities to accurately reproduce ENSO. Substantial work has been done to determine why many models have difficulty simulating an ENSO that

matches observations in amplitude and frequency. The CLIVAR ENSO working group's analysis of process-based variables in CMIP 3/5 – which quantifies a GCM's ability to simulate key ENSO processes – is underway (Guilyardi, 2012). That important work is squarely focused on determining exactly how the simulation of both ENSO events and the underlying ENSO processes can be improved in GCMs included in the CMIPs of the future.

# CHAPTER 4: THE G4FOAM EXPERIMENT: GLOBAL CLIMATE IMPACTS OF REGIONAL OCEAN ALBEDO MODIFICATION

## 4.1. Methods

Is it possible to cool Earth while concurrently maintaining or increasing precipitation in highly populated and heavily cultivated regions, particularly in regions dependent on monsoon precipitation by employing a specific regional ocean albedo modification regime? I address this question by prescribing regional albedo changes, which are a first step in simulating the impacts of the stable, nondispersive, highly reflective microbubble foam suitable for climate engineering along the lines of what was developed by Aziz et al. (2014) to evaluate whether geoengineering can cool the planet without bringing about reductions in tropical precipitation?

In G4Foam I raised the albedo of the ocean surface is raised from a daily average 0.06 to a fixed daytime value of 0.15 over the subtropical ocean gyres in the SH, specifically 20°N-20°S, 90°W-170°W (South Pacific), 20°N-20°S, 30°W-0°E (South Atlantic) and 20°N-20°S, 55°E-105°E (South Indian). These regions were chosen because of their low cloud fraction, high insolation, low wind speeds, weak currents, and lack of biological productivity in addition to the likelihood that the surface cooling in this area will advect well within the SH.

I used the Community Land Model (CLM) version 4.0 with prescribed satellite phenology (CLM4SP) instead of the version of CLM with a carbon–nitrogen cycle, coupled with CAM4–chem. This configuration allows for evaluation of photosynthesis rates on land, but the carbon-nitrogen cycle is turned off, as those simulations, while useful, would require a prohibitively large amount of computer time. Vegetation photosynthesis is calculated under the assumption of prescribed phenology and no

explicit nutrient limitations (Bonan et al., 2011; Xia et al., 2016). Dynamic vegetation is not turned on in this study, which could limit the ability of the climate to respond to changes in temperature and precipitation. The ocean model does not include any biogeochemical responses, which should be assessed in future studies that deal more squarely with impacts on the ocean brought about by perturbing the ocean surface.

The fundamental question I wish to answer concerns representation of the physical processes that lead to realistic simulation of tropical precipitation. The Asian monsoon is of great importance in this investigation. Fortunately, monsoon processes and regimes are depicted well in the atmospheric component, CAM4 (Meehl et al., 2012). Some important features of CAM4 that illustrate its very good monsoon representation include the amount and location of precipitation over the southern Tibetan Plateau and over the Western Ghats (a mountain range near the west coast of south India). This is improved when compared to earlier versions of the model. The rain shadow leeward of this range is often not resolved by GCMs. However, CAM4 shows some evidence of this rain shadow. These changes related to orography and horizontal resolution are important and likely generalize to similar land surface features outside of India, where model biases have not been as carefully studied as they have been in heavily populated southern India. This improvement can be attributed to the CCSM4 finite-volume dynamical core, which replaces the spectral version of the CCSM3 and the interconnected higher horizontal resolution. Additionally, large-scale features are improved. For example, the representation of the ITCZ during NH winter southward migration over the maritime continent is improved (Meehl et al., 2011).

It does not impact the results of this experiment, but there is an important remote process associated with monsoon precipitation, that is pervasively wrong across CMIP5. Zonal mean absorbed shortwave radiation is too high over the Southern Ocean (Kay et al., 2016). This cloud problem leads to unrealistic warming over the Southern Ocean, which leads to anomalous SH atmospheric eddy flux to the subtropics from the extratropics, potentially damping the cooling response of the negative surface radiative forcing in the subtropical oceans. The effect of a transfer of heat from the SH extratropics into the Hadley Cell already causes a relatively weak negative bias in the amount of interhemispheric heat transport from the south to north. Therefore, the manifestation of this bias in G4Foam would be to partially offset the imposed cooling, lessening the need for interhemispheric energy transport to the SH and suppressing the surface return flow of moisture advection into the NH. Lower than observed interhemispheric energy transport would be associated with a weaker Asian monsoon.

I compare G4Foam to two control experiments. First is G4SSA (Xia et al., 2016). They used a prescribed stratospheric aerosol distribution roughly analogous to annual tropical emission into the stratosphere (at 60 mb) of 8 Tg $SO_2$ $yr^{-1}$ from 2020 to 2070. This produces a net radiative forcing of about −2.5 W $m^{-2}$. The G4SSA forcing ramps down from 2069-2071 and then the run continues without additional forcing from 2072-2089. In G4SSA, the prescribed stratospheric aerosols do not affect tropospheric aerosols. Neely et al. (2016) offers more detail on the prescription of stratospheric aerosols in CAM4–Chem. The second control, which serves as the reference simulation, for both G4Foam and G4SSA is the Representative Concentration Pathway 6.0 (RCP6.0) (Meinshausen et al., 2011) from 2004 to 2089. I have run three ensemble members each

for G4Foam. Three ensembles each were run of G4SSA and RCP6.0 for Xia et al. (2016).

Since the G4Foam experiment is so unique, I take this opportunity to explain why I have chosen this model configuration and address the plausibility of such a regime. Aziz et al. (2014) described a plausible technology to make quantities of long lasting foam, or engineered microbubbles to enhance ocean albedo. This pushes ocean albedo modification up the continuum of plausibility to the point that its plausibility is of the same order as that of other widely discussed potential geoengineering methods.

Seitz (2010) speculated that since air-water and air-sea interfaces are similarly refractive, dispersing microbubbles onto the surface of the ocean would reflect sunlight in much the same way as cloud droplets do. While engineering refractive or stable foams is commonly done and applied in both food science and firefighting, engineering a stable and refractive foam appropriate for a geoengineering scheme appeared fanciful until Aziz et al. (2014) produced a long lasting refractive foam made with biodegradable and non-toxic additives. Aziz et al. identified foam lifetime of three months or more per microbubble as lasting long enough that the input of energy to create the microbubbles would not be prohibitive. After experimenting with protein-only solutions, Aziz et al. (2014) added high methyl ester pectin to type A gelatin and created a foam in salt water, which was still intact and stable at the cessation of the experiment after 3 months. The reflectance of the foam was about 50%, which is comparable to that of whitecaps. The creation of these stable microbubbles makes enhancing ocean albedo in this manner feasible (Aziz et al. 2014). However, these stable microbubbles would not be deployable

in their current form due to issues of scale and the high density of the surfactant used to stabilize the microbubbles.

Safe, stable, highly reflective microbubbles were created in saltwater in a laboratory. However, this technology – like other SRM techniques – is still a long way from deployment. For example, what effect would bacteria in the ocean have on the surfactant? There are a number of other potential risks associated with microbubble deployment, even if the feasibility issues are set aside. Robock (2011) pointed out that vertical mixing in the ocean, changes in ocean circulation, impacts on photosynthesis, and risks to the biosphere could all impair the efficacy of this geoengineering approach. Robock (2011) also pointed out that a cooler ocean would serve as a more effective $CO_2$ sink, helping to offset the $CO_2$ increase that comes about as a feedback of warming, but this additional ocean acidification would also be detrimental to ocean life. Other potentially attractive attributes of this technique include the possibility that it could be deployed exclusively in the 20% of the world's oceans that are not biologically active (Aziz et al. 2014) and therefore have little impact on the biosphere, that there would be no risk to ozone in the stratosphere.

**4.2. Results**

G4Foam would reduce global mean surface temperature relative to RCP6.0. Precipitation over land globally, in the tropics, during JJA globally, and during JJA in the tropics is statistically significantly increased in G4Foam relative to both G4SSA and RCP6.0. The combination of cooling and increased precipitation over land in the tropics results in a statistically significant increase in precipitation minus evaporation on an annual mean basis over many heavily populated regions in G4Foam relative to G4SSA.

Much of the temperature and hydrological response is the result of powerful cloud feedbacks and changes in the tropical meridional overturning circulation induced by the placement of the ocean albedo forcing. G4Foam forcing is shown in Fig. 4.1 and the forced regions are enclosed by black boxes.

The following results compare the G4Foam climate with the climates in G4SSA and RCP6.0 averaged over the period 2030-2069. While G4Foam and G4SSA forcing commences in 2020, the first 10 years of both experiments are a period of transition. For that reason 2020-2029 is discarded from the comparisons.

The primary purpose of G4Foam would be to reduce global mean surface temperature without reducing monsoon precipitation. G4Foam would reduce global mean surface temperature relative to RCP6.0 by 0.60 K and global mean land surface temperature by 0.51 K relative to RCP6.0. In JJA, G4Foam is 0.70 K cooler than RCP6.0 over land in the tropics, 20°S-20°N (Table 4). This JJA cooling in the tropics is of particular importance due to the dense population and heavy agricultural demand in the tropics, particularly north of the Equator. The G4Foam cooling is achieved by a change in net clear sky top of atmosphere flux in G4Foam of -1.5 W $m^{-2}$ as well as cloud changes (Figs. 4.2 and 4.3).

G4Foam would not achieve the same amount of cooling as G4SSA, which would reduce global mean surface temperature by 0.92 K. This is achieved by a change in net clear sky top of atmosphere shortwave flux in G4Foam of –4.0 W $m^{-2}$. On a global mean basis and relative to RCP6.0, G4Foam achieves 66% of the cooling produced by G4SSA, while applying only 38% as much forcing as G4SSA (Fig. 4.3a). This implies that much

of the G4Foam cooling is the result of positive feedbacks, which enhance the cooling, as discussed below.

Fig. 4.3 shows a comparison of the spatial distribution of surface temperature changes between G4Foam and G4SSA and between G4Foam and RCP6.0 between 2030 and 2069. Over the SH ocean gyres that were brightened, there is a very robust cooling, reaching 2 K at the center of the South Pacific foamed region. However, the cooling mixes rather well throughout the SH. Cross equatorial flow and changes in the Hadley Cell transmit this cooling into the NH tropics through the mechanisms described above in section 1.7 of this thesis. Some of this cooling in the NH tropics is then transmitted to the NH extratropics, although the cooling is stronger at high-latitudes in the NH than at mid-latitudes, which is unexpected and requires further investigation.

G4Foam is significantly cooler ($p < 0.05$) than RCP6.0 in almost all locations south of 30°N, in mid latitude NH continental regions windward of the Atlantic and Pacific, and at very high latitudes. Fig. 4.4 shows that G4Foam is less effective in cooling extratropical NH land regions during JJA. This is reasonable, since continental heating in the NH JJA season is more dominated by local heating than the other seasons, in which meridional energy transport plays a larger role. Figs. 4.4a and 4.4c show that G4SSA is more effective in reducing surface temperature over NH continents than G4Foam.

Since the G4Foam forcing alone, with the amplitude of forcing applied in the current experiments, would be insufficient to achieve any of the objectives of the G4Foam experiment, positive feedbacks that enhance cooling and circulation responses must be triggered by the G4Foam forcing to enhance a resulting cooler, wetter climate.

Fig. 4.5 shows change in low cloud fraction both year-round and in the JJA season. The largest change is in the extreme northern edge of the regions where foam is applied, and the area to the north of those foamed regions. The changes in low clouds in these regions are both large and statistically significant.

The low-cloud fraction increase in the three areas to the north and northeast of the G4Foam-forced subtropical surface regions is likely due to a stronger than normal trade wind inversion (TWI). The inversion develops when warm air is trapped above the atmospheric mixed layer due to large-scale subsidence and surface mixing of cooler air above these relatively low SST regions. The increase in low-cloud fraction does not occur over the entire downwind area because SSTs increase from east to west, causing a change in the lower troposphere from east to west. Moving west, the stratocumulus layer, which is trapped under the inversion base, decouples from the mixed layer in the lower troposphere. The surface warming triggers more turbulence within the planetary boundary layer, which allows for enhanced cumulus mixing in the cloud layer, which entrains dry air and evaporates the marine stratocumulus layer.

The subtropical high-pressure systems are stronger in G4Foam, due to the stronger than normal Hadley cell, which enhances subsidence throughout the subtropics. Typically, a subsidence inversion is strongest over the center of the subtropical anticyclones, over cold currents (particularly the Peru Current), and over cooler than normal waters, which are subjected to enhanced upwelling in large part by trade winds on the periphery of the subtropical highs (DeSzoeke et al., 2016). The TWI becomes weaker and its base increases in height as it moves towards the west and towards the equator, as

SSTs increase. This pattern is particularly evident in the Pacific, due to the larger geographical extent of the forced area.

Specifically, under G4Foam conditions, the increased low-cloud fraction areas are the result of the combination of enhanced large-scale subsidence (stronger Hadley cell) and a cooler than normal ocean surface. The cooler than normal surface waters are due to general cooling throughout the SH, as well as an increase in wind-driven upwelling over these areas of increased low-cloud fraction, which are already prone to upwelling, a large fraction of low clouds, and high relative humidity.

In these areas north of the foamed areas, the subsidence inversion is not quite as strong as it is right under the subtropical high. However, SSTs are artificially low, due to general cooling of the hemisphere and enhanced upwelling, driven by anomalously strong winds, and mixing of this anomalously cool surface air within the planetary boundary layer keeps the lowest levels of the atmosphere cool, keeping the marine air inversion base above the lifting condensation level and allowing stratocumulus clouds to form at low altitude, below the base of the inversion. Additionally, since SST is lower than air temperature in the areas of enhanced low-clouds, the surface inversion is further maintained as a result of sensible heat flux from the atmosphere to the ocean. Ultimately, the strong inversion often results in more marine-layer cloud formation and longer times for the clouds to dissipate. This response is consistent through the 2030–2069 period. This enhanced low-cloud fraction response is similar to the seasonal cycle of marine low clouds around the periphery of the subtropical highs (Wood and Bretherton, 2004;

Chiang and Bitz, 2005; Wood and Bretherton, 2006; George and Wood, 2010; Mechoso et al., 2014).

The relationship between the strength of the subtropical high, inversion strength, and marine cloud prevalence can be elucidated by analogy to the behavior of the very well-observed marine low clouds off of the California coast. The strength of the inversion and the prevalence of marine low clouds are modulated by the annual cycle with annual maximum low-cloud extent in the summer, when the subtropical high is at its strongest. The increased low-cloud fraction response is not seen above the actual G4Foam-forced regions despite the cooler SST. The subsidence is so strong in these areas that the base of the inversion falls below the lifting condensation level, and few clouds form (Fig. 4.5).

Mauritsen (2016) attributes some of the decreased rate of warming during the 1998-2015 so-called hiatus to cooling cloud feedback related to a stronger than normal tradewind inversion brought about by changes in tropical Pacific SST patterns. In my experiment, however, extratropical forcing induces the strong TWI. However, regardless of the cause, the stronger TWI has the same cooling cloud feedback impact as observed in Mauritsen (2016), and this feedback contributes to the cooling achieved in G4Foam. Additionally, in the areas under the regions of coincident maximum cooling and cloud increase to the north of the Indian and Atlantic brightened regions, there was a marked decrease in convective precipitation that exceeded the decrease in overall precipitation. In the Pacific, the response was even stronger, with a large area of 25-50% reduction in convective precipitation just downwind of the maximum cooling and low cloud response.

Overall precipitation in this area is only decreased by10-25% (Figs. 4.4, 4.5 and 4.11). Based on the existing TWI literature, the TWI hiatus connection offered in Mauritsen (2016) and my findings regarding the strong inhibition of convection at tradewind latitudes equatorward of the foamed regions, it is rather clear that this TWI plays a large role in the G4Foam cooling.

Another striking G4Foam feature is the large and statistically significant increase in low clouds over land across central Africa, the Middle East and Southeast Asia. These low clouds are coincident with the large cooling in Africa and the Middle East, particularly during the JJA season relative to both G4SSA and RCP6.0 (Figs. 4.5c, 4.5d). These are very hot areas and heat related mortality and morbidity are of great concern. A similar increase in low clouds is evident in the tropical eastern Pacific. This is coincident with the mean northward displacement of the ITCZ in G4Foam with respect to G4SSA and RCP6.0, not with any changes in ENSO.

In G4Foam, clouds are the key to changing the radiation budget in the tropics. In G4Foam there is a change in shortwave cloud forcing of –2.32 W $m^{-2}$ annually and –2.59 W $m^{-2}$ during JJA, relative to G4SSA. Only very small increases in longwave cloud forcing of 0.42 W $m^{-2}$ annually, and 0.07 W $m^{-2}$ in JJA counter this negative forcing. The overall change in cloud radiative forcing in the tropics is –1.90 W $m^{-2}$ annually and –2.52 W $m^{-2}$ during JJA.

Total cloud fraction is shown in Fig. 4.6. Figs. 4.6c and 4.6d are particularly striking in showing the increase in clouds over Africa and Southeast Asia during the JJA wet monsoon season in those regions. Under G4Foam, these regions generally

experience cloudier and cooler summers relative to RCP6.0 and are cloudier and only very slightly warmer on average compared to G4SSA. Some parts of the Sahel and the Middle East are actually slightly cooler in G4Foam than RCP6.0. These changes in temperature and cloudiness play a key role in the changes in the hydrological cycle under G4Foam, which I discuss next.

**4.3 How does the hydrological cycle response in G4Foam compare to that in G4SSA and RCP6.0?**

Relative to G4SSA, precipitation in G4Foam over land in the tropics increases by 3.9% on an annual mean basis and by 4.9% during JJA (Table 4.1). Tropical precipitation in G4Foam over land in the tropics increases by 1.4% on an annual mean basis and by 2.02% during JJA, when compared to G4SSA. Each of these changes is statistically significant ($p < 0.05$). Regarding the temperature change relative to G4SSA, G4Foam is only about 0.3 K warmer in the tropics. The temperature dependence of precipitation, between 1.5% $K^{-1}$ and 3.0% $K^{-1}$, (Emori and Brown, 2005), explains only a fraction of the precipitation increase. The statistically significant increase in land-only precipitation in the tropics in G4Foam relative to RCP6.0 occurs in a climate in which RCP6.0 is between 0.6 K and 0.7 K warmer than G4Foam, depending on the season. Over the tropical oceans, in G4Foam, precipitation only increases by 0.8% on an annual mean basis and 0.7% during JJA relative to G4SSA and there is a decrease of 1.6% on an annual mean basis and a decrease of 1.9% during JJA relative to RCP6.0.

Globally, over land, the response is similar, but the magnitude of change is a bit less. Precipitation is statistically significantly increased over land in G4Foam relative to

RCP6.0 by about 0.5%. Precipitation is statistically significantly increased in G4Foam relative to G4SSA over land by 3.5%.

The overall global precipitation difference between G4Foam and G4SSA or RCP6.0 when land and ocean are combined and all seasons and all latitudes are included are in line with the magnitude of the temperature dependence of precipitation. Globally, G4Foam is warmer than G4SSA by 0.3 K and there is 0.61% more precipitation. G4Foam is cooler than RCP6.0 by 0.6 K and drier by 1.98% (Table 4.1).

The spatial pattern of precipitation changes is shown in Fig. 4.7. Precipitation is greatly reduced over the ocean, particularly in the SH, relative to both G4SSA and RCP6.0. Changes in precipitation poleward of 40° latitude in either hemisphere are largely due to the temperature dependence of precipitation. The changes in the SH subtropics are dominated by the shortwave forcing applied over the ocean gyres, which reduces both evaporation and precipitation in those areas.

The changes in precipitation in the tropics are driven by the ITCZ's northward shift. Large precipitation anomalies occur in a narrow band north of the Equator and smaller positive anomalies occur in broader regions, primarily over NH monsoon regions. Importantly, there is a statistically significant increase in monsoon precipitation over the Sahel, the Middle East, the Indian subcontinent as well as Southwest Asia and the maritime continent on an annual mean basis in G4Foam relative to G4SSA (Fig. 4.7a). Relative to RCP6.0, these changes are not statistically significant over the Indian subcontinent or Southwest Asia, but there are only very isolated and small areas in these regions in which there is any precipitation reduction, either on the annual mean or during

JJA. Therefore, over much of heavily populated southern Asia, east of the Arabian Sea, G4Foam will be cooler than RCP6.0 without any notable precipitation differences.

Relative to both G4SSA and RCP6.0, there is a great deal more precipitation all year and particularly during JJA over central America, the northern Amazon, much of Africa, parts of the Arabian peninsula and the maritime continent. This response is more robust than the response over Southeast Asia due to the more direct dependence of rainfall in these regions on ITCZ position than in Southeast Asia, where the monsoon is also driven by numerous local and remote factors, including ENSO and the Indian Ocean Dipole (IOD). Gabriel et al. (2017) provides a more detailed discussion of how changes in the Indian Ocean, including the IOD, tend to dampen the magnitude of the precipitation increase over parts of Southeast Asia.

Although these G4Foam simulations are effective in enhancing moisture convergence over heavily populated and highly cultivated regions, particularly in the tropics, there are regions that would suffer under this regime. Precipitation patterns for islands in the South Pacific are largely governed by the position and strength of the South Pacific Convergence Zone (SPCZ), which changes substantially under G4Foam due in part to the cooling and to the movement of gradients of temperature and pressure. Precipitation deficits over Madagascar and some regions in Africa and South America exceed 10%. However, the very large precipitation deficits in G4Foam are largely confined to the SH oceans and the land areas that tend to be far less populated than in the areas where it will increase.

While the changes in precipitation are important and useful in describing the climate response in G4Foam, the change in precipitation minus evaporation between

G4Foam and G4SSA or RCP6.0 may be more determinative of overall water availability than precipitation alone, and may therefore be more relevant to how the changes in climate will actually impact people's lives. Fig. 4.8 shows precipitation minus evaporation. Specifically Fig. 4.8a shows that precipitation minus evaporation in G4Foam is increased, and this increase is significant relative to G4SSA, across the Sahel, all of South Asia, the Maritime Continent, Central America and the northern Amazon. These are all heavily populated regions that are heavily cultivated. Fig. 4.8b shows a similar pattern, albeit with the regions significantly gaining water slightly suppressed in coverage, when G4Foam is compared to the warmer RCP6.0 rather than G4SSA. Figs. 4.8c and 4.8d show changes in *P-E* during JJA, the NH wet monsoon season, when water may be needed the most. Due to variability in the monsoon, there is more heterogeneity in the JJA response than the annual response, particularly across Southeast Asia. The increase in *P-E* is, driven by a combination of increased precipitation, lower temperature and increased cloudiness in these heavily cultivated regions.

Fig. 4.9 shows the differences of annual cycles for 2030-2069 for zonal mean precipitation, zonal mean precipitation minus evaporation, and zonal mean precipitable water between G4Foam and G4SSA and between G4Foam and RCP6.0. They illustrate the northward displacement of the ITCZ, with positive precipitation anomalies progressing poleward as the boreal summer monsoon progresses. Fig. 4.9f shows the difference in the zonal mean annual cycle for column integrated precipitable water between G4Foam and RCP6.0. The striking feature here is that zonal mean precipitation is higher at key latitudes in the tropics, despite zonal mean column integrated precipitable water being much lower at the same latitude. This further illustrates the presence of

increased moisture convergence further north, at latitudes with more land and population, which explains the precipitation increase concurrent with the decrease in available water vapor.

In Fig. 4.10, the impacts on agriculture are quantified by looking at the photosynthesis rate anomalies between G4Foam and RCP6.0. There are small but statistically significant increases in photosynthesis rate in G4Foam relative to RCP6.0 in much of Southeast Asia. The most dramatic changes occur in Central America and parts of the northern Amazon, where the high $CO_2$, relatively cool and very wet conditions promote agriculture.

**4.4 Summary of the results of the G4Foam experiment**

To recap, G4Foam would reduce global mean surface temperature relative to RCP6.0 by 0.6 K for the 40-year period starting 10 years after the implementation of geoengineering. Clear sky top of atmosphere net shortwave flux is reduced by 1.5 W $m^{-2}$ in G4Foam relative to RCP6.0. This is achieved primarily by the shortwave forcing over the subtropical SH ocean gyres. Before accounting for feedbacks, temperature is more sensitive to the forcing applied in G4Foam than G4SSA. However, global mean surface temperature in G4SSA is 0.3 K lower than in G4Foam because of a larger change in clear sky top of atmosphere net shortwave flux of –4.0 W $m^{-2}$ (Fig. 4.2). Additionally, the latitudinal distribution of temperature reduction is different in G4Foam than in G4SSA. G4SSA is most effective in cooling the NH continents, while G4Foam most effectively cools the surface south of around 30°N (Fig. 4.3). Precipitation over land globally, in the tropics, during JJA globally, and during JJA in the tropics is statistically significantly increased in G4Foam relative to both G4SSA and RCP6.0 (Fig. 4.6). The combination of

cooling and increased precipitation over land in the tropics results in a statistically significant increase in *P-E* on an annual mean basis over Central America, the Northern Amazon, the Sahel, the Indian Subcontinent, the Maritime Continent and Southeast Asia in G4Foam relative to G4SSA (Fig. 4.7). All of these areas are very densely populated and heavily cultivated. Water scarcity is a major issue in these areas and G4Foam describes a climate model response in which there is global cooling but more water is made available to many people in regions on the brink of severe water shortages. Both the changes in the spatial pattern and magnitude of changes in temperature and precipitation are far too large to be explained by the forcing alone. Instead, much of the temperature and hydrological response is the result of powerful cloud feedbacks and changes in the tropical meridional overturning circulation induced by the placement of the ocean albedo forcing.

**4.5 The results of G4Foam come with important scientific and ethical caveats**

The technology does not presently exist to actually deploy a stable, highly reflective layer of microbubbles on the actual ocean surface. While a stable, highly reflective, nondispersive foam has been developed in a saltwater solution, appropriate for climate engineering, this foam has not been tested outside the laboratory, much less on the surface of a large area of rarely quiescent ocean. The foam has not been immersed in a medium in which bacteria are present, and the interaction between the bacteria and the protein surfactant could damage the layer of microbubbles. Also, even though the diameter of these microbubbles is on the order of $10^{-6}$ m, the demand for surfactant would likely overwhelm our current production capacity of whatever surfactant is chosen. The research on the engineering required to perform stratospheric geoengineering by sulfate

injection is much further along than research of microbubble deployment, which is still in its earliest stages.

However, since development of microbubble technology is underway, it is worthwhile to determine how such a technology could be applied in a manner that would address serious climate issues. The progress being made in research associated with stratospheric geoengineering actually enhances the relevance of researching the climate impact of this particular ocean surface geoengineering approach as G4Foam was designed with an eye toward concurrent deployment with stratospheric geoengineering in the event the stratospheric geoengineering were to cause the precipitation deficits relative to both picontrol and global warming scenarios that many model studies have shown that it might.

More fundamentally, the propriety of any attempt to impose a the G4Foam forcing in an attempt to achieve the modeled G4Foam climate is premised on a value judgment that it is desirable to develop a technology that could redistribute essential resources between nations in an attempt to achieve a net benefit to humanity as a collective when it unknowingly creates a local scarcity of these essential resources. To some extent, making this value judgment is germane and is a prerequisite to the discussion of any form of geoengineering. Even though G4Foam would be successful in increasing water supply in more heavily populated areas, water supply will almost certainly be reduced in remote regions, such as South Pacific islands. Is it ethical to pick winners and losers when the selection process is aimed at increasing the number of winners and decreasing the number of losers? Hypothetically, if G4Foam worked as described in this thesis, from a purely consequentialist perspective, and with the sole

objective being increased utility for the human collective, G4Foam could be considered beneficial.

Finally, Chapter 4 of this thesis which reports G4Foam only concerns the climate response to imposed surface albedo changes. I do not examine how placing an actual layer of microbubbles in the ocean would change ocean circulation or impact chemistry and biology in the ocean. Evaluating the changes in the ocean circulation that are caused by the surface albedo modification is one of the next issues to explore. The ocean regions I propose to brighten have low biological productivity and weak currents, but the possibility of remote impacts, due to changes in circulation having negative impacts on important ocean regions, is worth considering.

In the final chapter of this thesis I will combine G4Foam with G4SSA in an attempt to achieve global cooling everywhere, but still maintain tropical precipitation near current levels

# CHAPTER 5: COOLING THE PLANET BY COMBINING STRATOSPHERIC SRM WITH REGIONAL OCEAN ALBEDO MODIFICATION (G4SSAFOAM)

G4Foam alone is insufficient to cool the planet by more than a very small and highly spatially variable amount in the extratropical NH (Fig. 4.4). Can two methods of geoengineering be imposed concurrently to effectively cool the entire planet without simultaneously reducing precipitation in heavily populated and cultivated regions? Combining G4SSA with G4Foam would cool the planet more than G4SSA alone. Despite the cooler climate in G4SSAFoam than in G4SSA, could the combination of forcings in G4SSAFoam produce a climate in which there is a significantly smaller precipitation reduction, relative to RCP6.0, particularly over land in the tropics, than the reduction G4SSA alone?

## 5.1. Methods

G4SSAFoam consists of a 70-year simulation of G4Foam forcing, combined with G4SSA forcing, branched off of RCP6.0 (the experiments G4Foam and G4SSA are described in Chapters 3 and 4, above), starting in 2020 and ending in 2089. G4Foam forcing is removed after 2069, while G4SSA forcing is gradually reduced mostly during 2069. The simulations are performed with those forcings imposed on the model configuration described in section 4.1 (above) as well as in Xia et al. (2016) and Gabriel et al. (2017).

The surface SRM (the G4Foam forcing) would certainly be slightly less effective in terms of the amount of insolation reflected in the combined experiment than in the G4Foam only experiment due to the relatively uniform insolation reduction causing a slight decrease in shortwave radiation reaching the surface over the foamed regions as a

result of the stratospheric SRM also imposed. The years 2070-2089 are used to assess the termination effect, but as expected, there is a return to an RCP6.0-like climate within 5 to 10 years of termination as seen when G4Foam and G4SSA were run alone (Fig. 5.1 and 5.2). However, the termination effect could take longer if the G4SSAFoam introduced inertia into the climate by cooling more than G4Foam or G4SSA, maintaining sea ice more effectively than either method alone.

In assessing G4SSAFoam, I focus on several things. Will tropical precipitation shift sufficiently northward and landward as it did in G4Foam to avoid a decrease in rainfall in heavily populated and highly cultivated tropical regions, even in the presence of additional cooling? If the forcing generates feedbacks that lead to Hadley Cell intensification, and work similarly as they did in G4Foam, I expect G4SSAFoam to be about 0.5 K cooler than G4SSA and 1.5 K cooler than RCP6.0, with the precipitation amount during the 2030-2069 comparison period likely falling in between the amounts modeled in G4SSA and RCP6.0. However, the amount of anomalous northern migration of the ITCZ in G4SSAFoam may be influenced and possibly limited by the fact that G4SSA is most effective in cooling land, and since there is more land in the NH, G4SSA cools the NH more. Clouds will also play a major role. Also, G4SSAFoam may be so effective in cooling the tropics that the thermodynamic response to the temperature reduction could overwhelm the increased contribution of moisture convergence over land to precipitation over land. The results of G4SSAFoam are described below.

**5.2. Results**

In summary, G4SSAFoam would reduce global mean surface temperature relative to RCP6.0 and G4SSA. Global mean precipitation in G4SSAFoam decreases relative to

RCP6.0 and G4SSA, but under G4SSAFoam, tropical precipitation over land remains at or near RCP6.0 levels despite being 1.45 K cooler and this precipitation level is slightly above that in G4SSA, despite G4SSAFoam being 0.54 K cooler than G4SSA. The combination of cooling, increased cloud cover and increased precipitation over land in the tropics results in a statistically significant increase in *P-E* on an annual mean basis over many heavily populated tropical regions in G4SSAFoam relative to G4SSA and RCP6.0. However, some regions, including heavily populated parts of Southeast Asia, suffer negative *P-E* anomalies relative to RCP6.0, and the hydrological cycle in these areas is similar to that G4SSA, if not slightly weaker. However, mechanistically, the powerful cloud feedbacks and changes in the tropical meridional overturning circulation induced by the placement of the ocean albedo forcing are at play in G4SSAFoam as well, and these feedbacks bring about similar changes as in G4Foam in tropical cloud cover and hydroclimate, albeit in a cooler climate.

Immediately, upon combining the forcings from G4SSA to G4Foam, an important advantage of G4Foam is eliminated. Sulfur aerosols are placed in the stratosphere, which puts the risk of ozone loss on the table, as well as all of the other risks attendant to putting sulfur in the stratosphere (Robock, 2016). G4SSAFoam is not a potentially low ecological impact regional geoengineering approach. It is, put simply, a patch designed to cover up some of the regional inequalities created by stratospheric SRM alone.

In G4SSAFoam, the all-sky short wave flux at the top-of-the-atmosphere in G4SSAFoam remains an average of 4.2 W $m^{-2}$ below that in RCP6.0 and 1.2 W $m^{-2}$ below that in G4SSA throughout the 2020-2069 simulation of geoengineering (Fig. 5.1a), albeit with some fluctuation as cloud and surface reflectivity change over time. A small

decrease in global mean clear-sky shortwave (Fig. 5.2a), all-sky shortwave flux (Fig. 5.1a) and temperature (Fig. 5.2b) is seen in G4SSAFoam between 2025-2030. In addition, the maximum cooling (Fig. 5.3) throughout the period is not seen under the center of the albedo modification region, or in the area of maximum increased cloudiness equatorward of the South Pacific foamed region, but rather in the polar and sub polar latitudes of the Southern Ocean. Also, between 2025-2030, global mean shortwave cloud forcing becomes less negative than in G4SSAFoam during the 2025-2030 period, meaning the change is not attributable to clouds, making it very likely that sea-ice growth begins to occur in the SH during the first decade or so of G4SSAFoam. However, after 2030, the likely ice growth stops, and both all-sky and clear-sky shortwave at the top of the atmosphere increase by about 1 W $m^{-2}$ over the period 2030-2069, trending slowly upward by the same amount as RCP6.0.

Additional research will be done in this RCP6.0, G4SSA, G4Foam, G4SSAFoam and G4SSA-solar GeoMIP testbed to determine the impacts of each simulation on sea-ice and possibly ice sheets as well. That future work would also seek to explore whether Southern Ocean circulation anomalies induced by the different radiative forcings create nonlinearities in the ice sheet response that might make one or more of the geoengineering approaches that have been simulated in this testbed more or less appealing from the perspective of wanting to restore sea ice and limit ice sheet loss.

The anomalous circulation features in the G4SSAFoam climate are very similar to the G4Foam climate. However, the increase in low clouds is much more limited near the northern edge of the South Pacific foam region (Fig. 5.4). The same is not true for the increase in total clouds over tropical land regions, particularly in the JJA season, which

results in a very strong cooling of 1.7 K relative to RCP6.0 during JJA in the tropics. The spatial pattern of the large reduction in temperature coincides with the areas of increased total cloud fraction (Figs. 5.5 and 5.6). While it is not possible to infer a decrease in heat related mortality and morbidity in the tropics from a decrease in the mean only, this reduction is so significant, particularly considering the fact that tropical temperatures are relatively stable, it is not unreasonable to think that G4SSAFoam would effectively eliminate the risk of global warming induced increase in the risk of heat related morbidity and mortality in the tropics.

The intensified G4SSAFoam Hadley Cell results in a strong northward migration of the tropical rainbelts. The pattern of precipitation anomalies in G4SSAFoam relative to both G4SSA and RCP6.0 is similar to the pattern of anomalies in the same comparisons made between G4Foam and RCP6.0 and G4SSA over the Pacific, the Atlantic, Africa and the Americas. This northward shift is particularly robust over the Pacific and over the Americas, where large positive precipitation anomalies shift drastically northward.

However, there is not a northward shift in the maximum Asian monsoon rainfall and the general northward migration of the tropical rainbelts misses the most heavily populated and cultivated regions in the tropics (Fig. 5.6). Additionally, there is a great deal of regional heterogeneity in the *P-E* response over southeast Asia, with some areas gaining *P-E* and some areas experiencing negative *P-E* anomalies relative to both G4SSA and RCP6.0 (Fig. 5.7). While in the aggregate tropical precipitation remains near RCP6.0 levels in G4SSAFoam, G4SSAFoam is not broadly effective in cooling heavily cultivated regions of Southeast Asia without weakening the hydrological cycle. This is

despite a large northward jump in the ITCZ (Fig. 5.8). Finally, the low cloud pattern in the region equatorward of the foamed regions, where the TWI exists, is not as pronounced as it is in G4Foam. Additionally, convective precipitation actually increases more than total precipitation, or increases while total precipitation remains unchanged at the latitude of the TWI just north of the SP foam region (Fig. 5.9). However, while the TWI may be weaker, there is a very pronounced decrease in convection right along the equator in the heart of the Niño3 and Niño4 regions, which may imply a La Niña-like mean state in G4SSAFoam (Fig. 5.9). Further investigation could explore whether the strong cooling in G4SSAFoam in the absence of a low cloud response as strong as G4Foam is attributable to the La Niña-like mean state burying heat in the tropical Pacific. As future research, I intend to run a simulation G4SSAFoamPacific to further elucidate the La Niña-like mean state mechanism and its consequences. The Pacific zone of the G4Foam forcing is somewhat similar to the artificial MCB design used in the Hill and Ming (2012) experiment that produced a La Niña-like mean state due to MCB in the SH Eastern Pacific.

Looking at aggregate precipitation and temperature statistics both globally and in the tropics, there is a 4.7% decrease in global precipitation in G4SSAFoam relative to RCP6.0. However, the reduction over land was much less: 2.7% globally, 1.2% in the tropics and just 0.5% during JJA in the tropics (Table 5.1). Relative to G4SSA, G4SSAFoam was 0.5 K cooler than G4SSA alone. This cooling caused a 0.2% decrease in global precipitation, and an increase of 1.0% in the tropics and 1.9% during JJA in the tropics. On a global mean basis and on a tropical mean basis, the G4SSAFoam climate features mid 21$^{st}$ century precipitation with mid 20$^{th}$ century temperature levels. Also,

while negative *P-E* anomalies over land on G4SSAFoam are not particularly large relative to RCP6.0 or G4SSA in the SH extratropics, the cooling is so strong in that region, 2.0 K, that precipitation decreases by 5.9%. This large reduction in precipitation in the SH extratropics may also caution against a combined G4SSAFoam geoengineering scheme.

**5.3 G4SSAFoam Summary**

A concurrent deployment of stratospheric geoengineering and ocean albedo modification could cool the entire planet while maintaining or enhancing the hydrological cycle, in the aggregate in the tropics. However, the spatial pattern of the precipitation change is complex, with both winners and losers in the tropics, and the precipitation reduction in the SH extratropics of 5.9% could be hard to adapt to. While the use of a combination of geoengineering techniques to offset undesirable regional climate disparities that using one method of geoengineering alone could induce is certainly an area worthy of careful research, it may prove difficult to compensate for regional disparities in climate impacts brought about by geoengineering, as most regional interventions necessarily involve inducing circulation anomalies, which simply redistribute climate risks and benefits.

Now that the climate impacts of both G4Foam and G4SSAFoam have both been examined, it is important to understand what would be required to successfully raise the albedo of large regions of the SH ocean. Is it feasible to deploy of sheets of microbubbles the size of continents onto the surface of the remote ocean, have the layer remain there without degrading and not dramatically disturb processes that occur at the air-sea interface? This question will ultimately determine whether a geoengineering

option like G4Foam is a policy option to address the dilemma of global warming or potential regional inequalities of geoengineering or not.

**5.4 Placing an actual layer of microbubbles on the ocean surface would be incredibly difficult and is presently not possible**

The ability to use a computer model to harness the dynamics of the atmosphere to excite cooling climate feedbacks in the manner of G4Foam is interesting on its own merits. However, there is a good deal of work to be done before geoengineering with microbubble foam rises to the level of same level of plausibility as stratospheric SRM or even MCB and becomes policy relevant in the short term. There are fundamental differences between the foam developed by Aziz et al. (2014) and the modeled sub micron diameter diffuse (~1 ppmv) microbubbles that achieved a reflectivity of 0.22 in a model simulation from Seitz et al. (2010). The discovery by Aziz et al. (2014) is not a step toward the Seitz (2010) microbubbles, but instead potentially the beginning of an independent route to discovery.

Proteins serve as macromolecular surfactants for stable foams. Use of proteins in this manner is common in emulsion-type and foam-based food products. The function of proteins as surfactants in producing stable (long-lasting) foams for food products is ultimately a consequence of the structure and properties of the chosen protein adsorbed (held on an external or internal surface as a thin film) layers at the air-water interface (Damodoran, 2005). Stable and reflective foams are also used in firefighting and for medical applications (Patino et al., 2008; Dickinson et al., 2011). This foam stability property is also essential, and probably prerequisite, to the development of foams for climate engineering.

While foams produced by natural whitecaps have been observed to have reflectivites as high as 0.4-0.6 (Whitlock et al., 1982), they are ephemeral and due to this short-lived nature have only a small impact on the surface radiative budget. An ocean mirror effect, which is needed to raise the ocean albedo from around 0.06 to around 0.15, requires foam stability. Aziz et al. (2014) estimate that to work as an ocean mirror, the microbubbles making up the foam would need to last three months or longer.

Aziz et al. (2014) present the first successful work creating a foam product in the laboratory that combines high foam reflectivity with high foam stability. The experiment was conducted in a saltwater medium and the product was deemed by the authors of Aziz et al. (2014) to be appropriate for climate engineering because of stability and high reflectivity. However, stability and reflectivity are only two of the requirements of a foam that would be useful for climate engineering on the scale described in G4Foam. A useful foam would need to be deployable at a large scale and be diffuse enough so that it does not greatly impact processes that occur at the air-sea interface, including evaporation of water. The foam must be able to withstand ocean mixing and rainfall; rather than dissolving on contact with the ocean, it must form a stable reflective layer on the air-sea interface despite the waves and wind. The foam must stay generally where it is put, and the surfactant must not interact with proteins, such as those found on the surface of bacteria, that already exist naturally at and near the surface of the ocean, in such a way as to make the foam degrade quickly.

The issue of bacteria in the ocean is particularly important. The surfactants are made in large part of pectin or protein and are degraded by proteins on the surface of the bacteria due to the high aqueous solubility of the surfactants. So, since degradation of the

foam is inevitable as it interacts with naturally ocean surface constituents, upon degradation, the foam would have to be designed to sink to the bottom of the ocean or biodegrade , which is possible (Ngata et al., 2004; Cheng et al., 2004). Despite the risk of degradation related to interaction with bacteria, proteins and pectins are still excellent surfactants for the purpose of creating a highly reflective, stable foam at an air-sea interface for several reasons. They increase surface viscosity of a liquid foam, prevent coalescence and foam ripening (which is the tendency of small crystals in suspensions to dissolve and redeposit onto smaller crystals, which is undesirable when losing surface area leads to a reduction in reflectivity), and steric interactions are modified by interactions of positively and negatively charged groups, which could promote stability (Pugh, 1996; Wirenga et al., 2006).

While it is not impossible to do so, Aziz et al. (2014) do not attempt to prepare microbubbles with diameters on the order of 10 microns by sonication, frit and disc generation and microfluidics because such methods that produce such tiny bubbles, which would likely be even more reflective than the coarse, polydisperse foam that they do create, would require a copious amount of surfactant. The surfactant demand for microbubbles created by sonication, frit and disc generation and microfluidics increases proportionally with the surface area to volume ratio, making reflectivity related to the amount of surfactant used and could not be scalable. Therefore they turn to attempting to develop a coarser foam with microbubbles of varying sizes (polydisperse) with bubble diameters on the order of 1 mm, several orders of magnitude larger than the perfectly located network of diffuse bubbles modeled by Seitz et al. (2010).

Aziz et al. (2014) were not initially successful in developing a stable, reflective

foam. They tried numerous types of unary protein solutions and several gelling methods and failed. To generate the bubbles, they first tried using compressed air using nozzles, but that foaming method produced bubbles that weree too large to be effective for the purpose of reflectance. Eventually the foaming method of choice was an off-the-shelf food mixer, which produced a polydisperse foam, with bubble diameter of ~1 mm. The food mixer was capable of producing large pectin gelatin cells, visible to the naked eye. This process involved lengthy mixing, heating and drying.

Ultimately, several recipes were successful in creating stable foams. Foams that were stable for the three-month experiment (after three months, drainage had effectively stopped in all cases and the foams were deemed stable) remained stable as a result of electrostatic interactions between gelatin, positively charged, and pectin, negatively charged. These electrostatic interactions produced the persistent, highly reflective foam at the surface that Aziz et al. (2014) propose as suitable for climate engineering. The reflectance of this stable foam was between 0.50 and 0.55 in the visible spectrum.

However, these foams have concentrations of pectin and gelatin of between 0.3% and 0.5% of the total weight of the foam. Solutions consisting only of whey protein isolate, albumin, or gelatin type A and B showed rapid liquid drainage. Other research on polydisperse protein-only foams had shown the same fast drainage. The unsuitability of protein additives alone provides additional evidence of the electrostatic interaction between pectin and gelatin being a dominant source of foam stability.

While the headline finding of the Aziz et al. (2014) experiment was stabilization with high methyl ester pectin to type A gelatin, because that is potentially possible to re-create at a larger scale, foams produced from solutions derived from red seaweed

produced stable foam with smaller bubbles that were more reflective, 0.65 to 0.75. Such a foam derived from something as natural as seaweed would most likely have little negative impact on biology (Xu et al., 2004; Aziz et al., 2014).

As constituted, the Aziz et al. (2014) foam is certainly not deployable. It is nearly as dry and probably as stable as Styrofoam and contains very large concentrations of pectin and gelatin. It is made of salt and soluble polymers, so if it were exposed to rain and to the ocean, it would dissolve.

**5.5 A proposal to develop a foam based on Aziz et al. (2014) to use in G4Foam**

It is possible to stop there and deem the Aziz et al. (2014) foam undeployable. However, it may be more useful to consider whether it is possible to get closer to foam deployability by suggesting research toward a similar foam. This foam has many of the properties of the Aziz et al. (2014) foam and if fabricated in this manner, there might be a path to deployability at some scale. Therefore, I assume for the sake of exploring the deployability issue further that the stable foam created by Aziz et al. (2014) could instead have been designed as a reflective suspension of pectin gelatin cells, probably suspended in 10-20% ethanol, that could sit on the surface of the ocean and would not dissolve into the ocean upon contact. Of course the ocean is rarely quiescent, so the ability to sit on the surface is a huge assumption. The envisioned foam containing the Aziz et al. (2014) stable gelatin pectin cells is similar to an aqueous suspension used in preparing solutions of drugs, such as injectable antibiotics. Proteins are often sold as aqueous ethanol suspensions and used in medical research. Surfactant suspensions in ethanol also exist (Gülseren et al., 2012). A common example of a protein in ethanol suspension is Protein-A Sepharose, used in chromatography, and is sold as an aqueous ethanol suspension.

Pectin is also frequently suspended in ethanol. The large pectin gelatin cells would need to be suspended in a solution like ethanol. In reality, an ethanol suspension might not be appropriate because dumping ethanol into the ocean could be dangerous. So I additionally assume that the ethanol suspension could be engineered to be nontoxic or to be so thin and so persistent so as to make the accretion of ethanol into the ocean minimal. Alternatively, another, more innocuous, aqueous suspension could be used, rather than an ethanol-based suspension.

It is rather difficult to predict, for example, at what rate this theorized foam, composed of large pectin gelatin cells stabilized by steric interactions, in an aqueous suspension would evaporate. Even if it is assumed that this film did not degrade (or could be easily and infrequently replaced) and could be permanently fixed to the air-sea interface, unperturbed by wind or waves, the properties of the film would be variable and difficult to determine, as relatively large quantities of surface constituents occur naturally at the air-sea interface and would interact with and become part of the surfactant suspension.

Polysaccharides like pectin, or proteins like whey protein isolate, are large polymers that differ from the large polymer hydrocarbons deposited in the sea after oil spills in terms of what functional groups are part of the polymer structure. However, there is a body of research on how oil spills behave at the air-sea interface and their evaporation rates are highly variable. Also, oil spills may be an apt analogy, because proteins and pectins are often suspended in ethanol, sometimes together with whey protein, so it is possible that this foam, as described above, would contain large concentrations of ethanol. Given the relatively low concentrations of surfactant (0.5% of

the weight of the foam), the tendencies of hydrocarbons, pectins and proteins to interact with natural surface constituents, and the possibility that the surfactant could be suspended in ethanol, it is likely that the evaporation rates of either a spill of hydrocarbons or a liquid foam containing a suspension of particles in ethanol or some similar solution will be highly variable and impossible to predict based on the properties of only the known substances in the film that would for at the air-sea interface.

Since evaporation of hydrocarbons is an important process that is considered in oil spill behavior, it is known that very light crude oils are reduced in volume in the water by as much as 75% within a few days, while some very heavy crude oils only lose 5% of their volume. These evaporating hydrocarbons are actually composed of hundreds of types of molecules and can differ greatly based on source. Further, the processes that are determinative of hydrocarbon evaporation are very different from those associated with evaporation of water from the ocean (Fingas, 1999). Evaporation of oil spills is not dependent upon conditions in the PBL, unlike evaporation of water, which is PBL dependent. For oil spills, evaporation rates are estimated from a simple equation relating evaporation rate to the product of a constant (derived from known distillation properties of the oil type and the surface temperature) and the logarithm of time. Wind velocity, turbulence level, area, thickness, or scale need not be considered, rather only time and temperature matter for evaporation rate (Fingas, 1999).

In summary, the Aziz et al. (2014) foam would dissolve in real world conditions. Even if it did not dissolve, it would degrade over time and need to be engineered to sink upon degradation, in part because of interactions with bacteria on the ocean surface, it would be displaced by convection, wind and waves in the ocean. And even if it dissolved

or was applied in such a way to form a wet film of foam suspended in a dilute surfactant solution that coated the ocean surface and sat on the ocean surface, impervious to the forces exerted by the water and the wind, it would evaporate. The rate of evaporation would be difficult to estimate and highly variable both because of variable composition of the film and the polydisperse nature of the substance. Also, the amount of protein surfactant required to cover up to 10% of the ocean is not available. Lastly, if a lot of ethanol were required to constantly replenish the suspended foam, dumping ethanol into even a biologically unproductive ocean could be dangerous if enough ethanol were able to advect and coalesce into a biologically active area and could not be recovered from the ocean before it got to that area. The proteins being used in the protein iterations of the Aziz et al. (2014) are very specific and derived from sources like porcine skin, which is a relatively finite resource. Pectin is probably more available, but demand would still exceed supply unless a massive production effort were embarked upon, the scale of which could not be determined until it could be determined how much pectin would be demanded by the foam.

However, Aziz et al. (2014) did isolate an actual, stable foam that is highly reflective (0.50-0.55) and this stability means that the amount of energy needed to create an ocean mirror via microbubbles would not be prohibitive. The development of an appropriate, scalable source of pectin and gelatin that could be prepared in such a way to be deployable and exhibit the same steric interaction and large cell formation would be worth exploring if there was a proof-of-concept of a foam that could survive real-world conditions.

Lastly, the evaporation of water could be very different in an environment where much of, or all of, the air-sea interface was covered with a relatively thick foam of surfactant suspension, mixed with the other naturally occurring materials that interact with the suspension. If the water were covered by the Aziz et al. (2014) relatively dry Styrofoam-like foam, evaporation would be massively reduced, such as it is in an area polluted with plastic debris or in an area, such as a desert reservoir, where debris is intentionally added to limit evaporation.

For water, unlike hydrocarbons and possibly surfactant suspensions, the properties of air in the PBL regulate the evaporation rate. The saturation vapor pressure varies with temperature and humidity. In a poorly mixed, wind-free boundary layer, the air above the water saturates very quickly, and evaporation rates can slow by orders of magnitude. Water actually evaporates at a tiny fraction of its maximum rate due to PBL saturation. Water evaporation is a function of the mass transfer rate of the evaporating water, the concentration of the water as a mass per volume, a factor describing the intensity of turbulence, and a factor accounting for the level of saturation of the boundary layer above the evaporating water. Less mass transfer occurs when less surface area of water is exposed to the air-sea interface and when there is resistance to evaporation of liquid as a result of the vapor permeability of the film at the air-sea interface makes it more difficult to pass the water vapor through the film than it would through the air.

This has also been observed in the study of oil spills. Films of oil on an ocean surface reduce water evaporation rate by 15% to 33% due to this diffusion resistance as well as other properties of surface-active substances at the film-water interface (Anikiev et al., 1988). An additional risk of the foam is a reduction of gas exchange at the air-sea

interface, which may lead to toxic increases in oxygen concentration in the ocean water underlying the film. A decrease in the evaporation of water as a result of these surface processes is one of many factors, also including changes in surface roughness and the lack of a diurnal cycle in the reflectivity of the modeled G4Foam, that would make the actual boundary layer conditions, and therefore potentially the mesoscale, synoptic scale and global scale feedbacks of the forcing quite different if all processes were accounted for rather than just the prescribed albedo increase.

For all of the reasons described above, the Aziz et al. (2014) foam should be viewed as only as being crucial in that concurrently reflective and stable bubbles can be formed in salt water, mostly as a result of preparation of stable cells of positively charged gelatin and negatively charged pectin in a food mixer, but not necessarily meaning substantial innovation is not needed before anything is suitable to be deployed. While the Seitz et al. (2010) model results are interesting, there has been little if any work since to develop the incredibly diffuse (1 ppmv), sub-micron diameter microbubbles modeled in that experiment and that specific idea may be fanciful. Since that line of research has effectively ended, the Aziz et al. (2014) strand of foam development is likely the most feasible and most likely to be built upon, and there is no reason to discuss the future potential of the Seitz et al. (2010) microbubbles if and until laboratory work begins on that concept. The properties of Seitz et al. (2010) are based on an optimal bubble diameter and a very specific distribution of the bubbles, which may not be physically realistic for several reasons. For example, since the bubble lifetime matters, and the properties of a surfactant are not formally taken into account in modeling the bubbles, the bubbles must either be instantaneously replenished as needed or have permanent

lifetimes.

Absent breakthroughs in microbubble research, the ability to excite climate feedbacks with ocean mirrors is currently and may remain impossible for a very long time. However, the G4Foam feedbacks could be what is needed if stratospheric SRM caused a weakened tropical hydrological cycle and if stratospheric SRM along were insufficient to limit the damage of heat stress in the tropics. It would be wonderful to see more research in this area, as microbubble deployment in biologically unproductive areas of the ocean could be an effective and low-impact form of geoengineering.

# CHAPTER 6: CONCLUSIONS

Changes in ENSO are either not present in GeoMIP G1-G4 output, or not detectable, due to the short simulation duration and to the large inherent variability of ENSO. The changes in precipitation distribution and monsoon strength relative to AGW or the historical climate under G1-G4 cannot be attributed to changes in ENSO.

After determining that no possible MCB scheme could be an effective method of cooling Earth without reducing tropical precipitation, in heavily populated, highly cultivated tropical regions, I developed the G4Foam experiment, which achieved significant global cooling and a large redistribution of precipitation from ocean to land. No direct forcing was applied to tropical latitudes, but G4Foam cooled the tropics by 0.6 K, while increasing precipitation in most areas, including areas that typically get drier with global warming. However, the SH regional forcing was, as expected, not effective in cooling NH continents.

In an attempt to cool the entire planet while maintaining tropical precipitation at present day levels, I combined stratospheric SRM and regional ocean albedo enhancement in designing the G4SSAFoam experiment. In this experiment, 1.5 K of global mean cooling was achieved and tropical precipitation remained at or near RCP6.0 levels and slightly above G4SSA levels. However, the spatial distribution of positive and negative precipitation and *P-E* anomalies in the tropics was heterogeneous, with some heavily populated areas experiencing large increases, while others would suffer large decreases. The severe cooling of about 2 K in the SH extratropics would cause a precipitation reduction of almost 6% in G4SSAFoam when compared to RCP6.0. While *P-E* anomalies over land in the SH were only negative in certain regions, future research

would be needed to determine if these SH extratropical temperature and precipitation perturbations are too large to adapt to. Deployment of microbubbles in the ocean is currently not possible and significant innovation would need to occur if a need to conduct geoengineering in the manner of G4Foam arose, for example, in the event of a stratospheric SRM deployment that reduced tropical precipitation too much or reduced tropical temperature too little.

The question of whether it is possible to cool the entire planet without causing regional inequities in precipitation and temperature remains open. The question of whether it is possible to apply regional climate forcings in an attempt to trigger global scale feedbacks that lead to cooling climate feedbacks and changes in the distribution of precipitation is important. While many simulations show that most, if not all, regions of Earth will experience less climate change related damage under a regime of stratospheric SRM than under global warming alone, it is possible that disparate regional impacts may need to be addressed.

Supplementing stratospheric SRM with regional geoengineering may be a way to address this potential problem. This is not only important to the regions that may potentially experience these impacts, but to regions of the world that benefit from geoengineering. If geoengineering can be done in such a way to avoid regional inequities that have impacts on human and ecological systems, the governance of geoengineering would likely exist in a background of international comity about the geoengineering program. However, if regional inequities resulted in objections from particular nations or political subdivisions, these inequities could be the basis for be significant disagreement

about the nature, intensity and duration of any geoengineering program that is implemented.

The success in achieving specific climate objectives through regional geoengineering, as simulated in G4Foam and G4SSAFoam, requires manipulating the dynamics of the ocean-atmosphere system. Changing the atmospheric circulation in the way demonstrated in G4Foam and G4SSFoam brought about a climate in which deficits of precipitation were triggered as a consequence of the circulation anomalies induced. These circulation anomalies induced by the forcing enhance or maintain precipitation in highly cultivated and heavily populated tropical regions, including the large area across the southern Arabian peninsula and the Sahel which is prone to drought, but cause severe rainfall deficits across the Pacific Islands and Madagascar. Therefore, the type of regional geoengineering applied in this thesis has its own profile regional inequities, which must also be considered.

Additionally, it is not known what climate objectives will be chosen, how they will be chosen or to what extent the process of identifying and addressing these objectives will be subjective. In the conceptually simpler case of identifying the best uniform aerosol optical depth in the context of stratospheric SRM, it is possible that different regions will have different preferences and there is no fully objective arbiter of what is best for the human collective in place to decide what aerosol optical depth would be best. Therefore, the decision as to what aerosol optical depth is chosen may be made in such a way to benefit some more than others.

For the sake of simplicity, it is useful to pose the results of G4Foam in the simplest way possible. G4Foam is a method of regional geoengineering that creates more

precipitation in heavily populated areas and reduces population in less heavily populated areas. But people in the less populated areas still need robust agriculture and commerce. It would require research from other disciplines to determine whether imposing such a regime would be ethical. It would require economic and agricultural modeling to determine if the redistribution of precipitation would create such severe problems in smaller, but still not unpopulated regions, that there would be a significant global burden to take care of these inequities.

There are ways in which I could have arranged the placement of the foam that I did not do because I do not have the expertise to be certain that even doing the experiment in a way to achieve other, less benevolent climate objectives, and reporting the results, would be ethical. Adding regional geoengineering that has the impacts of G4Foam and G4SSAFoam to the list of available geoengineering techniques would greatly broaden the range of climate objectives that could be achieved. The large array of potential climate objectives may cause much larger disagreements between regions about what form of geoengineering should be imposed than the simple, but still very difficult to address dilemma of setting a uniform aerosol optical depth. This dichotomization of regional interests would force the imposition of a governance regime in a context where many conflicting interests would need to be represented and reconciled. Should regional geoengineering receive additional attention, future research should address its governability and to what extent to range of regional geoengineering options could be constrained to only include strategies that would benefit the human collective. Even then it is unknowable whether knowingly disrupting Earth that hurts some people but benefits the human collective in the aggregate is ethical.

## References

Alterskjaer, K., Kristjánsson, J.E., Boucher, O., Muri, H., Niemeier, U., Schmidt, H., Schulz, M. and Timmreck, C.: Sea-salt injections into the low-latitude marine boundary layer: The transient response in three Earth system models, J. Geophys. Res. Atmos., 118, 12,195–206, doi:10.1002/2013JD020432, 2013.

Anikiev, V.V., Mishukov, V.F. and Moiseevsky, G.N.: The effect of oil films on water evaporation and oxygen content in sea water, GeoJournal, 16:19-24, 1988.

Arora, V. K., Scinocca, J. F., Boer, G. J., Christian, J. R., Denman, K. L., Flato, G. M., Kharin, V. V., Lee, W. G., and Merryfield, W. J.: Carbon emission limits required to satisfy future representative concentration pathways of greenhouse gases, Geophys.Res. Lett., 38, L05805, 2011.

Aziz, A., Hailes, H.C., Ward, J.M. and Evans, J.R.G.: Long-term stabilization reflective foams in seawater. Royal Society of Chemistry, 95, 53028–53036. 2014.

Bellenger, H., Guilyardi, E., Leloup, J., Lengaigne, M., and Vialard, J.: ENSO representation in climate models: from CMIP3 to CMIP5, Clim. Dyn., 42, 1999-2018, 2013.

Bjerknes, J.: Atmospheric teleconnections from the equatorial Pacific, Mon. Wea. Rev., 97, 163–172, 1969.

Bonan, G. B., Lawrence, P. J., Oleson, K. W., Levis, S., Jung, M., Reichstein, M., Lawrence, D. M., and Swenson, S. C.: Improving canopy processes in the Community Land Model version 4 (CLM4) using global flux fields empirically inferred from FLUXNET data, J. Geophys. Res., 116, G02014, doi:10.1029/2010JG001593, 2011.

Broccoli, A. J., Dahl, K. A. and Stouffer, R.J.: The response of the ITCZ to Northern Hemisphere cooling. Geophys. Res. Lett., 33, L01702, doi:10.1029/2005GL024546, 2006.

Cai W., Van Rensch P., Cowan T. and Hendon H.H.: Teleconnection pathways for ENSO and the IOD and the mechanism for impacts on Australian rainfall, J. Climate, 24:3910–3923, doi:10.1175/2011JCLI4129.1, 2011.

Cai, W., Wang G., Santoso, A., McPhaden, M., Wu, L., Jin, F-F, Timmermann, A., Collins, M., Vecchi, G., Lengaigne, M., England, M., Dommenget, D., Takahashi, K., and Guilyardi, E.: Increasing frequency of extreme El Niño events due to greenhouse warming. Nature Climate Change, 4, 111-116, 2014.

Cai, W., Wang, G., Santoso, A., McPhaden, M., Wu, L., Jin F-F., Timmermann, A., Collins, M., Vecchi, G., Lengaigne, M., England, M., Dommenget, D., Takahashi, K., and Guilyardi, E.: Increased frequency of extreme La Niña events under greenhouse warming. Nature Climate Change, 5, 132-137, 2015.

Caldeira, K., and Myhrvold, N. P.: Projections of the pace of warming following an abrupt increase in atmospheric carbon dioxide concentration. Environ. Res. Lett., 8, 034039, 2013.

Cheng Y, Li S.M., Leithead A., Brickell P.C., and Leaitch, W.R.: Characterizations of cis-pinonic acid and n-fatty acids on fine aerosols in the Lower Fraser Valley during Pacific 2001 Air Quality Study, Atmospheric Environment, 38:5789–5800, 2004.

Chiang, J. C. H. and Bitz, C. M.: Influence of high latitude ice cover on the marine Intertropical Convergence Zone. Climate Dynamics 25, 477–496, 2005.

Clement, A. C., Seager, R., Cane, M.,A. and Zebiak, S.,E.: An ocean dynamical thermostat. J. Climate, 9, 2190-2196, 1996.

Cobb, K. M., Westphal, N., Sayani, H. R., Watson, J. T., Di Lorenzo, E., Cheng, H., Edwards, R. L., and Charles, C. D.: Highly variable El Niño-Southern Oscillation throughout the Holocene, Science, 339 (6115), 67-70, 2013.

Collins, W. J., Bellouin, N., Doutriaux-Boucher, M., Gedney, N., Halloran, P., Hinton, T., Hughes, J., Jones, C. D., Joshi, M., Liddicoat, S., Martin, G., O'Connor, F., Rae, J., Senior, C., Sitch, S., Totterdell, I., Wiltshire, A., and Woodward, S.: Development and evaluation of an Earth-System model – HadGEM2, Geosci. Model Dev., 4, 1051–1075, 2011.

Chiang, J. C. H. and Bitz, C. M. Influence of high latitude ice cover on the marine Intertropical Convergence Zone, Climate Dynamics 25, 477–496, 2005.

Crutzen, P.: Albedo enhancement by stratospheric sulfur injections: A contribution to solve a policy dilemma?, Climatic Change, 77, 211–219, 2006.

Cvijanovic, I., Caldeira, K., and MacMartin, D.G.: Impacts of ocean albedo alteration on Arctic sea ice restoration and Northern Hemisphere climate, Environmental Research Letters, 10, 044020, doi:10.1088/1748-9326/10/4/044020, 2015.

D'Agostino, R. B., Belanger A., and Ralph B.: A suggestion for using powerful and informative tests of normality. The American Statistician 44, 316–321, 1990.

Dai, Y., Zeng X. B., Dickinson R. E., Baker I., Bonan, G. B., Bosilovich, M. G., Denning A. S., Dirmeyer P. A., Houser P. R., Niu G. Y., Oleson K. W., Schlosser C. A., and Yang Z.-L.: The Common Land Model (CLM), Bull. Am. Meteorol. Soc., 84, 1013–1023, 2003.

Damodaran, S.: Protein Stabilization of Emulsions and Foams J. Food Sci., 70, R54–R66, 2005.

Decarlo, L.T.: On the meaning and use of kurtosis, Psychological Methods 2, 292-307, 1997.

DeSzoeke, S. P., Verlinden, K. L., Yuter, S. E., and Mechem, D. B.: The Time Scales of Variability of Marine Low Clouds, J. Climate, 29, 6463–6481, doi:10.1175/JCLI-D-15-0460.1, 2016.

Dickinson, E.: Food colloids research: historical perspective and outlook.

Adv. Colloid Interface Sci., 165, 7–13, 2011.

Dufresne, J. L., Foujols, M. A., Denvil, S., Caubel, A., Marti, O., Aumont, O, Balkanski, Y., Bekki, S , Bellenger, H., Benshila, R., Bony, S., Bopp, L., Braconnot, P., Brockmann, P., Cadule, P., Cheruy, F , Codron, F , Cozic, A , Cugnet, D., de Noblet, N., Duvel, J,P., Ethé, C., Fairhead, L., Fichefet, T., Flavoni, S., Friedlingstein, P., Grandpeix, J. Y., Guez, L., Guilyardi, E., Hauglustaine, D., Hourdin, F., Idelkadi, A., Ghattas, J., Joussaume, S., Kageyama, M., Krinner, G., Labetoulle, S., Lahellec, A., Lefebvre, M. P., Lefevre, F., Levy, C., Li, Z. X., Lloyd, J., Lott, F., Madec, G., Mancip, M., Marchand, M., Masson, S., Meurdesoif, Y., Mignot, J., Musat, I., Parouty, S., Polcher, J., Rio, C., Schulz, M., Swingedouw, D., Szopa, S., Talandier, C., Terray, P., Viovy, N., and Vuichard, N.: Climate change projections using the IPSL-CM5 Earth System Model: from CMIP3 to CMIP5, Clim. Dynamics, 40, 2123-2165, 2013.

Dykema J.A., Keith D.W., Anderson J.G., Weisenstein, D.: Stratospheric controlled perturbation experiment: a small-scale experiment to improve understanding of the risks of solar geoengineering, Phil. Trans. R. Soc. A 372, 20140059, doi:10.1098/rsta.2014.0059, 2014.

Emile-Geay, J., Seager, R., Cane, M. A., Cook, E. R., and Haug, G.H.: Volcanoes and ENSO over the past millennium, J. Climate, 21(13), 3134–3148, 2007.

Emori, S. and Brown, S.J.: Dynamic and thermodynamic changes in mean and extreme precipitation under changed climate, Geophysical Research Letters, 321,17, doi: 10.1029/2005GL023272, 2005**.**

Fingas, M.F.: The Evaporation of Oil Spills: Development and Implementation of New Prediction Methodology. International Oil Spill Conference Proceedings, No. 1, 281-287, 1999.

Fischbach, J.R., Lempert, R.J., Molina-Perez, E., Tariq, A.A., Finucane, M.L., Hoss, F.: Managing water quality in the face of uncertainty: A robust decision making demonstration for EPA's national water program, Santa Monica, CA: RAND Corporation, http://www.rand.org/pubs/research_reports/RR720.html. Also available in print form, 2015.

Fleitmann, D., Burns, S.J., Mudelsee, M., Neff, U., Kramers, J., Mangini, A., Matter, A., 2003a. Holocene forcing of the Indian monsoon recorded in a stalagmite from Southern Oman, Science, 300, 1737–1739.

Folland, C. K., Parker, D. E and Palmer, T. N.: Sahel rainfall and worldwide sea temperatures 1901–85, Nature, 320, 602–607, 1986.

Frierson, D. M. W. and Hwang, Y-T: Extratropical influence on ITCZ shifts in slab ocean simulation of global warming, J. Clim. 25, 720–733, 2012.

Fuss S., Canadell J.G. and Peters G.P.: Betting on negative emissions. Nat Clim Chang 4: 850–853, 2014.

Gabriel, C. J. and Robock, A.: Stratospheric geoengineering impacts on El Niño/Southern Oscillation, Atmos. Chem. Phys., 15, 11949-11966, doi:10.5194/acp-15-11949-2015, 2015.

Gabriel, C. J., Robock, A., Xia, L., Zambri, B., and Kravitz, B.: The G4Foam Experiment: global climate impacts of regional ocean albedo modification, Atmos. Chem. Phys., 17, 595-613, doi:10.5194/acp-17-595-2017, 2017.

Gergis J. L., and Fowler, A.M.: How unusual was late twentieth century El Niño-Southern Oscillation? Adv. Geosci., 6, 173–79, 2006.

Giorgetta, M. A., Jungclaus, J. H., Reick, C. H., Legutke, S., Bader, J., Böttinger, M., Brovkin, V., Crueger, T., Esch, M., Fieg, K., Glushak, K., Gayler, V., Haak, H., Hollweg, H.-D., Ilyina, T., Kinne, S., Kornblueh, L., Matei, D., Mauritsen, T., Mikolajewicz, U., Mueller, W. A., Notz, D., Pithan, F., Raddatz, T., Rast, S., Redler, R., Roeckner, E., Schmidt, H., Schnur, R., Segschneider, J., Six, K., Stockhause, M., Timmreck, C., Wegner, J., Widmann, H., Wieners, K.-H., Claussen, M., Marotzke, J., and Stevens, B.: Climate and carbon cycle changes from 1850 to 2100 in MPI-ESM simulations for the coupled model intercomparison project phase 5. J. Adv. Modeling Earth Sys., 5, 572-597, 2013.

Guilyardi E., Wittenberg, A., Fedorov, A., Collins, M., Wang, C., Capotondi, A., Oldenborgh, G. J. V., and Stockdale, T.: Understanding El Niño in ocean-atmosphere general circulation models : progress and challenges. Bull. Amer. Met. Soc., 90, 325-340, 2009.

Guilyardi E., Bellenger, H., Collins, M., Ferrett, S., Cai, W., and Wittenberg, A.: A first look at ENSO in CMIP5. CLIVAR Exchanges, 58, 29-32, 2012.

Gülseren, I., Fang, Y. and Corredig, M.: Complexation of high methoxyl pectin with with ethanol desolvated whey protein nanoparticles: physico-chemical properties and encapsulation behavior, 3, 859-866, 2012.

Hardman-Mountford, N. J.,Polimene, L., Hirata, T., Brewin, R. J. W. and Aiken, J.: Impacts of light shading and nutrient enrichment geoengineering approaches on the productivity of a stratified, oligotrophic ocean ecosystem, J. R. Soc. Interface, 10, 20130701, doi:10.1098/rsif.2013.0701, 2013.

Haywood, J. M., Jones, A., Bellouin, N. and Stephenson, D.: Asymmetric forcing from stratospheric aerosols impacts Sahelian rainfall, Nat. Clim. Change, 3(7), 660–665, doi:10.1038/nclimate1857, 2013.

Held, I. M. and Soden, B. J.: Robust responses of the hydrological cycle to global warming, J. Climate, 19, 5686–5699, 2006.

Held, I. M., Winton, M., Takahashi, K., Delworth, T., Zeng, F., and Vallis, G. K.: Probing the fast and slow components of global warming by returning abruptly to preindustrial forcing. J. Climate, 23, 2418–2427, 2010.

Hill, S., and Y. Ming, Y.: Nonlinear climate response to regional brightening of tropical marine stratocumulus, Geophys. Res. Lett., 39, L15707, doi:10.1029/2012GL052064, 2012.

Hurley, J. V. and Boos, W. R.: Interannual variability of monsoon precipitation and local subcloud equivalent potential temperature. J. Climate, 26, 9507–9527, 2013.

Hwang, Y.-T., Frierson, D. M. W. and Kang, S. M.: Anthropogenic sulfate aerosol and the southward shift of tropical precipitation in the late 20th century, Geophys. Res. Lett., 40, doi:10.1002/grl.50502, 2013.

IPCC: Summary for Policymakers, in: Climate Change 2013: The Physical Science Basis. Contribution of Working Group I to the Fifth Assessment Report of the Intergovernmental Panel on Climate Change, edited by: Stocker, T. F., Qin, D., Plattner, G.-K., Tignor, M., Allen, S. K., Boschung, J., Nauels, A., Xia, Y., Bex, V., and Midgley, P. M., Cambridge University Press, Cambridge, UK and New York, NY, USA, 2013.

Irvine, P. J., Ridgwell, A. and Lunt, D. J.: Climatic effects of surface albedo geoengineering, J. Geophys. Res., 116, D24112, doi:10.1029/2011JD016281, 2011.

Jenkins, A. K. L., Forster, P. M., and Jackson, L. S.: The effects of timing and rate of marine cloud brightening aerosol injection on albedo changes during the diurnal cycle

of marine stratocumulus clouds, Atmos. Chem. Phys., 13, 1659-1673, doi:10.5194/acp-13-1659-2013, 2013.

Jones A., Haywood, J. and Boucher, O.: Climate impacts of geoengineering marine stratocumulus clouds, J. Geophys. Res., 114, D10106, doi:10.1029/2008JD011450, 2009.

Jones, A., Haywood, J., Boucher, O., Kravitz, B., and Robock, A.: Geoengineering by stratospheric $SO_2$ injection: Results from the Met Office HadGEM2 climate model and comparison with the Goddard Institute for Space Studies ModelE. *Atmos. Chem. Phys.*, **10**, 5999-6006, 2010.

Kang, S. M., Held, I. M., Frierson, D. M. W and Zhao, M.: The response of the ITCZ to extratropical thermal forcing: Idealized slab-ocean experiments with a GCM, J. Climate, 21, 3521–3532, 2008.

Kaplan, A., Cane, M., Kushnir, Y., Clement, A., Blumenthal, M., and Rajagopalan, B.: Analyses of global sea surface temperature 1856-1991, J. Geophys. Res., 103, 18,567-18,589, 1998.

Kay J. E., Wall C., Yettella V., Medeiros B., Hannay C., Caldwell P., and Bitz C.: Global climate impacts of fixing the Southern Ocean shortwave radiation bias in the community earth system model (CESM), J. Climate, 96, 1333–13349, doi:10.1175/JCLI- D-15-0358, 2016.

Keith, D. W., Duren, R. and MacMartin, D.G.: Field experiments on solar geoengineering: report of a workshop exploring a representative research portfolio. Philosophical Transactions of the Royal Society A., 372-20140175, 2014.

Kirtman, B. P., and Schopf, P. S.: Decadal variability in ENSO predictability and prediction. J. Climate, 11, 2804–2822, 1998.

Kravitz, B., Robock, A., Boucher, O., Schmidt, H., Taylor, K., Stenchikov, G. and Schulz, M.: The geoengineering model intercomparison project (GeoMIP), Atm. Sci. Lett., 12, 162-167, doi: 10.1002/asl.316. 201, 2011.

Kravitz, B., Rasch, P.J., Forster, P.M., Andrews, T., Cole, J.N.S., Irvine, P.J., Ji, D., Kristjánsson, J.-E., Moore, J.C., Muri, H., Niemeier, U., Robock, A., Singh, B., Tilmes, S., Watanabe, S. and Yoon, J.-H.: An energetic perspective on hydrological cycle changes in the Geoengineering Model Intercomparison Project (GeoMIP), J. Geophysical Research, 118, 13,087-13,102, doi:10.1002/2013JD020502, 2013.

Kravitz, B., Robock, A., Tilmes, S., Boucher, O., English, J. M., Irvine, P. J., Jones, A., Lawrence, M. G., MacCracken, M., Muri, H., Moore, J. C., Niemeier, U., Phipps, S. J., Sillmann, J., Storelvmo, T., Wang, H., and Watanabe, S.: The Geoengineering Model Intercomparison Project Phase 6 (GeoMIP6): simulation design and

preliminary results, Geosci. Model Dev. Discuss., 8, 4697–4736, doi:10.5194/gmdd-8-4697-2015, 2015.

Kravitz, B., MacMartin, D. G., Wang, H., and Rasch, P. J.: Geoengineering as a design problem, Earth Syst. Dynam., 7, 469-497, doi:10.5194/esd-7-469-2016, 2016.

Jones A., Haywood, J. and Boucher, O.: Climate impacts of geoengineering marine stratocumulus clouds, J. Geophys. Res., 114, D10106, doi:10.1029/2008JD011450, 2009.

Kay J.E., Wall C., Yettella V., Medeiros B., Hannay C., Caldwell P. and Bitz C.: Global climate impacts of fixing the Southern Ocean shortwave radiation bias in the community earth system model (CESM), J Climate, doi:10.1175/JCLI-D-15-0358, 2016.

Lamarque, J.-F., Emmons, L. K., Hess, P. G., Kinnison, D. E., Tilmes, S., Vitt, F., Heald, C. L., Holland, E. A., Lauritzen, P. H., Neu, J., Orlando, J. J., Rasch, P. J., and Tyndall, G. K.: CAM-chem: description and evaluation of interactive atmospheric chemistry in the Community Earth System Model, Geosci. Model Dev., 5, 369–411, doi:10.5194/gmd-5-369-2012, 2012.

Latham, J.: Control of global warming?, Nature, 347, 339–340, 1990.

Latham, J., Bower, K., Choularton, T., Coe, H., Connoly, P., Cooper, G., Craft, T., Foster, J., Gadian, A., Galbraith, L., Iacovides, H., Johnston, D., Launder, B., Leslie, B., Meyer, J., Neukermans, A., Ormond, B., Parkes, B., Rasch, P., Rush, J., Salter, S., Stevenson, T., Wang, H., Wang, Q., and Wood, R.: Marine cloud brightening, Phil. Trans. R. Soc. A, 370, 4217–4262, doi:10.1098/rsta.2012.0086, 2012.

Li, J., Xie, S.-P., Cook E. R., Morales, M., Christie, D., Johnson, N., Chen, F., D'Arrigo, R., Fowler, A., Gou, X., and Fang, K.: El Niño modulations over the past seven centuries. Nature Climate Change, 3, 822–826, 2013.

MacMartin, D.G. and Tziperman, E.: Using transfer functions to quantify El Niño Southern Oscillation dynamics in data and model, Proceedings of The Royal Society A, 470(2169):20140272, 2014.

Maher, N., McGregor, S., England, M. H., and Gupta, A. S.: Effects of volcanism on tropical variability. Geophys. Res. Lett., 42(14): 6024-6033, 2015.

Manabe, S. and Stouffer, R. J.: Sensitivity of a global climate model to an increase of $CO_2$ concentration in the atmosphere, J. Geophys. Res.. 85, 5529–5554, 1980.

Mann, M. E., Cane, M. A., Zebiak, S. E., and Clement, A.: Volcanic and solar forcing of the tropical Pacific over the past 1000 years, J. Climate, 18, 447-456, 2005.

Mauritsen, T.: Global warming: Clouds cooled the Earth, Nature Geoscience, 9, 12, 865-867, 2016, 10.1038/ngeo2838, 2016.

McGregor, S., Timmermann, A., England, M. H., Elison Timm, O., and Wittenberg, A. T.: Inferred changes in El Niño–Southern Oscillation variance over the past six centuries, Clim. Past, 9, 2269-2284, 2013.

McPhaden, M. L., Zebiak, S. E., and Glantz, M. H.: ENSO as an integrating concept in earth science. Science, 314, 1739–1745, 2006.

Mechoso, C., Wood, R., Weller, R., Bretherton, C. S., Clarke, A., Coe, H., Fairall, C., Farrar, J. T., Feingold, G., and Garreaud, R.: Ocean-cloud-atmosphere-land interactions in the southeastern Pacific: The VOCALS Program, B. Am. Meteorol. Soc., 95, 357–375, 2014.

Meehl, G. A., Arblaster, J. M., Caron, J. M., Annamalai, H., Jochum, M., Chakraborty, A., and Murtugudde, R.: Monsoon regimes and processes in CCSM4. Part I: The Asian-Australian Monsoon, J. Climate, 25, 2583–2608, 2012.

Meinshausen, M., Smith, S. J., Calvin, K., Daniel, J. S., Kainuma, M. L. T., Lamarque, J.-F., Matsumoto, K., Montzka, S. A., Raper, S. C. B., Riahi, K., Thomason, A., Velders, G. J. M., and van Vuuren, D. P. P.: The RCP greenhouse gas concentrations and their extension from 1765 to 2300, Climatic Change, 109, 213– 241, doi:10.1007/s10584-011-0156-z, 2011.

Mengis, N., Martin, T., Keller, D. P., and Oschlies, A.: Assessing climate impacts and risks of ocean albedo modification in the Arctic, J. Geophys. Res.-Oceans, 121, 3044–3057, doi:10.1002/2015JC011433, 2016.

Miller, K. G., Kopp, R.E., Horton, B.P., Browning, J.V. and Kemp, A.C.: A geological perspective on sea-level rise and its impacts along the U.S. mid-Atlantic coast. Earth's Future 1, 3–18. doi: 10.1002/ 2013EF000135, 2013.

Nagata, T., Meon, B. and Kirchman, D.L.: Microbial degradation of peptidoglycan in seawater, Limnol. Oceanogr., 48, 745–754, 2004.

Neely III, R. R., Conley, A. J., Vitt, F., and Lamarque, J.-F.: A consistent prescription of stratospheric aerosol for both radiation and chemistry in the Community Earth System Model (CESM1), Geosci. Model Dev., 9, 2459-2470, doi:10.5194/gmd-9-2459, 2016.

Partanen, A.-I., Kokkola, H., Romakkaniemi, S., Kerminen, V.-M., Lehtinen, K.E.J., Bergman, T., Arola, A. and Korhonen, H.: Direct and indirect effects of sea spray geoengineering and the role of injected particle size, J. Geophys. Res., 117, D02203, doi:10.1029/2011JD016428, 2012.

Partanen, A.-I., Keller, D.P., Korhonen, H. and Matthews, H.D.: Impacts of sea spray geoengineering on ocean biogeochemistry, Geophys. Res. Lett., 43, 7600–7608, doi:10.1002/2016GL070111, 2016.

Patino, J. M. R., Sanchez, C.C. and Nino, M.R.R.: Implications of interfacial characteristics of food foaming agents in foam formulations, Adv. Colloid Interface Sci., 140, 95–113, 2008.

Phipps, S. J., Rotstayn, L. D., Gordon, H. B., Roberts, J. L., Hirst, A. C., and Budd, W. F.: The CSIRO Mk3L climate system model version 1.0 - Part 1: Description and evaluation, Geoscientific Model Dev., 4, 483-509, 2011.

Phipps, S. J., Rotstayn, L. D., Gordon, H. B., Roberts, J. L., Hirst, A. C., and Budd, W. F.: The CSIRO Mk3L climate system model version 1.0 - Part 2: response to external forcings, Geoscientific Model Dev., 5, 649-682, 2012.

Power, S. B., and Smith, I. N.: Weakening of the Walker Circulation and apparent dominance of El Niño both reach record levels, but has ENSO really changed? Geophys. Res. Lett., 34, L18702, 2007.

Pugh, R.J.: Foaming, foam films, antifoaming and defoaming, Adv. Colloid Interface Sci., 64, 67–142, 1996.

Rasch P. J., Latham, J. and Chen, C.C.: Geoengineering by cloud seeding: influence on sea ice and climate system, Environmental Research Letters, 4, 45-112. doi:10.1088/1748-9326/4/4/045112, 2009.

Reason, C. J. C.: Subtropical Indian Ocean SST dipole events and southern African rainfall Geophys. Res. Lett., 28, 2225-2228, 10.1029/2000GL012735, 2001.

Robock, A., L. Oman, L., and Stenchikov, G.: Regional climate responses to geoengineering with tropical and Arctic $SO_2$ injections, Journal of Geophysical Research, 113, D16101, doi: 10.1029/2008JD010050, 2008.

Robock, A.: 20 reasons why geoengineering may be a bad idea, Bull. Atomic Sci., 64, 14–18, doi:10.2968/064002006, 2008.

Robock, A., Marquardt, A., Kravitz, B., and Stenchikov, G.: The benefits, risks, and costs of stratospheric geoengineering. Geophys Res. Lett., 36, L19703, doi:10.1029/2009GL039209, 2009.

Robock, A.: Bubble, bubble, toil and trouble. An editorial comment, Climatic Change, 105, 383-385, doi:10.1007/s10584-010-0017-1, 2011.

Robock, A.: Stratospheric aerosol geoengineering, Issues Env. Sci. Tech. (special issue "Geoengineering of the Climate System"), 38, 162-185, 2014.

Russell, L. M., et al.: Ecosystem impacts of geoengineering: A review for developing a science plan, Ambio, 41(4), 350–69, doi:10.1007/s13280-012-0258-5, 2012.

Salter, S., Sortino, G., and Latham, J.: Sea-going hardware for the cloud albedo method of reversing global warming., Philos. T. Roy. Soc. A, 366, 3989–4006, doi:10.1098/rsta.2008.0136, 2008.

Sanderson B.M., O'Neill B., Tebaldi C.: What would it take to achieve the Paris temperature targets?, Geophys Res Lett, 1, 10, doi:10.1002/2016GL069563, 2016.

Schmidt, G. A., Ruedy, R., Hansen, J. E., Aleinov, I., Bell, N., Bauer, M., Bauer, S., Cairns, B., Canuto, V., Cheng, Y., Del Genio, A., Faluvegi, G., Friend, A. D., Hall, T. M., Hu, Y., Kelley, M., Kiang, N. Y., Koch, D., Lacis, A. A., Lerner, J., Lo, K. K., Miller, R. L., Nazarenko, L., Oinas, V., Perlwitz, J. P., Perlwitz, J., Rind, D., Romanou, A., Russell, G. L., Sato, M., Shindell, D. T., Stone, P. H., Sun, S., Tausnev, N., Thresher, D., and Yao, M. S.: Present-day atmospheric simulations using GISS ModelE: Comparison to in situ, satellite and reanalysis data, J. Climate, 19, 153–192, 2006.

Seitz, R.: Bright water: hydrosols, water conservation and climate change. Climatic Change, 105, 365–381, 2010.

Siegenthaler, U., Stocker, T. F., Monnin, E., Luthi, D., Schwander J., Stauffer, B., Raynaud, D., Barnola, J. M., Fischer, H., Masson, Delmotte, V., and Jouzel, J.: Stable carbon cycle-climate relationship during the late Pleistocene, Science, 310, 1313–1317, 2005.

Stuart, G. S., Stevens, R. G., Partanen, A.-I., Jenkins, A. K. L., Korhonen, H., Forster, P. M., Spracklen, D. V., and Pierce, J. R.: Reduced efficacy of marine cloud brightening geoengineering due to in-plume aerosol coagulation: parameterization and global implications, Atmos. Chem. Phys., 13, 10385-10396, doi:10.5194/acp-13-10385-2013, 2013.

Taylor, K. E., Stouffer, R. J., and Meehl, G. A.: An overview of CMIP5 and the experiment design, B. Am. Meteorol. Soc., 93, 485–498, doi:10.1175/BAMS-D-11-00094.1, 2012.

Tilmes, S., Fasullo, J., Lamarque, J.-F., Marsh, D. R., Mills, M., Alterskjaer, K., Muri, H., Kristjánsson, J. E., Boucher, O., Schulz, M., Cole, J. N. S., Curry, C. L., Jones, A., Haywood, J., Irvine, P. J., Ji, D., Moore, J. C., Karam, D. B., Kravitz, B., Rasch, P. J., Singh, B., Yoon, J.-H., Niemeier, U., Schmidt, H., Robock, A., Yang, S., and Watanabe, S.: The hydrological impact of geoengineering in the Geoengineering Model Intercomparison Project (GeoMIP), J. Geophys. Res.-Atmos, 118, 11036–11058, doi:10.1002/jgrd.50868, 2013.

Tilmes, S., Mills, M. J., Niemeier, U., Schmidt, H., Robock, A., Kravitz, B., Lamarque, J.-F., Pitari, G., and English, J. M.: A new Geoengineering Model Intercomparison Project (GeoMIP) experiment designed for climate and chemistry models, Geosci. Model Dev., 8, 43-49, doi:10.5194/gmd-8-43-2015, 2015.

.

Tilmes, S., Lamarque, J.-F., Emmons, L. K., Kinnison, D. E., Marsh, D., Garcia, R. R., Smith, A. K., Neely, R. R., Conley, A., Vitt, F., Val Martin, M., Tanimoto, H., Simpson, I., Blake, D. R., and Blake, N.: Representation of the Community Earth System Model (CESM1) CAM4-chem within the Chemistry-Climate Model Initiative (CCMI), Geosci. Model Dev., 9, 1853-1890, doi:10.5194/gmd-9-1853-2016, 2016.

Tokinaga, H., Xie, S.P., Deser, C., Kosaka, A., and Okumura, Y. M.: Slowdown of the Walker Circulation driven by tropical Indo-Pacific warming, Nature, 491, 439-443, 2012.

Trenberth, K. E., and Hoar, T. J.: El Niño and climate change. Geophys. Res. Lett., 24, 3057–3060, 1997.

Trenberth, K. E., and Dai, A.: Effects of Mount Pinatubo volcanic eruption on the hydrological cycle as an analog of geoengineering, Geophys. Res. Lett., 34, L15702, doi:10.1029/2007GL030524, 2007.

Twomey, S.: Pollution and planetary albedo, Atmos. Environ., 8, 1251–1256, doi:10.1016/0004-6981(74)90004-3, 1974.

Vecchi, G. A., Soden, B. J., Wittenberg, A. T., Held, I. M., Leetmaa, A., and Harrison, M. J.: Weakening of tropical Pacific atmospheric circulation due to anthropogenic forcing, Nature, 7089, 73-76, 2006.

Vecchi, G. A., and Soden, B. J.: Global warming and the weakening of the tropical circulation, J. Climate, 20, 4316–4340, 2007.

Watanabe, S., Hajima, T., Sudo, K., Nagashima, T., Takemura, T., Okajima, H., Nozawa, T., Kawase, H., Abe, M., Yokohata, T., Ise, T., Sato, H., Kato, E., Takata, K., Emori, S., and Kawamiya, M.: MIROC-ESM 2010: Model description and basic results of CMIP5-20c3m experiments, Geosci. Model Dev., 4, 845–872, 2011.

Whitlock, C.H., Bartlett, D.S. and Gurganus, E.A.: Sea foam reflectance and influence on optimum wavelength for remote sensing of ocean aerosols, Gurganus, Geophys. Res. Lett., 9, 719–722, 1982.

Wierenga, P.A. and Gruppen H.: New views on foams from protein solutions Curr. Opin. Colloid Interface Sci., 15, 365–373, 2010.

Wittenberg A.T, Rosati A., Delworth T.L., Vecchi G.A., Zeng F.: ENSO modulation: Is it decadally predictable? J Clim., 27(7):2667–2681, 2014.

Wood, R. and Bretherton, C. S.: Boundary layer depth, entrainment, and decoupling in the cloud-capped subtropical and tropical marine boundary layer, J. Climate, 17, 3576–3588, 2004.

Wood, R. and Bretherton, C. S.: On the relationship between stratiform low cloud cover and lower-tropospheric stability, J. Climate, 19, 6425–6432, 2006.

Xia, L., Robock, A., Tilmes, S., and Neely III, R. R.: Stratospheric sulfate geoengineering could enhance the terrestrial photosynthesis rate, Atmos. Chem. Phys., 16, 1479-1489, doi:10.5194/acp-16-1479-2016, 2016.

Xie, S-P. and Philander, S. G. H. A coupled ocean-atmosphere model of relevance to the ITCZ in the eastern Pacific, Tellus, 46A, 340–350, 1994.

Xu, Y., Wang, C., Tam, . K. C. and Li, L. Salt-Assisted and Salt-Suppressed Sol−Gel Transitions of Methylcellulose in Water , Langmuir, 20, 646–652, 2004.

Yeh, S. W., Ham, Y.-G., and Lee, J.-Y.: Changes in the tropical Pacific SST trend from CMIP3 to CMIP5 and its implication of ENSO. J Climate, 25, 7764–7771, 2012.

Zebiak, S. E., and Cane M. L.: A model El Niño/Southern Oscillation. Mon. Wea. Rev., 115, 2262–2278, 1987.

**Publications arising from this research and my contribution to this work.** The work included in this thesis has generated two refereed publications in *Atmospheric Chemistry and Physics* (*ACP*): Stratospheric Geoengineering Impacts on El Niño/Southern Oscillation (Gabriel and Robock, 2015) and The G4Foam Experiment: Global Climate Impacts of Regional Ocean Albedo Modification (Gabriel et al., 2017). *A third manuscript will be submitted describing the G4SSAFoam experiment.*

The first step in writing this dissertation was to analyze GeoMIP output from as many modeling groups as possible. A list of those models is provided in Table 3.1. The simulations analyzed in the ENSO portion of this thesis were conducted by numerous modeling groups, all around the world. The paper was written under the direction and with the suggestions of Dr. Robock.

The first step in writing this dissertation was to perform geoengineering simulations using the CESM-CAM4-Chem. Two sets of simulations of three ensemble members each were run. The runs commenced from Simone Tilmes (NCAR) RCP6.0 runs and Simone Tilmes designed the G4SSA aerosol distribution. G4SSA was used as a control run and the G4SSA forcing was also used in G4SSAFoam. Lili Xia produced a figure, based on a figure used in Xia et al. (2016) showing global photosynthesis rate changes. Brian Zambri helped calculate statistical significance in many of the comparisons. I developed idea for G4Foam and G4SSAFoam with Alan Robock, who provided supervision and direction during the climate modeling and the writing process.

Chapter 2 was prepared as part of writing a report on Geoengineering for Ocean Conservancy, a charity based in Washington, DC and Santa Cruz, CA, that is primarily concerned with the condition of the ocean ecosystem and of marine biota. The report was

not published by Ocean Conservancy and I retain the right to publish the material at my unrestrained pleasure, as per our contractor contract agreement, signed in November, 2016.

**Table 3.1.** The names of the climate models used in this ENSO study, with short names and references. Asterisks indicate that the models were excluded from comparison due to unrealistic ENSO variability.

| Model | Model short name | Reference |
|---|---|---|
| *BNU-ESM | BNU | Dai et al. (2003) |
| CanESM2 | CanESM | Arora et al. (2011) |
| CSIRO-Mk3L | CSIRO | Phipps et al. (2011,2012) |
| GISS-E2-R | GISS | Schmidt et al. (2006) |
| HadGEM2-ES | HadGEM | Collins et al. (2011) |
| IPSL-CM5A-LR | IPSL | Dufresne et al. (2012) |
| *MIROC-ESM | MIROC | Watanabe et al. (2011) |
| *MIROC-ESM-CHEM | MIROC-C | Watanabe et al. (2011) |
| MPI-ESM-LR | MPI | Giorgetta et al. (2012) |

**Table 3.2.** Models analyzed in each experiment. Asterisks indicate that the models that did not produce a realistic ENSO and were excluded. For a discussion of the excluded models, see 3.2 Results. For examples of typical ENSO variability in simulations from the excluded models, see figures 3.3 and 3.4. The number of ensemble members for each experiment is given in parenthesis after the model name.

**a. Models in G1**

*BNU-ESM (2)
CanESM2 (3)
CSIRO-Mk3L (3)
GISS-E2- (3)
HadGEM2-ES (1)
IPSL-CM5A-LR (1)
*MIROC-ESM (1)
MPI-ESM-LR (1)

**b. Models in G2**

*BNU-ESM (3)
CanESM2 (3)
CSIRO-Mk3L (3)
GISS-E2-R] (3)
HadGEM2-ES (3)
IPSL-CM5A-LR (1)
*MIROC-ESM (1)
MPI-ESM-LR (1)

**c. Models in G3**

*BNU-ESM (1)
GISS-E2-R (3)
HadGEM2-ES (2)
IPSL-CM5A-LR (1)
MPI-ESM-LR (3)

**d. Models in G4**

*BNU-ESM (2)
CanESM2 (3)
CSIRO-Mk3L (3)
GISS-E2-R (3)
HadGEM2-ES (1)
IPSL-CM5A-LR (1)
*MIROC-ESM (1)
*MIROC-ESM-CHEM (1)
MPI-ESM-LR (1)

**Table 3.3.** Difference in linear trend of Niño3.4 Index (5°S-5°N, 120°W-170°W) between each experiment G1-G4 and its control.

| | |
|---|---|
| G1 minus 4xCO2 | -0.18 K decade$^{-1}$ |
| G2 minus +1% $CO_2$ yr$^{-1}$ | -0.24 K decade$^{-1}$ |
| G3 minus RCP4.5 | -0.14 K decade$^{-1}$ |
| G4 minus RCP4.5 | -0.07 K decade$^{-1}$ |

**Table 4.1** Changes in temperature and precipitation in G4Foam relative to both G4SSA and RCP6.0, for the entire globe and for the Tropics (20°S-20°N) annually and in Northern Hemisphere summer, for the 40-year period beginning 10 years after the start of climate engineering.

| **Global, 2030-2069** | **G4Foam – G4SSA (% change)** | **G4Foam – RCP6.0 (% change)** |
|---|---|---|
| Precipitation (mm/day) | +0.02 (+0.61) | -0.06 (-1.98) |
| Land precipitation (mm/day) | +0.07 (+3.19) | +0.01 (+0.32) |
| Ocean precipitation (mm/day) | –0.01 (–0.36) | –0.08 (–2.57) |
| Temperature (K) | +0.27 | –0.53 |
| Land temperature (K) | +0.63 | –0.44 |
| **Global, 2030-2069,** June-July-August | | |
| Precipitation (mm/day) | +0.02 (+0.70) | -0.05 (-1.85) |
| Land precipitation (mm/day) | +0.08 (+3.35) | +0.02 (+0.70) |
| Ocean precipitation (mm/day) | +0.01 (-0.29) | –0.08 (–2.51) |
| Temperature (K) | +0.32 | –0.60 |
| Land temperature (K) | +0.71 | –0.53 |
| **Tropical**, **2030-2069** | | |
| Precipitation (mm/day) | +0.06 (+1.59) | –0.03 (–1.06) |
| Land precipitation (mm/day) | +0.16 (+3.93) | +0.07 (+1.43) |
| Ocean precipitation (mm/day) | +0.03 (+0.77) | –0.07 (–1.92) |
| Temperature (K) | +0.21 | –0.60 |
| Land temperature (K) | +0.43 | –0.61 |
| **Tropical, 2030-2069,** June-July-August | | |
| Precipitation (mm/day) | +0.06 (+1.52) | –0.03 (–0.84) |
| Land precipitation (mm/day) | +0.16 (+4.66) | +0.07 (+2.02) |
| Ocean precipitation (mm/day) | +0.03 (+0.67) | –0.06 (–1.61) |
| Temperature (K) | +0.18 | –0.61 |
| Land temperature (K) | +0.37 | –0.70 |

**Table 5.1.** Changes in temperature and precipitation in G4Foam relative to both G4SSAFoam and RCP6.0, for the entire globe and for the Tropics (20°S-20°N) annually and in Northern Hemisphere summer, for the 40-year period beginning 10 years after the start of climate engineering.

| **Global, 2030-2069** | **G4SSAFoam – G4SSA (% change)** | **G4Foam – RCP6.0 (% change)** |
|---|---|---|
| Precipitation (mm/day) | -0.05 (-1.91) | -0.13 (-4.56) |
| Land precipitation (mm/day) | 0.00 (-0.19) | -0.06 (-2.74) |
| Ocean precipitation (mm/day) | –0.07 (–2.31) | –0.14 (–4.71) |
| Temperature (K) | -0.53 | –1.45 |
| Land temperature (K) | -0.47 | –1.66 |
| **Global, 2030-2069,** June-July-August | | |
| Precipitation (mm/day) | -0.05 (-1.83) | -0.13 (-4.47) |
| Land precipitation (mm/day) | +0.01 (+0.55) | -0.05 (-1.90) |
| Ocean precipitation (mm/day) | -0.08 (-2.48) | –0.15 (–4.80) |
| Temperature (K) | -0.52 | –1.44 |
| Land temperature (K) | -0.47 | –1.72 |
| **Tropical**, **2030-2069** | | |
| Precipitation (mm/day) | -0.05 (-1.19) | –0.15 (–3.90) |
| Land precipitation (mm/day) | +0.04 (+0.98) | -0.05 (-1.24) |
| Ocean precipitation (mm/day) | -0.08 (+0.77) | –0.19 (–4.80) |
| Temperature (K) | -0.50 | –1.31 |
| Land temperature (K) | -0.52 | –1.58 |
| **Tropical, 2030-2069,** June-July-August | | |
| Precipitation (mm/day) | -0.05 (-1.29) | –0.14 (–3.61) |
| Land precipitation (mm/day) | +0.06 (+1.87) | -0.02 (-0.47) |
| Ocean precipitation (mm/day) | -0.09 (-2.14) | –0.18 (–4.47) |
| Temperature (K) | -0.54 | –1.34 |
| Land temperature (K) | -0.62 | –1.71 |

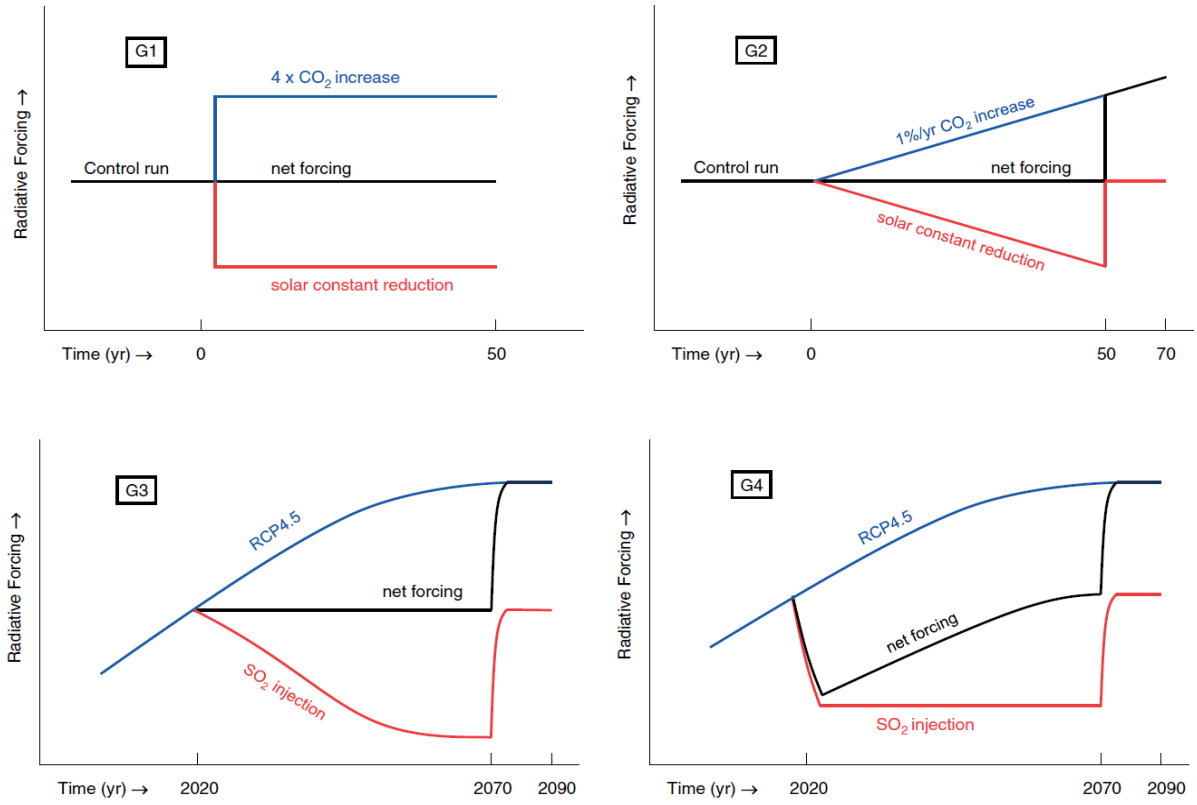


**Figure 3.1.** GeoMIP G1-G4 experiment designs. Figures 1-4 from Kravitz et al. (2011).

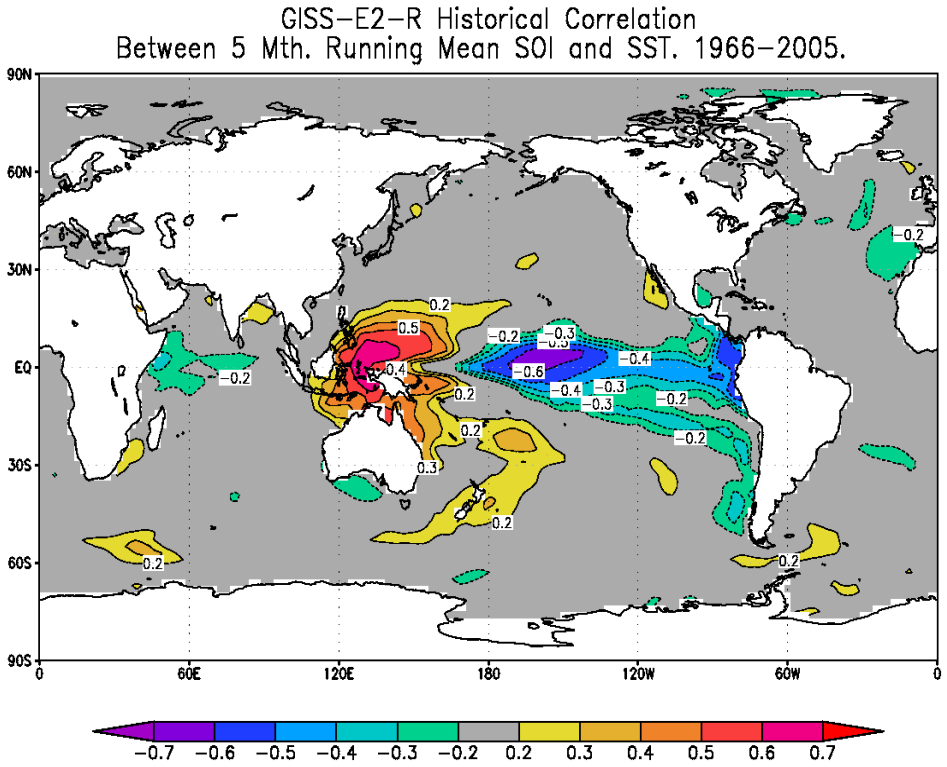


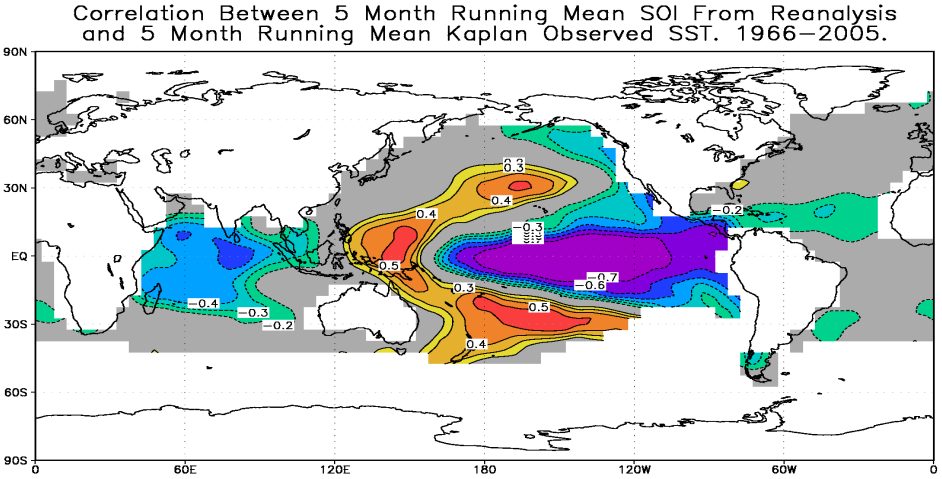


**Figure 3.2.** Top panel shows spatial correlation between GISS historical sea surface temperature (SST) and the Southern Oscillation Index (SOI). The area of strong negative correlation is confined to a small region in the central Pacific, relative to the broad area of strong negative correlation in the observations in the bottom panel, which shows the spatial correlation between NCEP SLP reanalysis and the Kaplan SST observations data set.

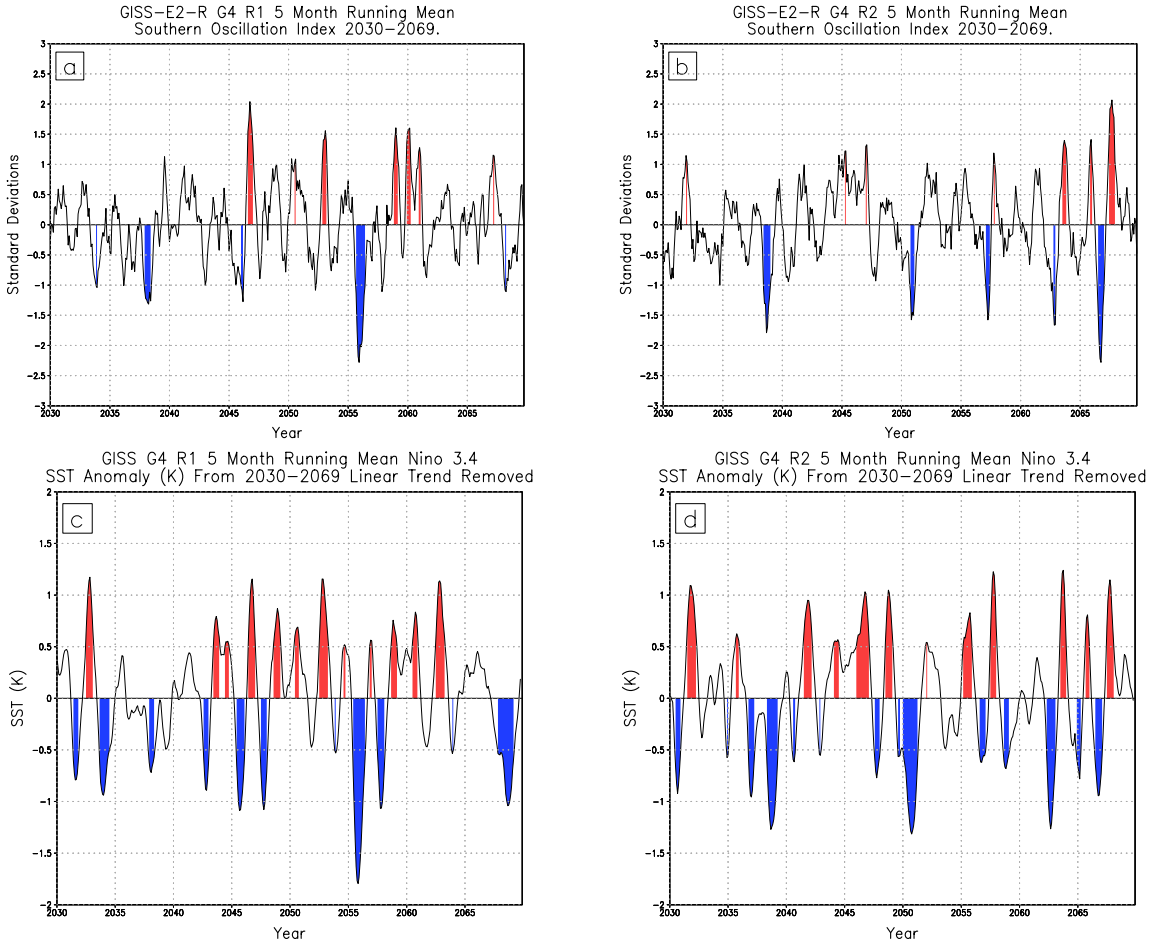


**Figure 3.3.** Time series of normalized Southern Oscillation Index (SOI) for (a) GISS G4 Run 1 and (b) GISS G4 Run 2. In the context of SOI, ENSO events are defined as departures of 0.5 standard deviations from zero. SOI warm events are highlighted in red, while cold events are highlighted in blue. No highlight is applied during an ENSO neutral phase. Time series of SST in Niño3.4 region for (c) GISS G4 Run 1 and (d) GISS G4 Run 2. The SST-based index in the bottom panel depicts more realistic ENSO variability, and therefore SOI is not used as an SST proxy.

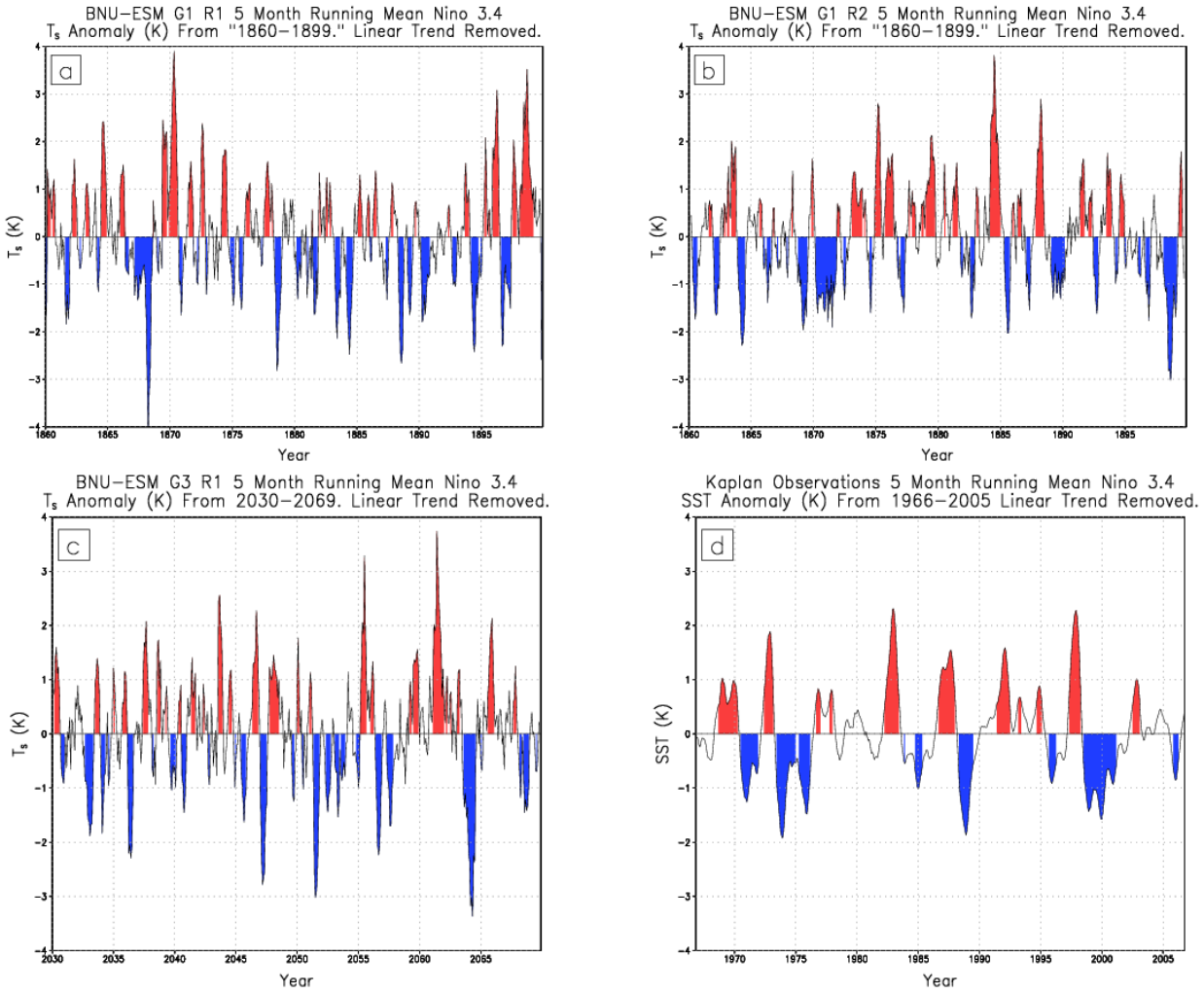


**Figure 3.4.** Time series of Niño3.4 anomalies from three experimental runs, (a) G1 run 1, (b) G1 run 2, and (c) G3 run 1, of the BNU-ESM model compared to observations (d). Red coloring indicates ENSO warm events, while blue shading indicates ENSO cold events. The model is excluded due to unrealistic variability and amplitude.

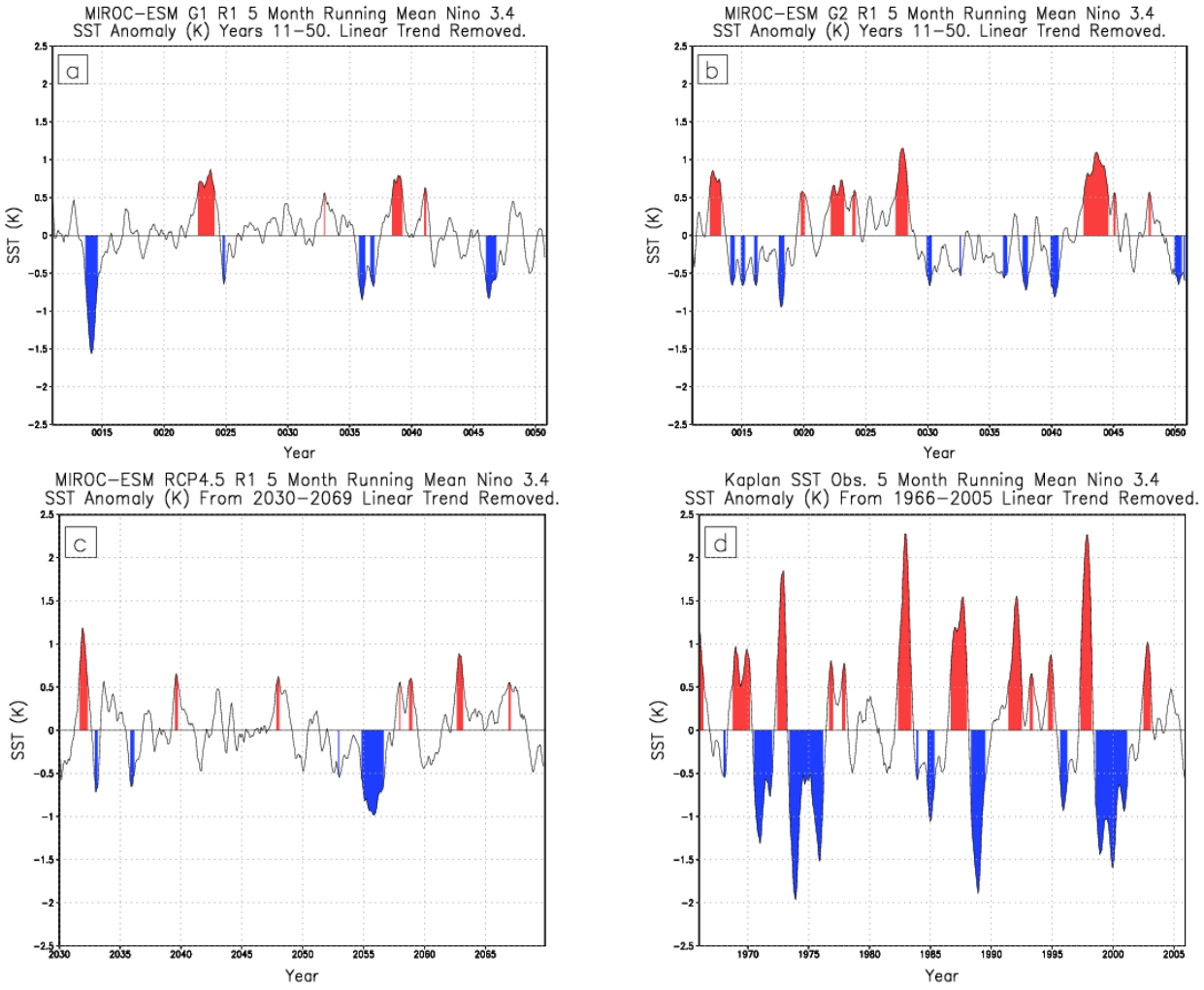


**Figure 3.5.** Niño3.4 anomalies for MIROC-ESM. Time series of (a) G1, (b) G2 and (c) RCP4.5 from each model all show significantly muted variability and amplitude compared to (d) observations, with few, if any, warm events exceeding a 1 K anomaly. All other MIROC family experiments showed the same muted variability. Cold event amplitude is essentially muted, with no 1 K or greater departures. The inability of the MIROC-ESM to depict a plausible ENSO cycle is also seen in the MIROC-ESM-CHEM. Therefore, both sets of model output were excluded.

**ENSO warm (red) and cold (blue) events per 40 year period. Mean of all ensembles from all models within each experiment or control. Error bars indicate one standard deviation.**

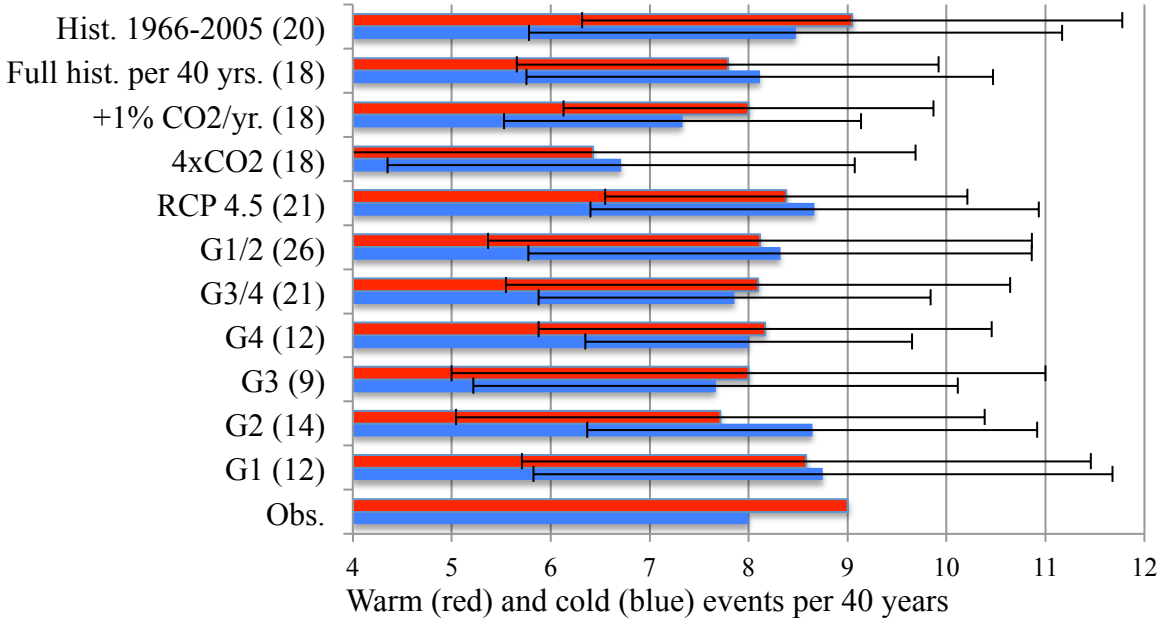


| | Obs. | G1 (12) | G2 (14) | G3 (9) | G4 (12) | G3/4 (21) | G1/2 (26) | RCP4.5 (21) | 4XCO2 (18) | +1% $CO_2$ /yr. (18) | 1850-2005 /40 yr. (18) | 1966-2005 (18) |
|---|---|---|---|---|---|---|---|---|---|---|---|---|
| Warm events | 9.00 | 8.58 | 7.71 | 8.00 | 8.17 | 8.10 | 8.12 | 8.38 | 6.43 | 8.00 | 7.79 | 9.05 |
| Cold events | 8.00 | 8.75 | 8.64 | 7.67 | 8.00 | 7.86 | 8.32 | 8.67 | 6.71 | 7.33 | 8.11 | 8.48 |

**Figure 3.6.** Number of ENSO warm (red) or cold (blue) events simulated or observed between 2030-2069 for G3, G4, RCP4.5, Years 11-50 for G1, G2, +1% $CO_2$ $yr^{-1}$ increase and 4x CO2, and 1966-2005 for historical simulations and observations for the CanESM, CSIRO, GISS, HadGEM, IPSL and MPI models. The full historical record spans 1850-2005 and the number of events reported for this period is the per 40 year frequency of warm or cold events in this full record. Values in parentheses are the number of ensemble members for each experiment or family of experiments. Error bars represent plus or minus one standard deviation of ENSO events relative to the experiment mean. A table of values is provided under the graph.

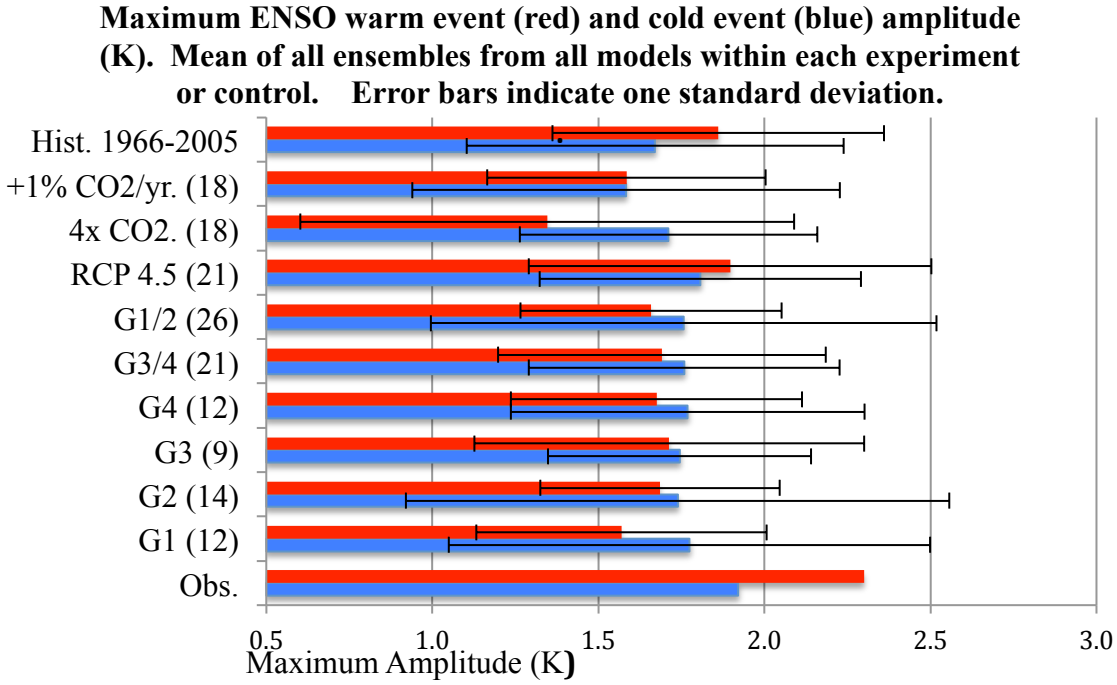


| | Obs. | G1 (12) | G2 (14) | G3 (9) | G4 (12) | G3/4 (21) | G1/2 (26) | RCP4.5 (21) | 4XCO2 (18) | +1% $CO_2$/yr. (18) | 1966-2005 (18) |
|---|---|---|---|---|---|---|---|---|---|---|---|
| Warm amp. | 2.30 | 1.57 | 1.69 | 1.71 | 1.68 | 1.69 | 1.66 | 1.90 | 1.35 | 1.58 | 1.86 |
| Cold amp. | 1.92 | 1.77 | 1.74 | 1.74 | 1.77 | 1.76 | 1.76 | 1.81 | 1.71 | 1.58 | 1.67 |

**Figure 3.7.** Maximum amplitude (K) of ENSO warm (red) or cold (blue) events simulated or observed between 2030-2069 for G3, G4, RCP4.5, Years 11-50 for G1, G2, +1% $CO_2$ $yr^{-1}$ increase and 4x CO2, and 1966-2005 for historical simulations and observations . Values in parenthesis following y-axis (model name) labels indicate the number of ensemble members, inclusive of all experiment designs, run by the particular model. Error bars show plus or minus one standard deviation relative to the model mean. A table of values is provided under the graph.

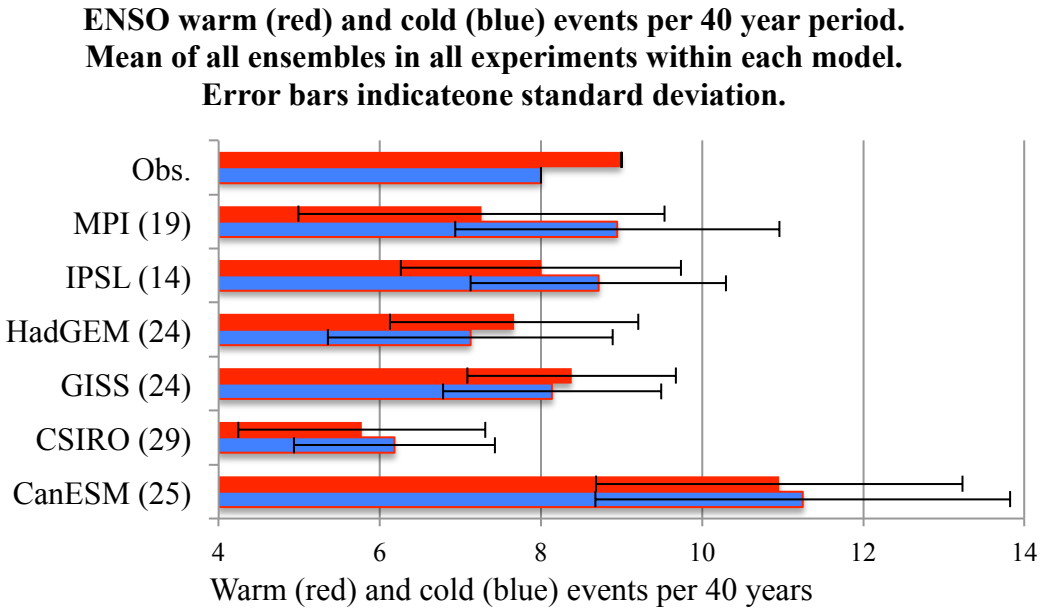


| | Obs. | CanESM (25) | CSIRO (25) | GISS (24) | HadGEM (24) | IPSL (14) | MPI (19) |
|---|---|---|---|---|---|---|---|
| Warm Events | 9.00 | 10.96 | 5.78 | 8.38 | 7.67 | 8.00 | 7.26 |
| Cold Events | 8.00 | 11.25 | 6.19 | 8.14 | 7.13 | 8.71 | 8.95 |

**Figure 3.8.** Number of ENSO warm (red) or cold (blue) events observed or simulated in the applicable 40-year comparison period for the CanESM, CSIRO, GISS, HadGEM, IPSL and MPI models. Values in parentheses are the number of ensemble members for each experiment or family of experiments. Error bars represent plus or minus one standard deviation of ENSO events relative to the experiment mean. A table of values is provided under the graph.

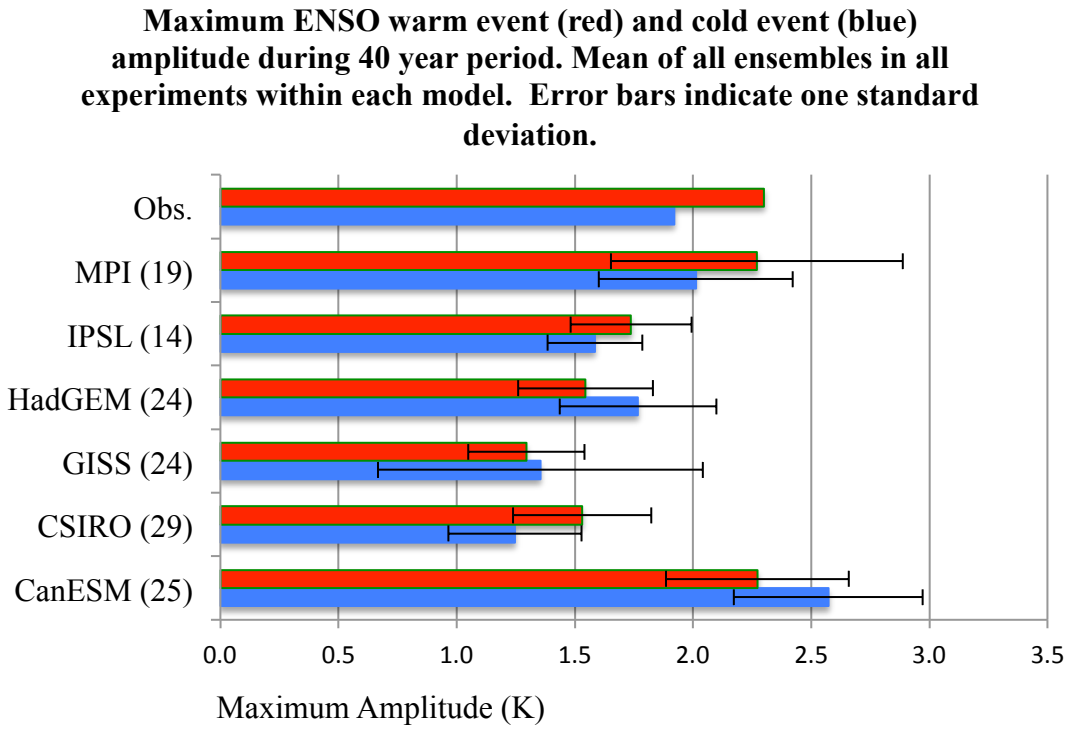


| | Obs. | CanESM (25) | CSIRO (25) | GISS (24) | HadGEM (24) | IPSL (14) | MPI (19) |
|---|---|---|---|---|---|---|---|
| Warm amp. | 2.30 | 2.27 | 1.53 | 1.29 | 1.54 | 1.74 | 2.27 |
| Cold amp. | 1.92 | 2.57 | 1.25 | 1.35 | 1.77 | 1.58 | 2.01 |

**Figure 3.9.** Maximum amplitude (K) of ENSO warm (red) or cold (blue) events observed or simulated in the applicable 40-year comparison period. Values in parenthesis following y-axis (model name) labels indicate the number of ensemble members, inclusive of all experiment designs, run by the particular model. Error bars show plus or minus one standard deviation relative to the model mean. A table of values is provided under the graph.

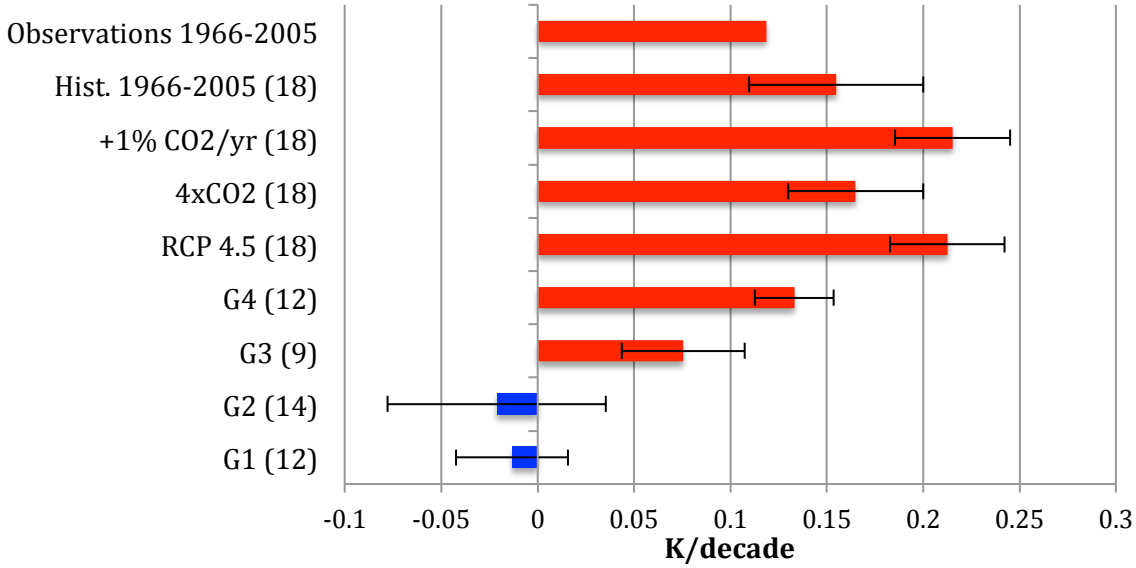


**Figure 3.10.** Linear trend in Niño3.4 Index (5°S-5°N, 120°W-170°W) during the applicable 40-year comparison periods. The applicable comparison periods are 1966-2005 for historical simulations; years 11-50 for G1, G2, +1% $CO_2$ $yr^{-1}$ and 4xCO2; 2030-2069 for G3, G4 and RCP4.5; and 1966-2005 for historical simulations and observations. The values in parenthesis are the number of ensemble members for each experiment. Red bars indicate a warming trend. Blue bars indicate a cooling trend. Error bars indicate one standard deviation.

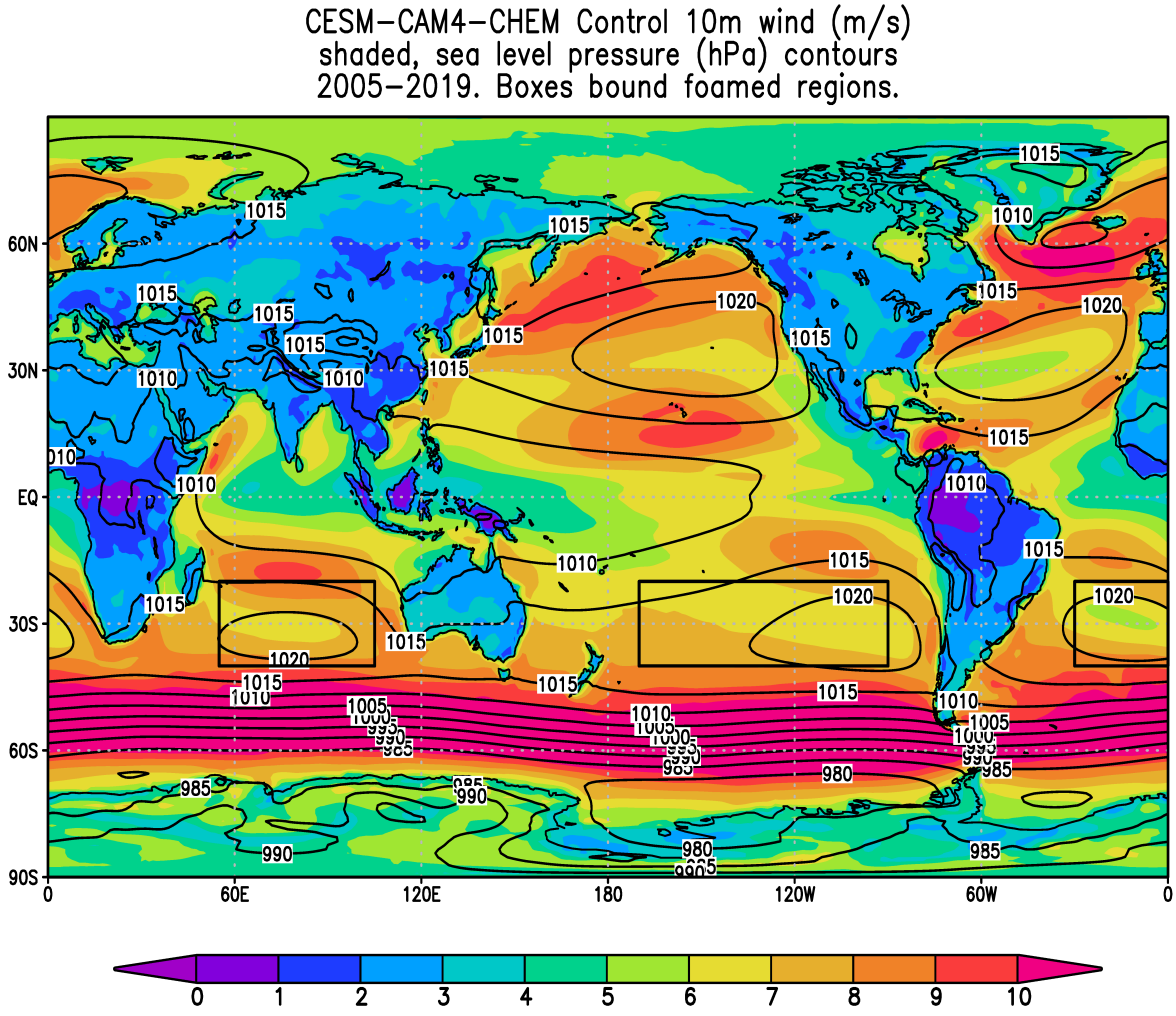


**Figure 4.1.** Applied forcing and global mean temperature response. Ocean albedo changed from daily average of 0.0]6 to a fixed value of 0.15 over "foam regions," 20°N-20°S, 90°W-170°W (South Pacific), 20°N-20°S, 30°W-0°E (South Atlantic) and 20°N-20°S, 55°E-105°E (South Indian). Each "foamed" region is outlined in black. Control run sea level pressure (mb) is shown with contours and 10-m winds (m/s) are shaded.

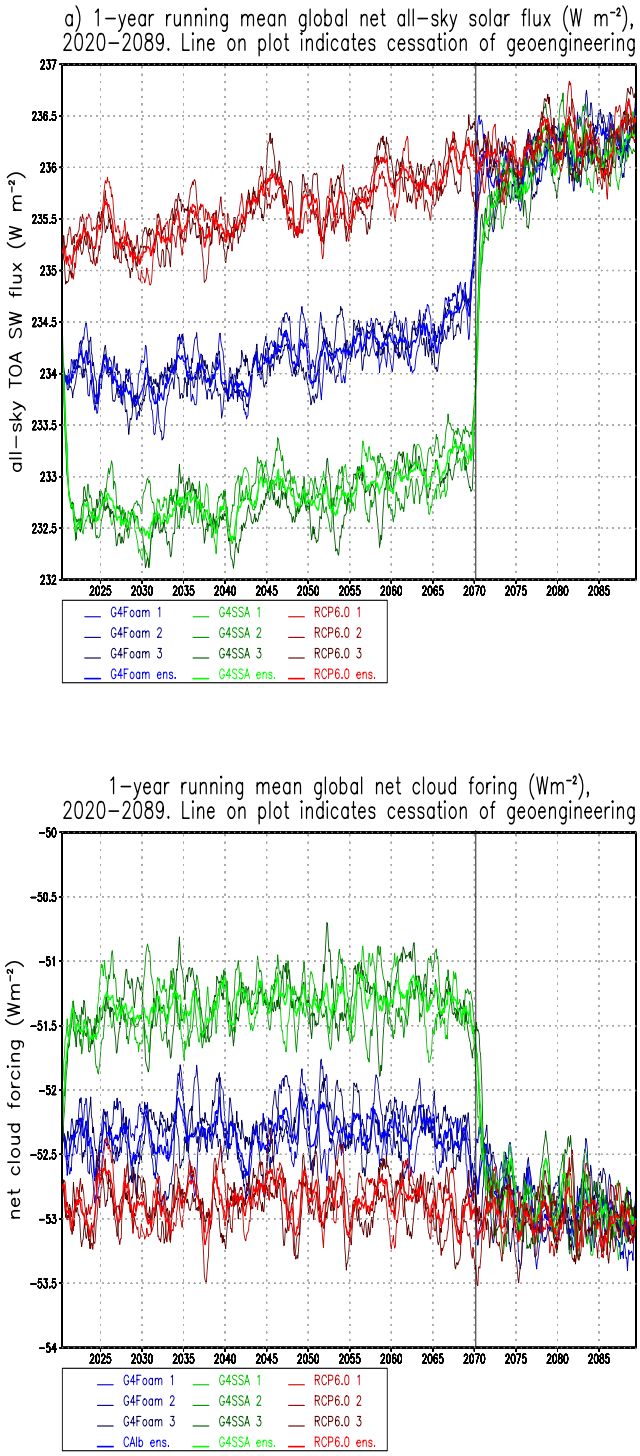


**Figure 4.2.** (a) Net all-sky SW flux at top of atmosphere and (b) time series of global mean net cloud forcing. Each ensemble member and the ensemble mean are shown for each forcing.

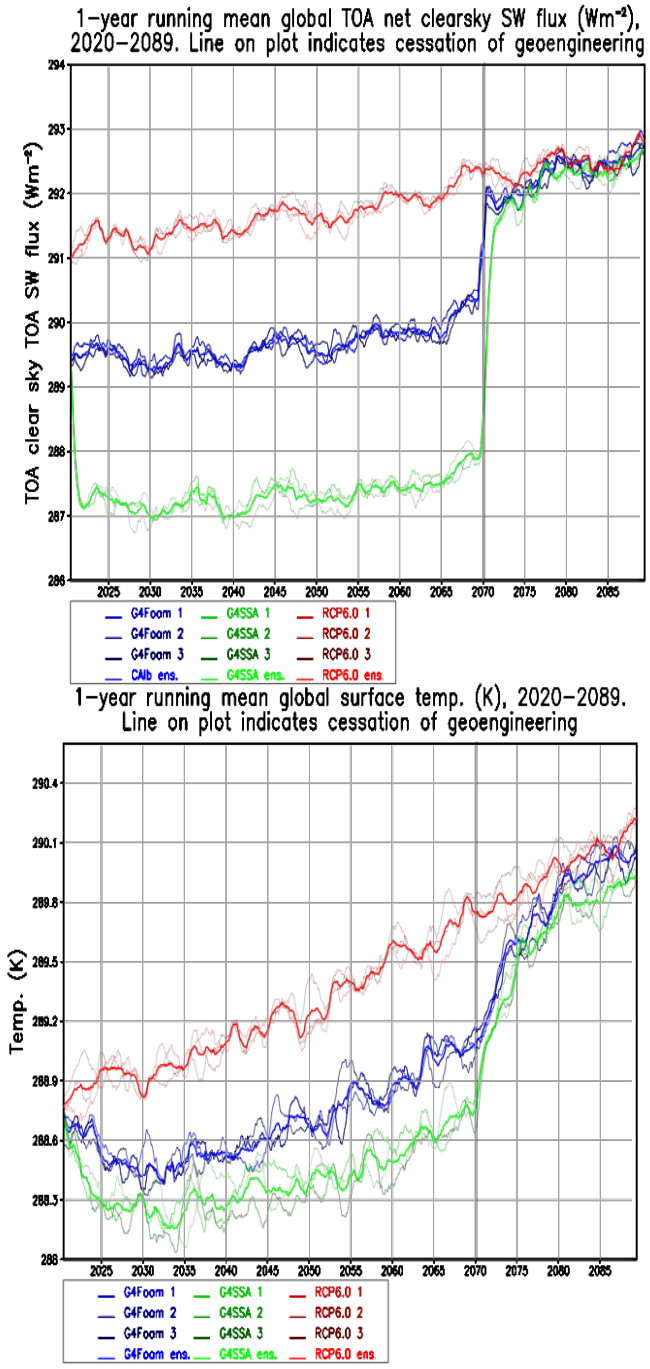


**Figure 4.3**. (a) Net clear sky SW flux at top of atmosphere, which includes the effects of changes in radiation caused by changes in ocean surface albedo or land albedo (ice and snow), as well as stratospheric aerosols (stratospheric geoengineering) and (b) Time series of global mean temperature. In G4Foam, temperature is more than twice as sensitive to ocean albedo forcing as it is to stratospheric geoengineering, as applied in G4SSA, albeit with very different latitudinal distributions of temperature changes. Each ensemble member and the ensemble mean are shown for each forcing.

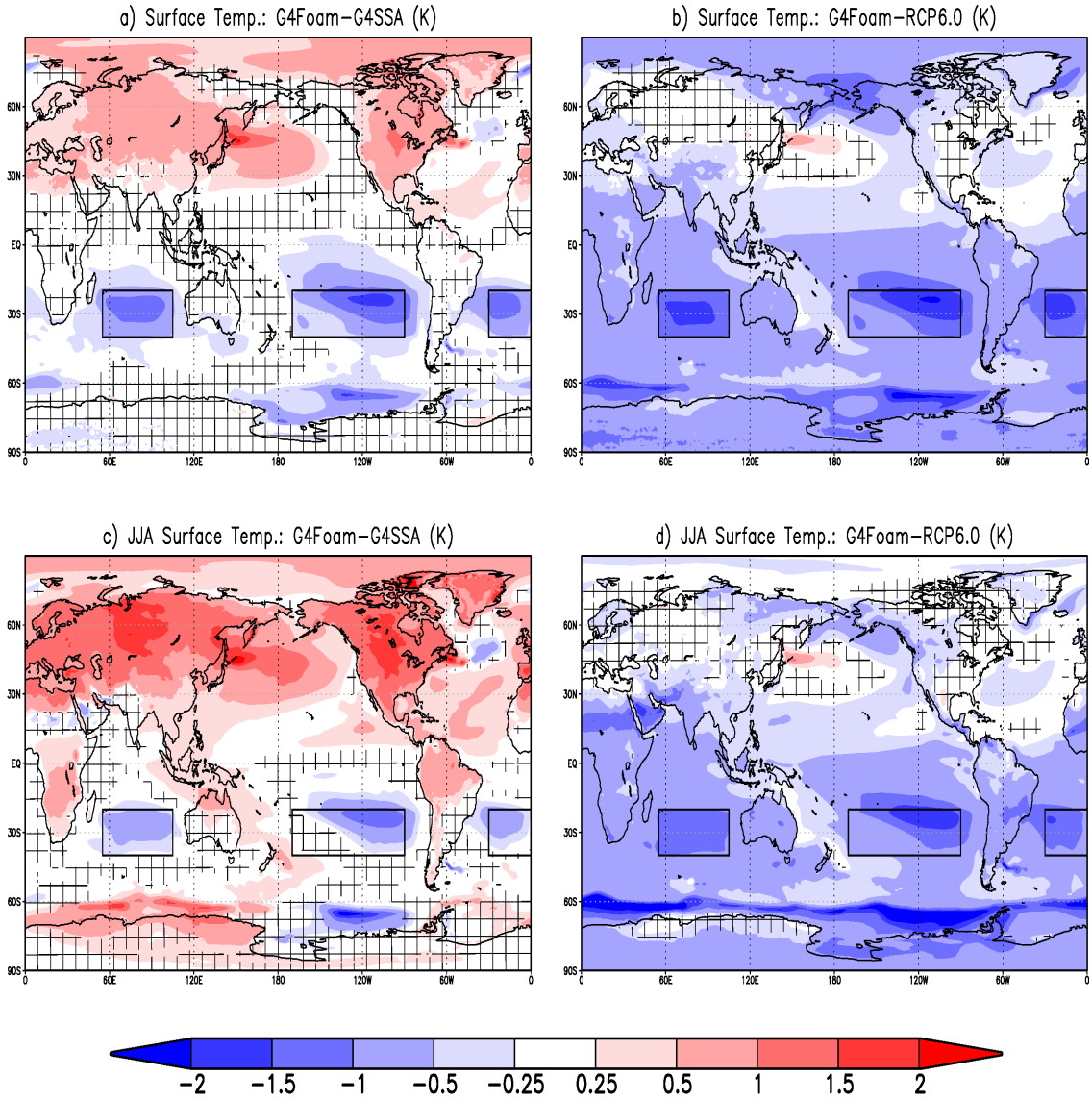


**Figure 4.4.** 2030-2069 surface temperature differences (K) between G4Foam and (a) G4SSA, (b) RCP6.0, (c) G4SSA during JJA, and (d) RCP6.0 during JJA. Hatched regions are areas with $p > 0.05$ (where changes are not statistically significant based on a paired *t*-test). Black boxes enclose foamed regions.

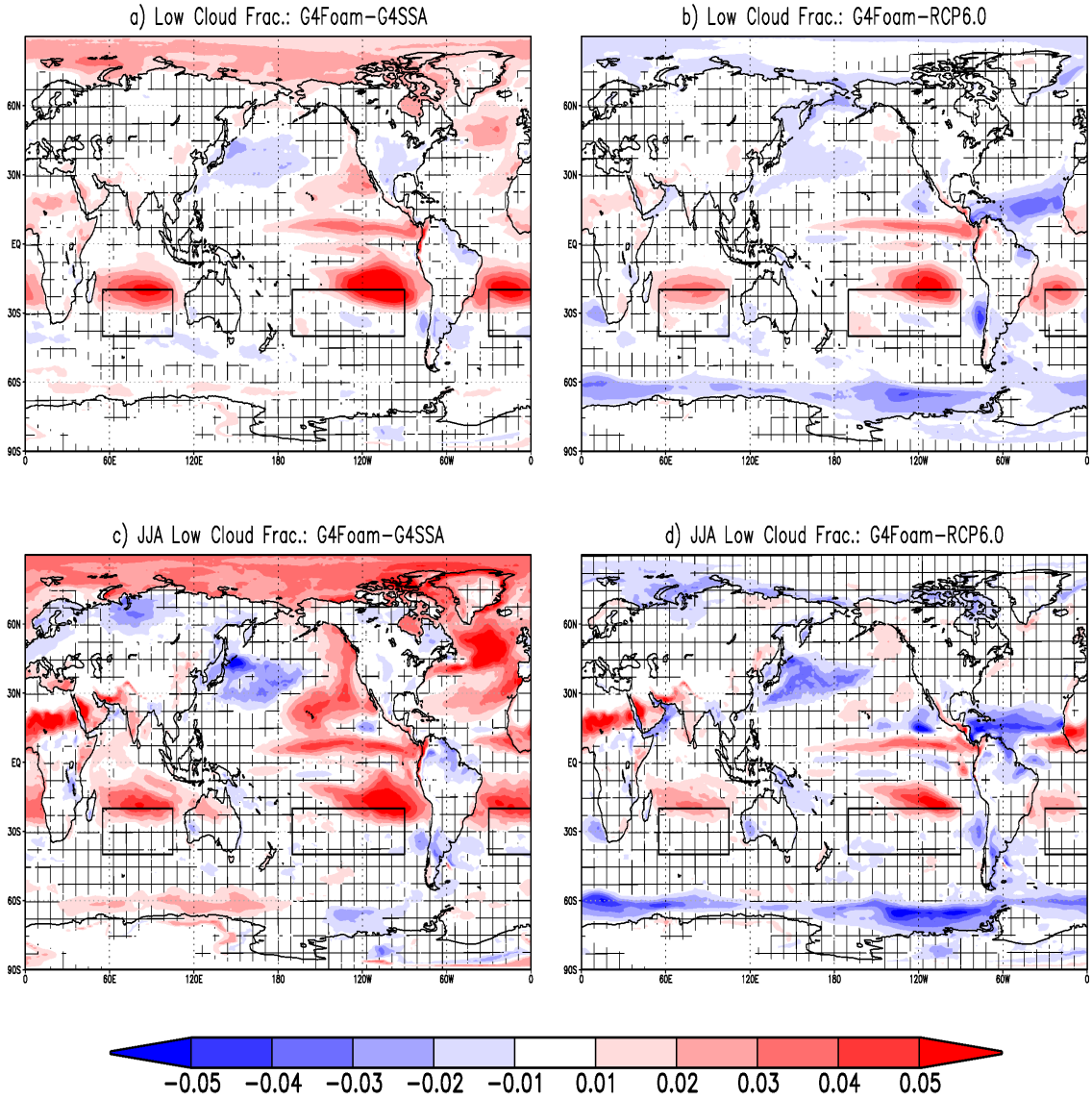


**Figure 4.5.** 2030-2069 low cloud fraction difference (unitless) between G4Foam and (a) G4SSA, (b) RCP6.0, (c) G4SSA during JJA, and (d) RCP6.0 during JJA. Hatched regions are areas with $p > 0.05$ (where changes are not statistically significant based on a paired *t*-test). Black boxes enclose foamed regions.

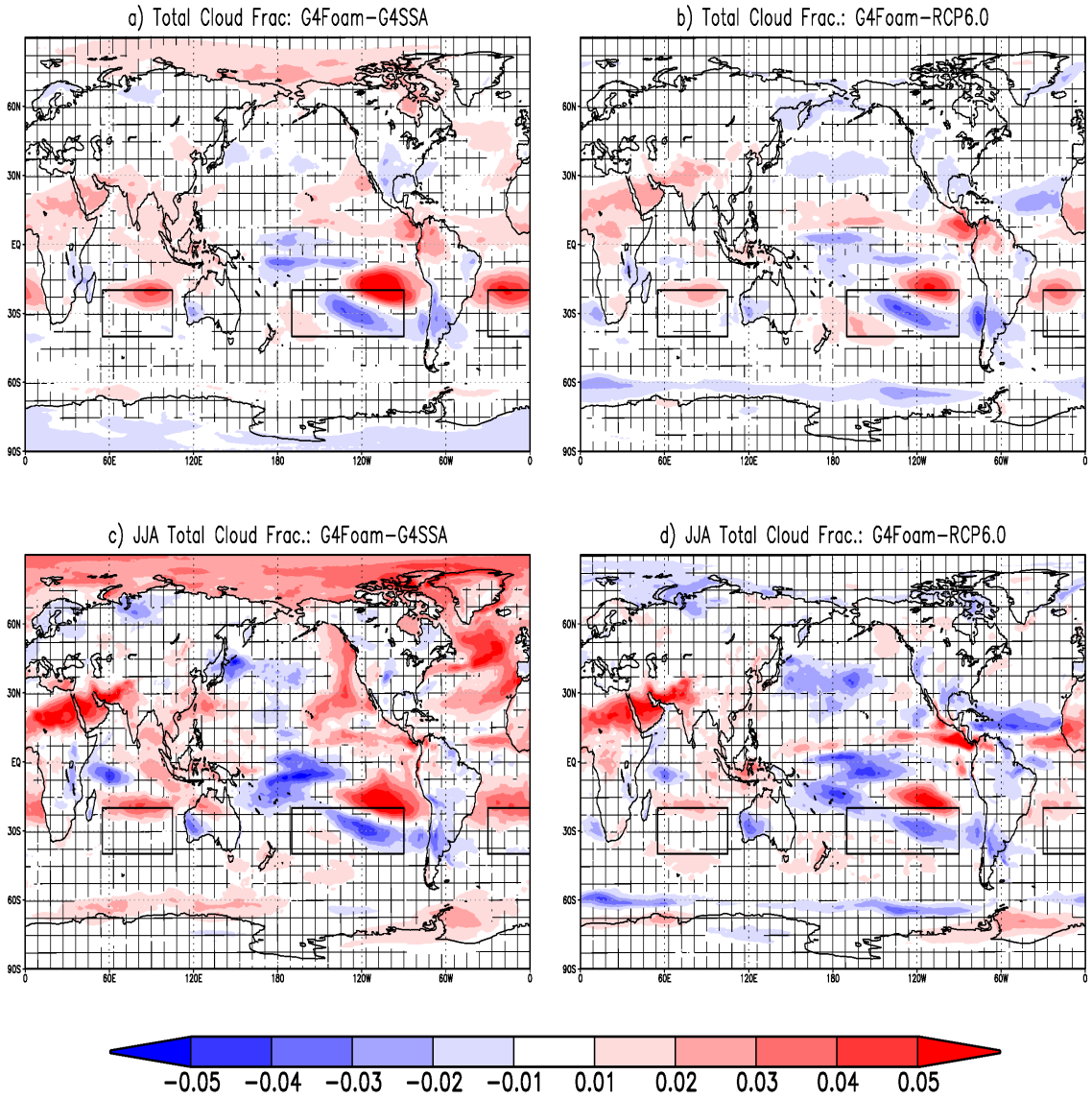


**Figure 4.6.** 2030-2069 total cloud fraction difference (unitless) between G4Foam and (a) G4SSA, (b) RCP6.0, (c) G4SSA during JJA and (d) RCP6.0 during JJA. Hatched regions are areas with $p > 0.05$ (where changes are not statistically significant based on a paired *t*-test). Black boxes enclose foamed regions.

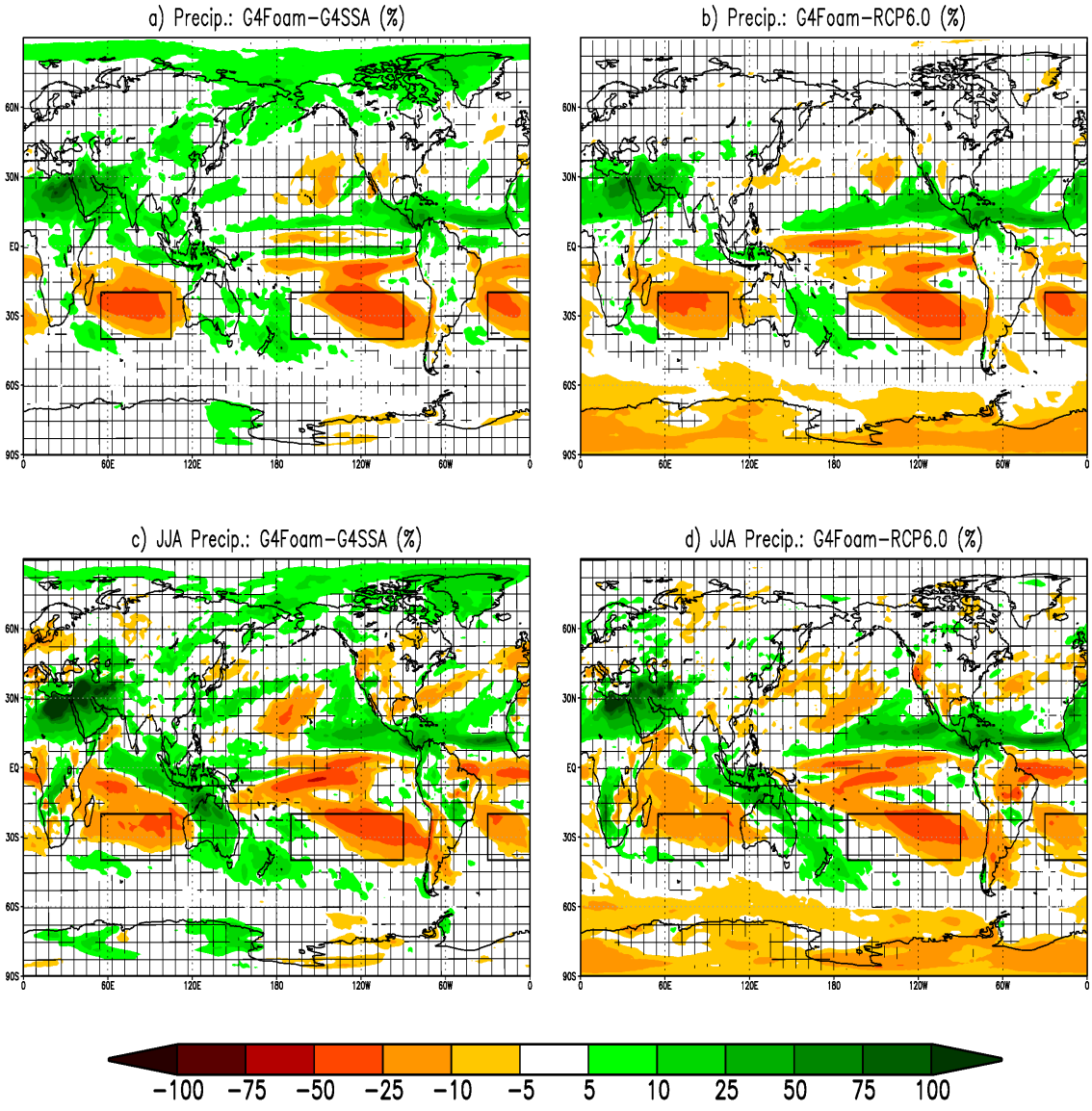


**Figure 4.7.** 2030-2069 precipitation difference (%) between G4Foam and (a) G4SSA, (b) RCP6.0, (c) G4SSA during JJA and (d) RCP6.0 during JJA. Hatched regions are areas with $p > 0.05$ (where changes are not statistically significant based on a paired *t*-test). Black boxes enclose foamed regions.

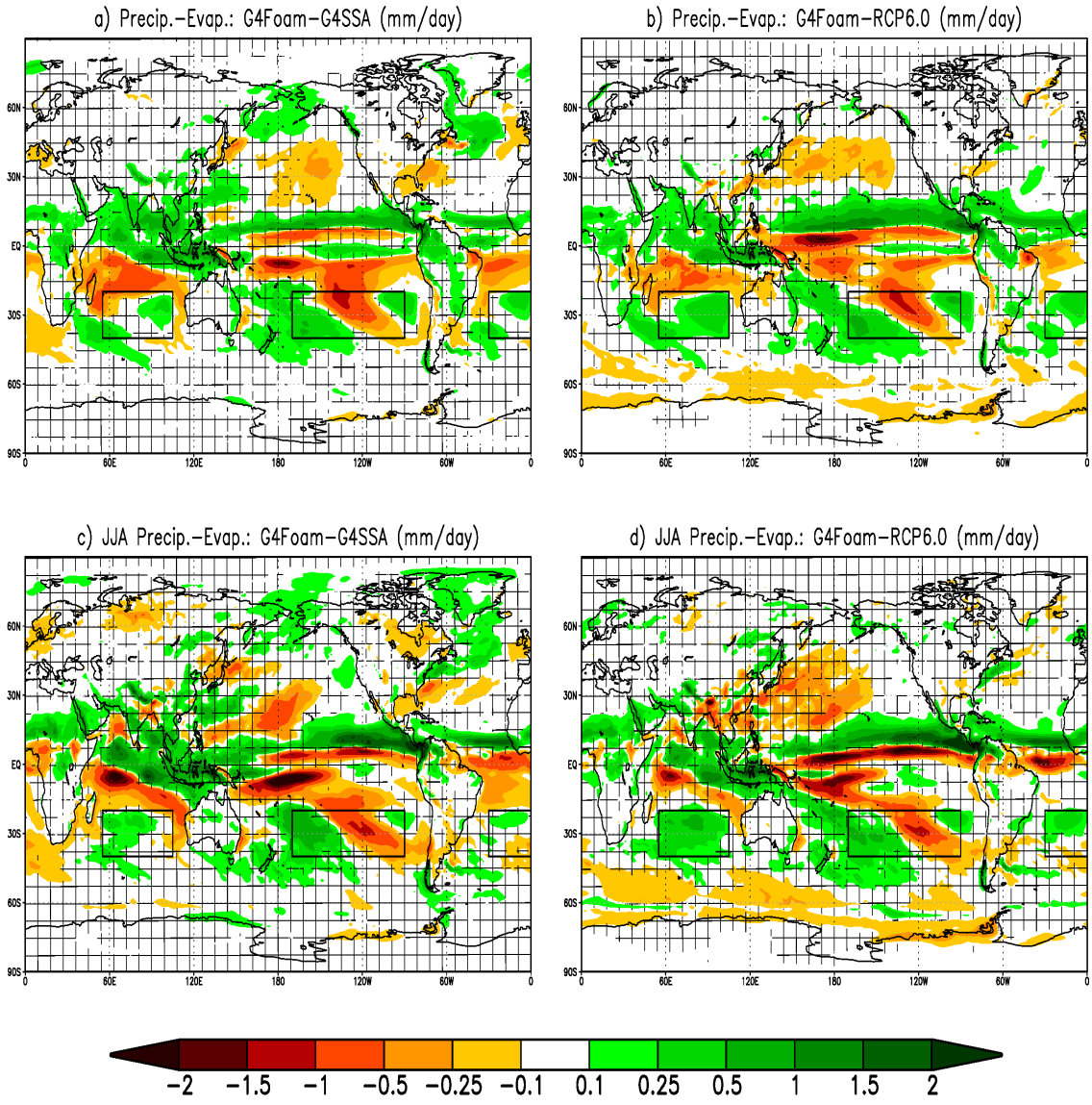


**Figure 4.8.** 2030-2069 precipitation minus evaporation difference (mm/day) between G4Foam and (a) G4SSA, (b) RCP6.0, (c) G4SSA during JJA and (d) RCP6.0 during JJA. Hatched regions are areas with $p > 0.05$ (where changes are not statistically significant based on a paired *t*-test). Black boxes enclose foamed regions.

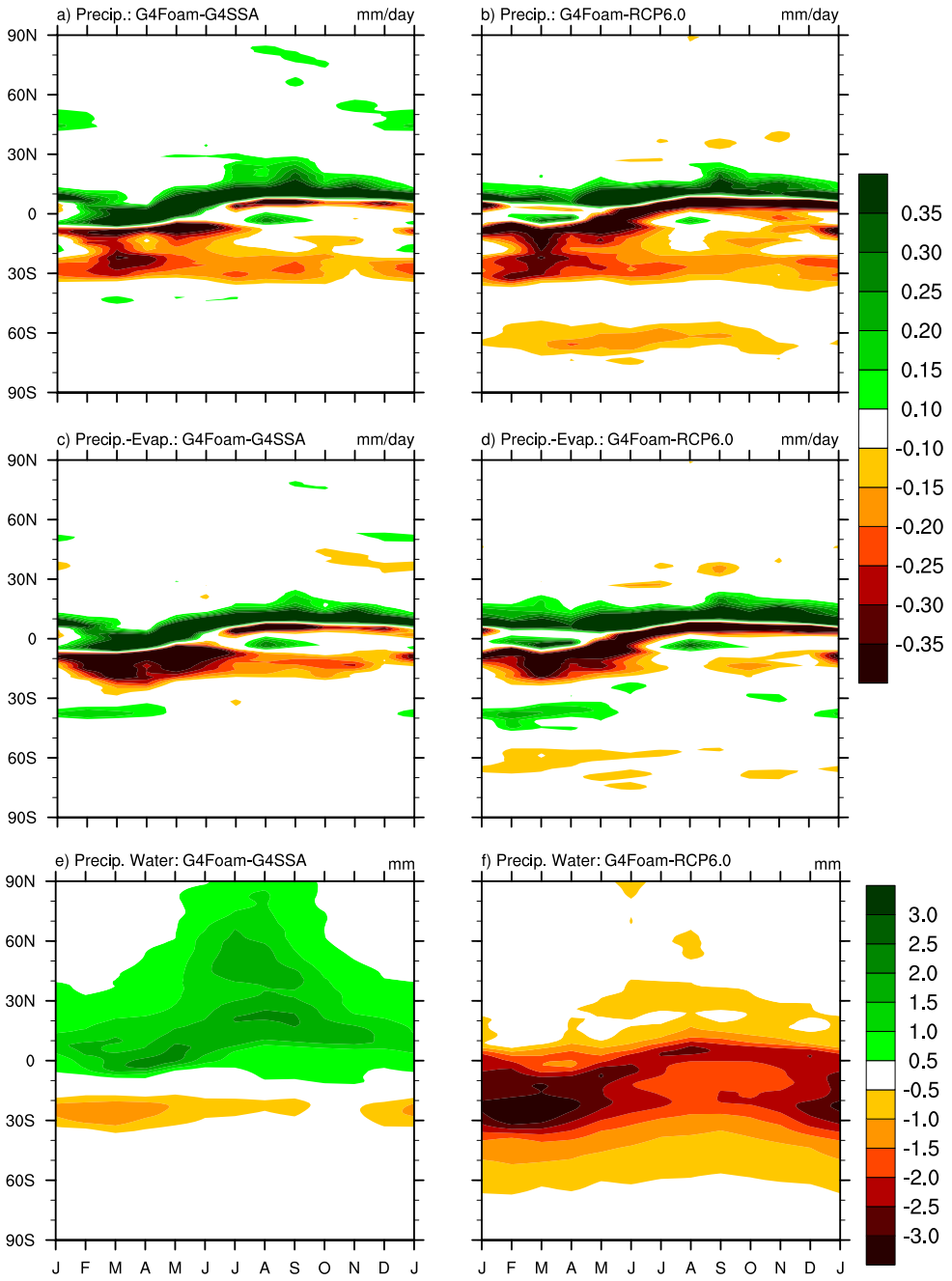


**Figure 4.9.** 2030-2069 monthly mean annual cycle of zonal mean precipitation (mm/day) for (a) G4Foam minus G4SSA and (b) G4Foam minus RCP6.0, precipitation minus evaporation (mm/day) for (c) G4Foam minus G4SSA and (d) G4Foam minus RCP6.0, and total precipitable water (mm) for (e) G4Foam minus G4SSA and (f) G4Foam minus RCP6.0.

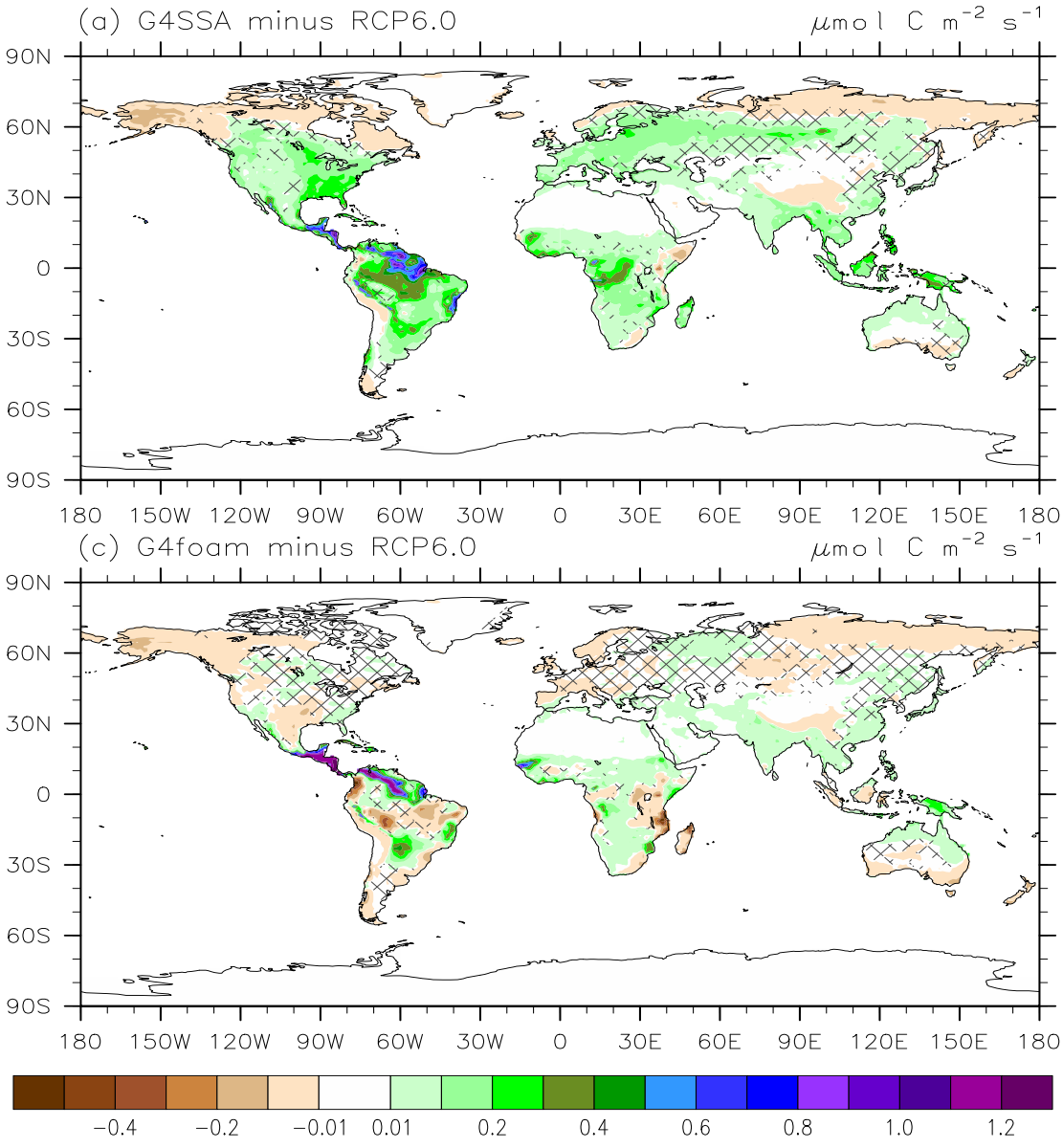


**Figure 4.10.** (a) Photosynthesis rate differences between G4SSA and RCP6.0 during years 2030–2069 (sulfate injection period, excluding the first 10 years) (Fig. 4a from Xia et al., 2016). (b) Photosynthesis rate anomaly between G4Foam and RCP6.0 during years 2030–2069 of solar reduction. Hatched regions are areas with $p > 0.05$ (where changes are not statistically significant based on a paired t test).

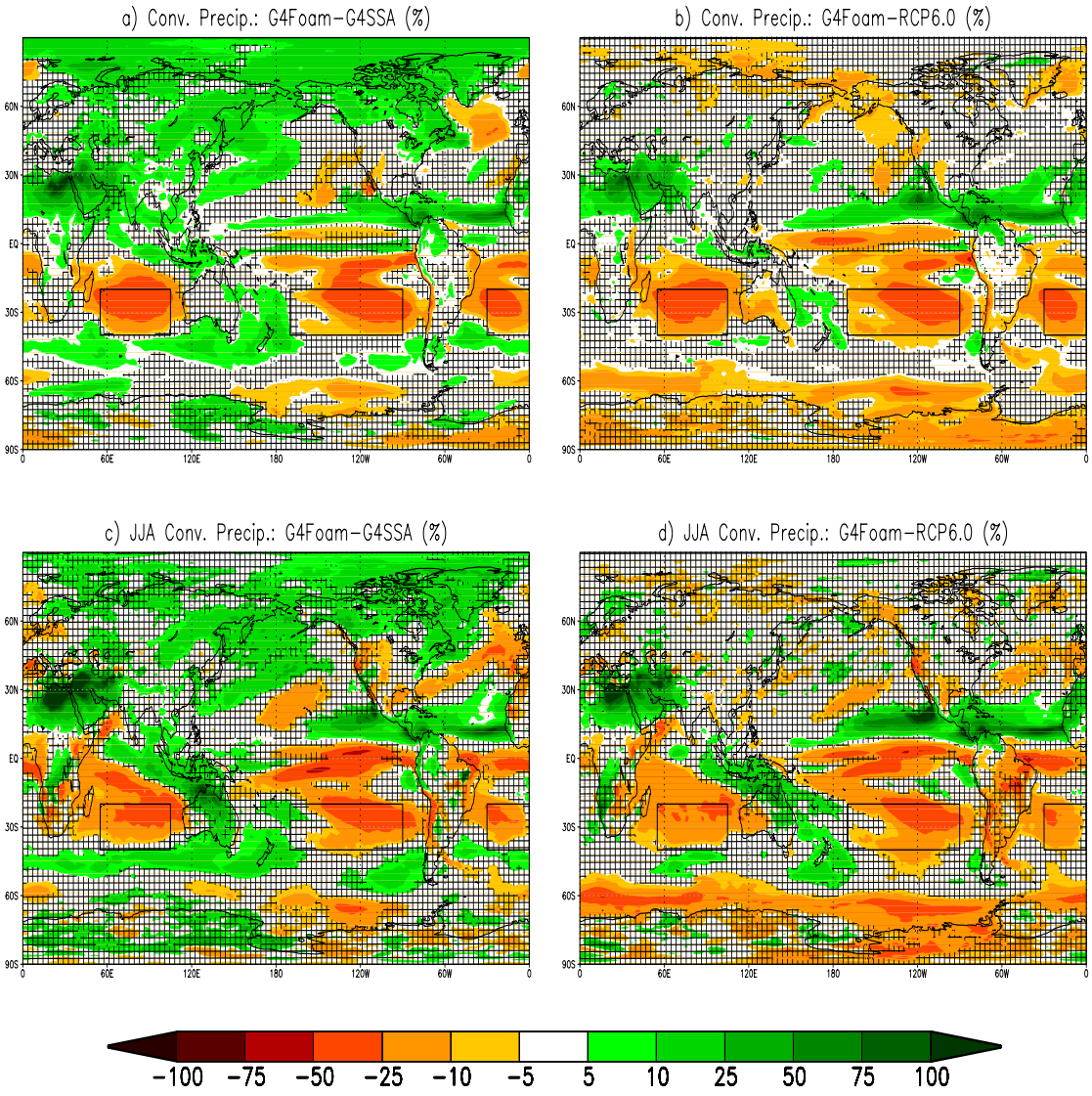


**Figure 4.11.** 2030-2069 convective precipitation difference (%) between G4Foam and (a) G4SSA, (b) RCP6.0, (c) G4SSA during JJA and (d) RCP6.0 during JJA. Hatched regions are areas with $p > 0.05$ (where changes are not statistically significant based on a paired *t*-test). Black boxes enclose foamed regions.

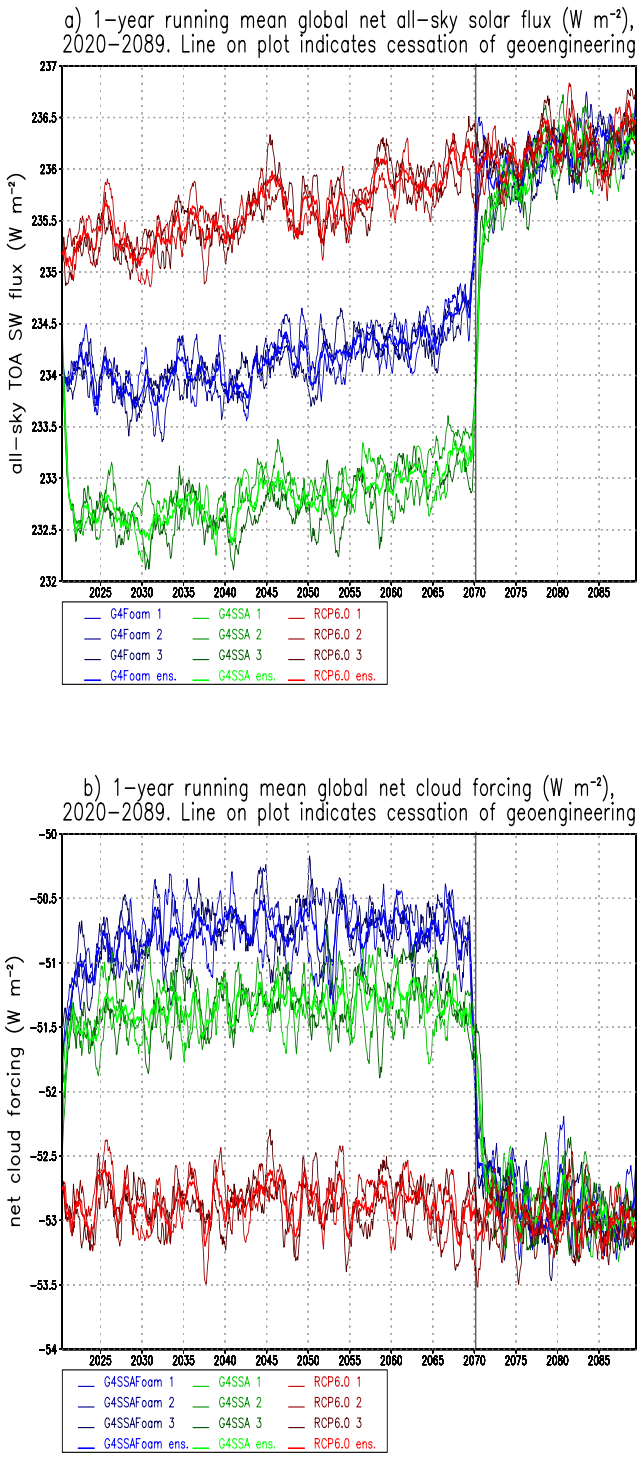


**Figure 5.1.** (a) Net all-sky SW flux at top of atmosphere and (b) time series of global mean net cloud forcing. Each ensemble member and the ensemble mean are shown for each forcing.

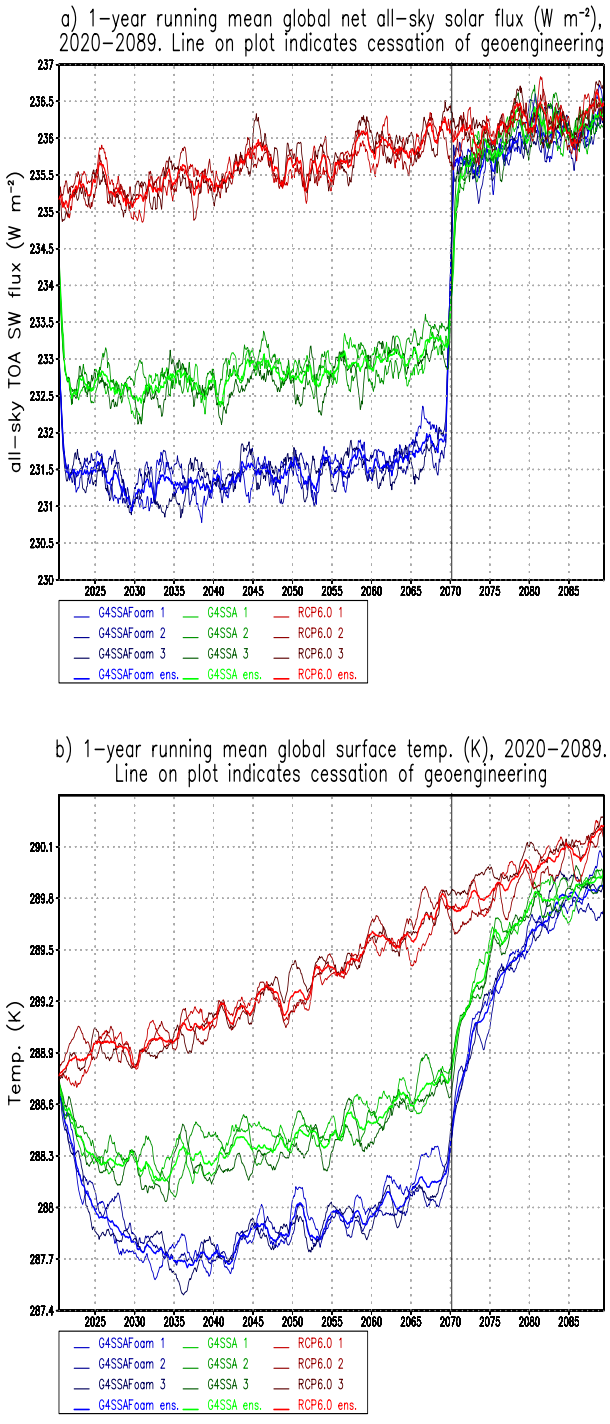


**Figure 5.2. (**a) Net clear sky SW flux at top of atmosphere, which includes the effects of changes in radiation caused by changes in ocean surface albedo or land albedo (ice and snow), as well as stratospheric aerosols (stratospheric geoengineering) and (b) Time

series of global mean temperature. Each ensemble member and the ensemble mean are shown for each forcing.

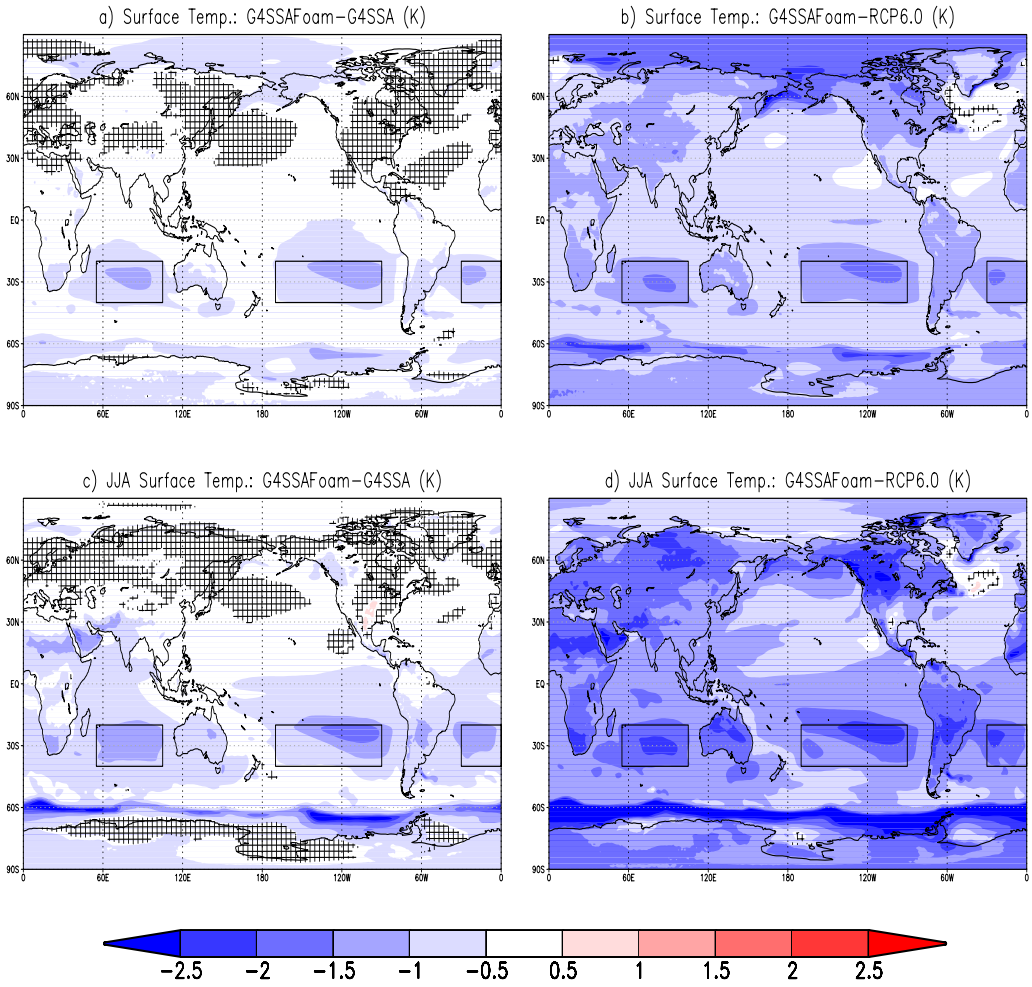


**Figure 5.3.** 2030-2069 surface temperature differences (K) between G4SSAFoam and (a) G4SSA, (b) RCP6.0, (c) G4SSA during JJA, and (d) RCP6.0 during JJA. Hatched regions are areas with $p > 0.05$ (where changes are not statistically significant based on a paired *t*-test). Black boxes enclose foamed regions.

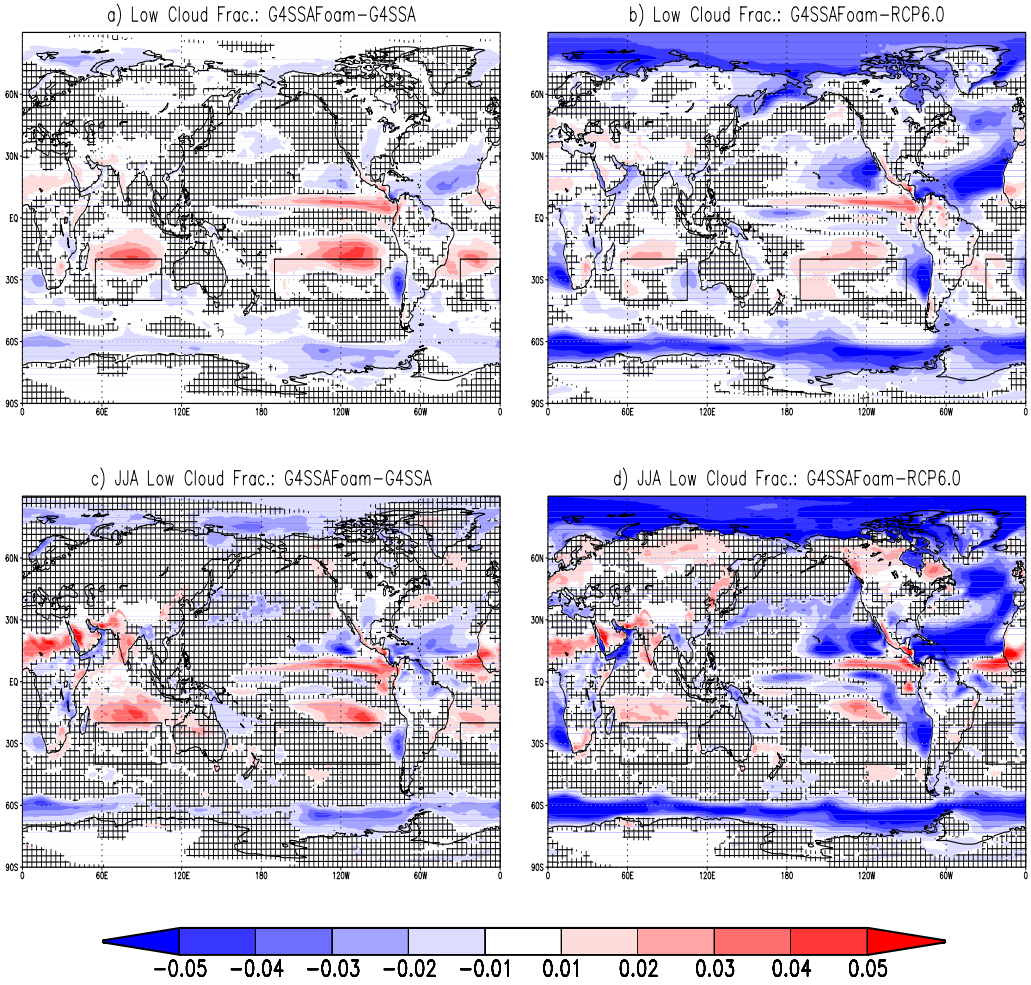


**Figure 5.4.** 2030-2069 low cloud fraction difference (unitless) between G4SSAFoam and (a) G4SSA, (b) RCP6.0, (c) G4SSA during JJA, and (d) RCP6.0 during JJA. Hatched regions are areas with $p > 0.05$ (where changes are not statistically significant based on a paired *t*-test). Black boxes enclose foamed regions.

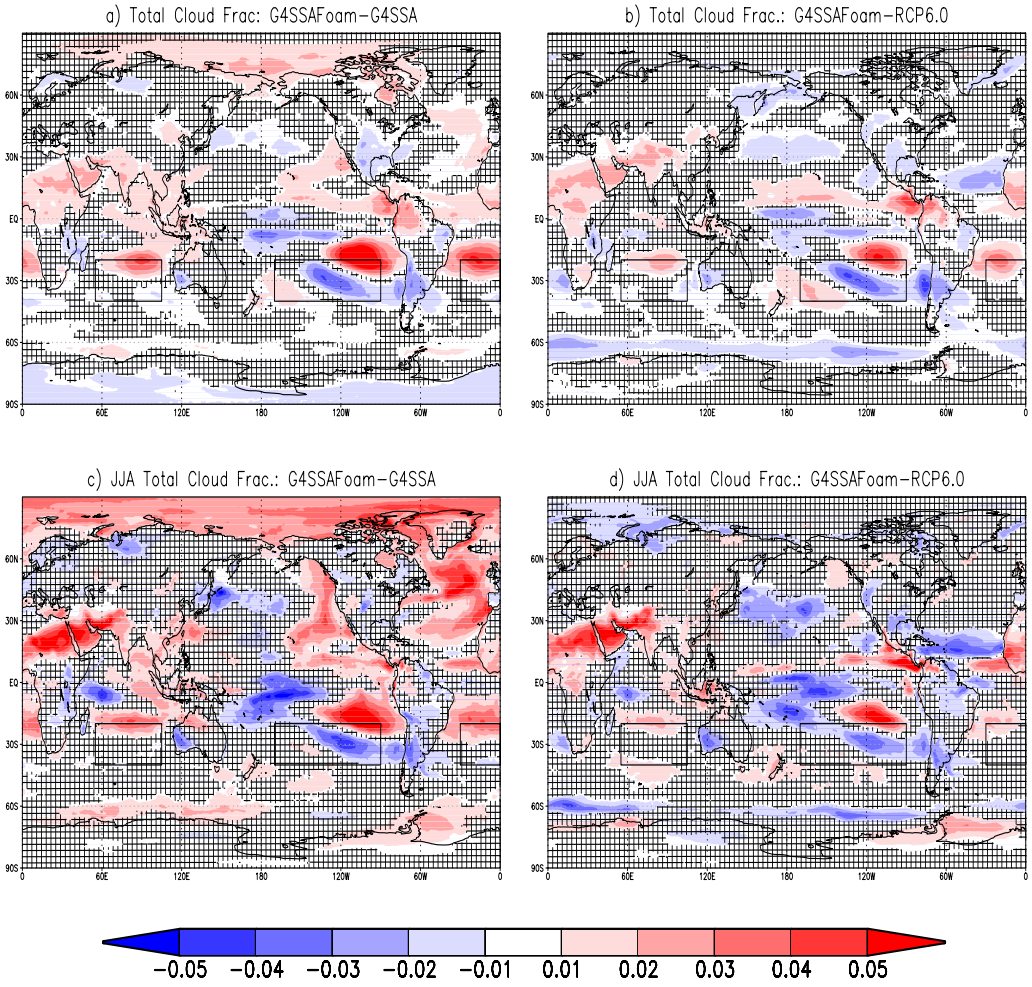


**Figure 5.5.** 2030-2069 total cloud fraction difference (unitless) between G4SSAFoam and (a) G4SSA, (b) RCP6.0, (c) G4SSA during JJA and (d) RCP6.0 during JJA. Hatched regions are areas with $p > 0.05$ (where changes are not statistically significant based on a paired *t*-test). Black boxes enclose foamed regions.

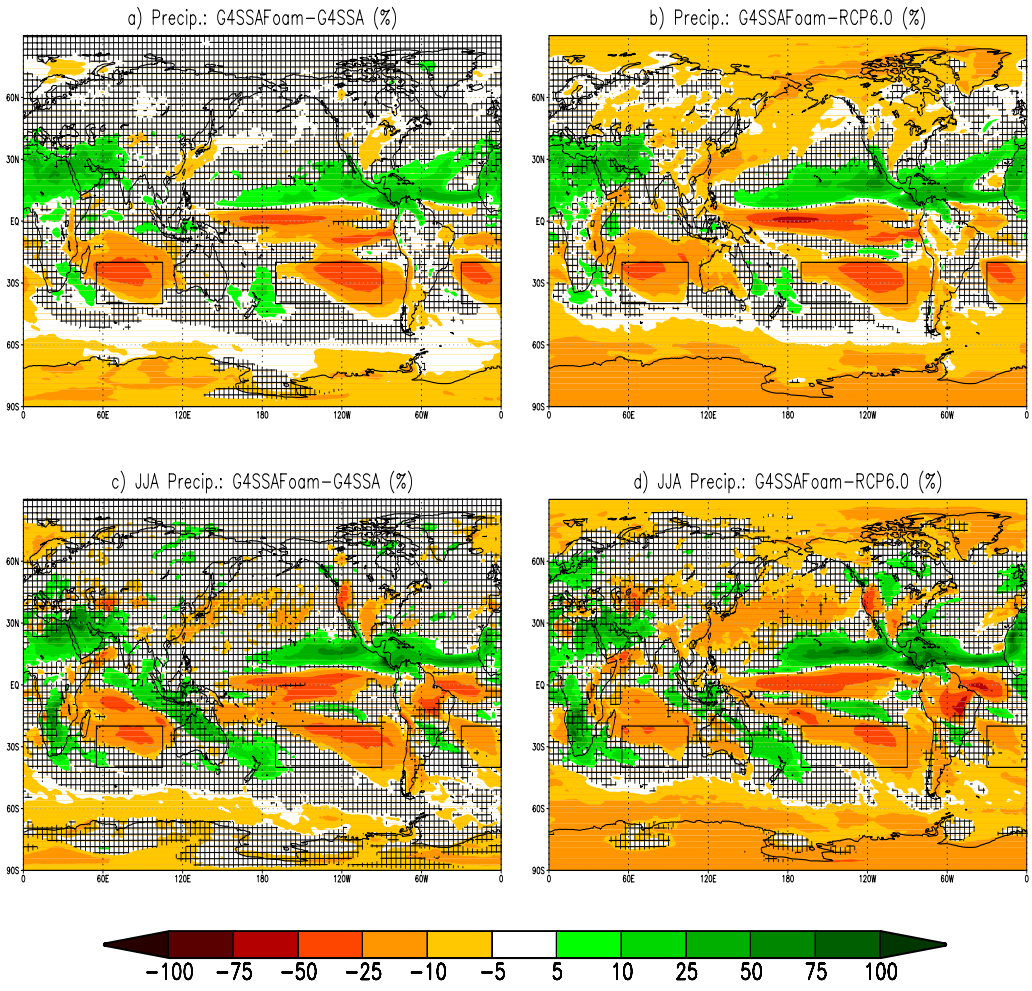


**Figure 5.6.** 2030-2069 precipitation difference (%) between G4SSAFoam and (a) G4SSA, (b) RCP6.0, (c) G4SSA during JJA and (d) RCP6.0 during JJA. Hatched regions are areas with $p > 0.05$ (where changes are not statistically significant based on a paired *t*-test). Black boxes enclose foamed regions.

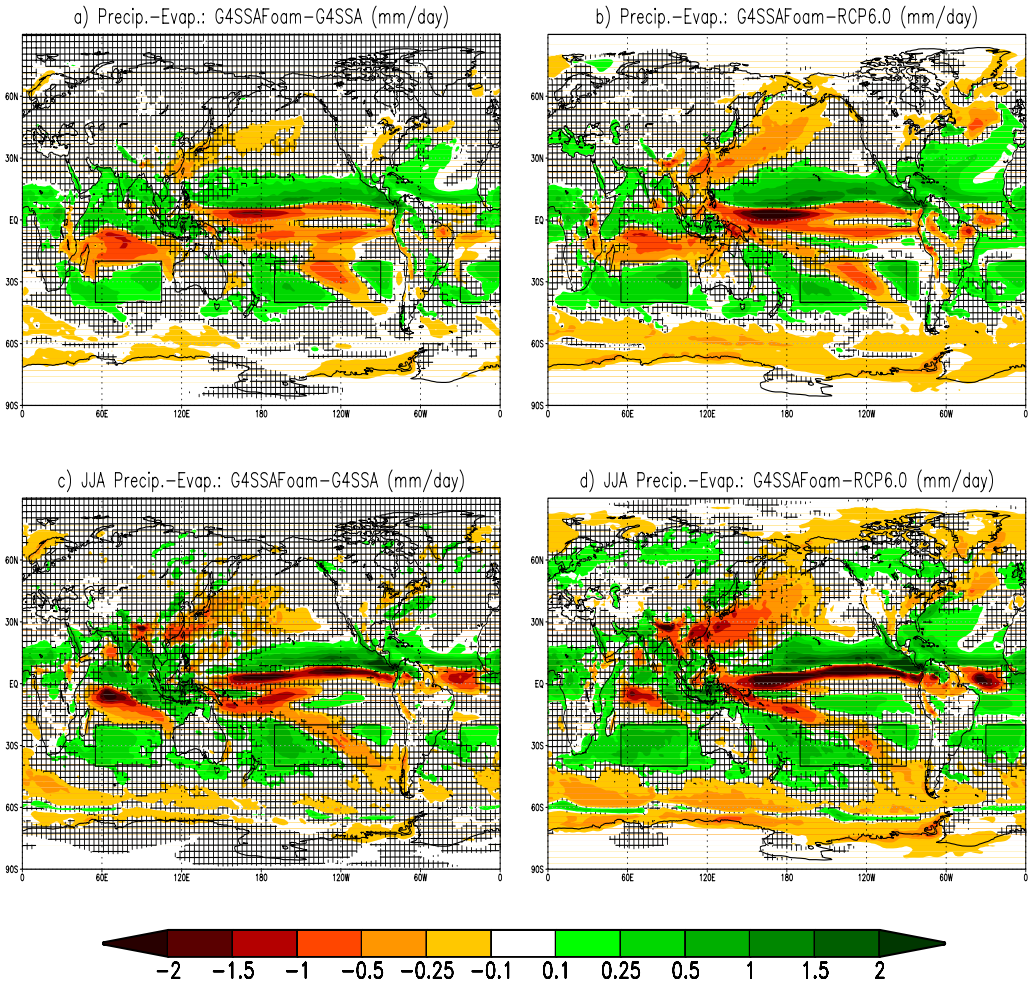


**Figure 5.7.** 2030-2069 precipitation minus evaporation difference (mm/day) between G4SSAFoam and (a) G4SSA, (b) RCP6.0, (c) G4SSA during JJA and (d) RCP6.0 during JJA. Hatched regions are areas with $p > 0.05$ (where changes are not statistically significant based on a paired $t$-test). Black boxes enclose foamed regions.

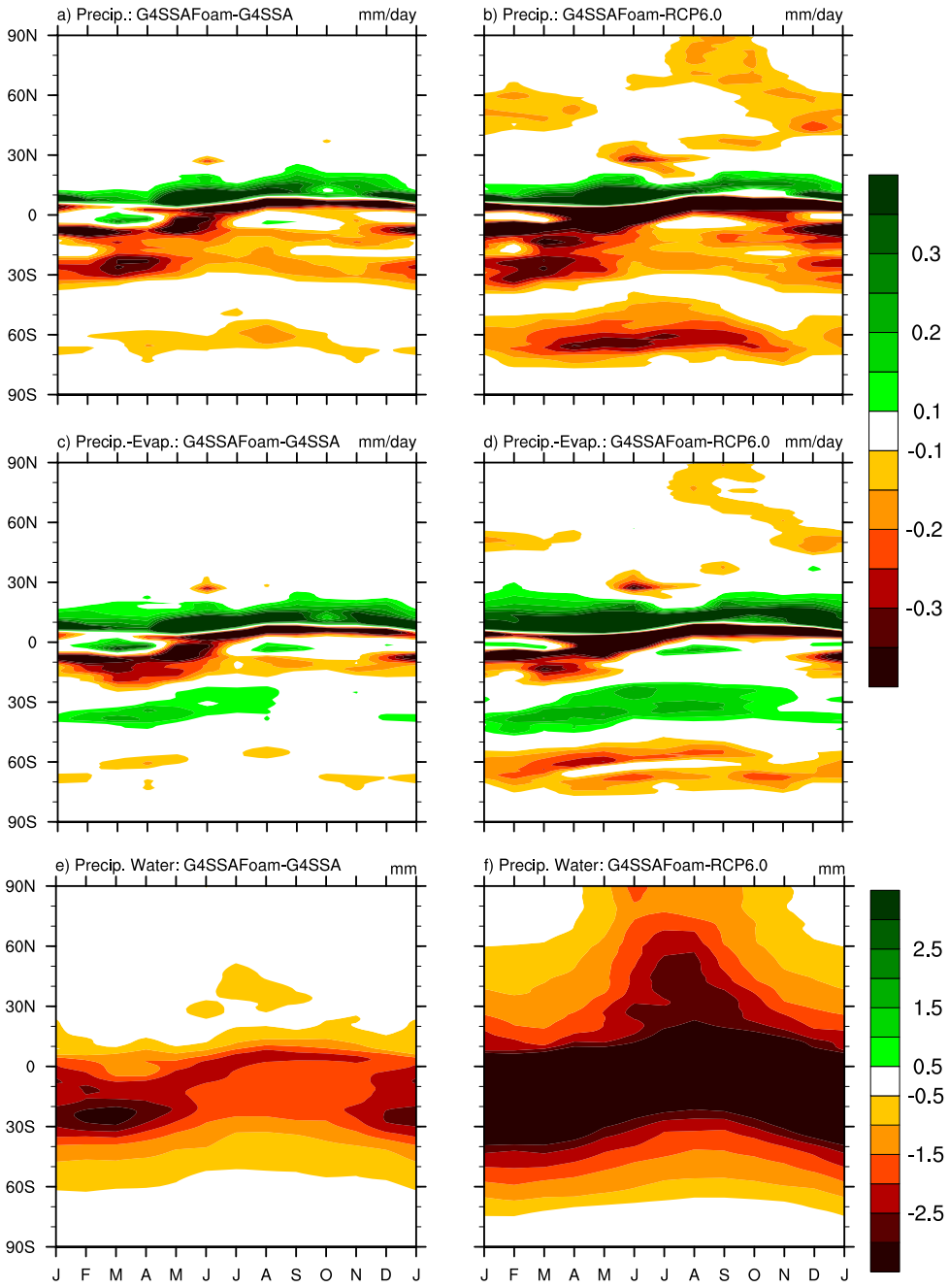


**Figure 5.8.** 2030-2069 monthly mean annual cycle of zonal mean precipitation (mm/day) for (a) G4SSAFoam minus G4SSA and (b) G4SSAFoam minus RCP6.0, precipitation minus evaporation (mm/day) for (c) G4SSAFoam minus G4SSA and (d) G4SSAFoam minus RCP6.0, and total precipitable water (mm) for (e) G4SSAFoam minus G4SSA and (f) G4SSAFoam minus RCP6.0.

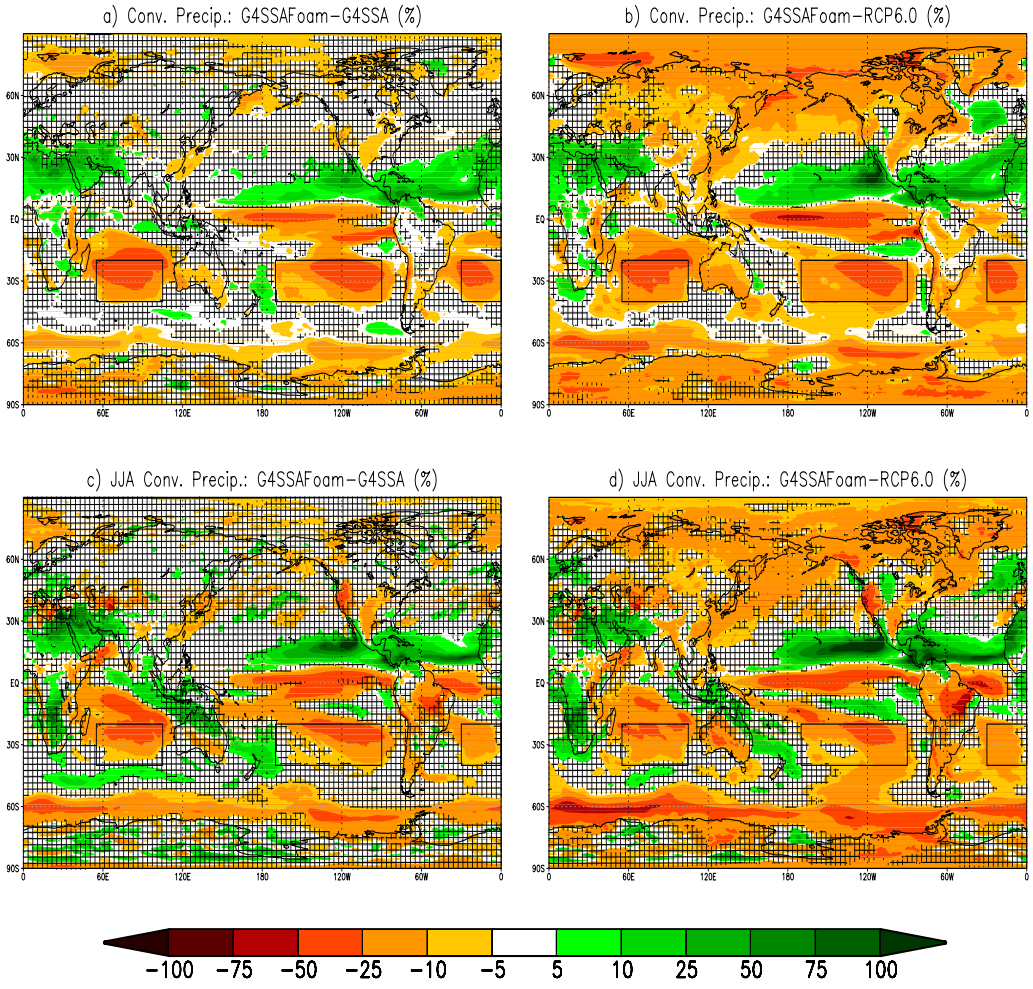


**Figure 5.9.** 2030-2069 convective precipitation difference (%) between G4SSAFoam and (a) G4SSA, (b) RCP6.0, (c) G4SSA during JJA and (d) RCP6.0 during JJA. Hatched regions are areas with $p > 0.05$ (where changes are not statistically significant based on a paired *t*-test). Black boxes enclose foamed regions.